UNIVERSITY OF CALIFORNIA,
IRVINE

KCNQ2 Channels: Dynamic Molecular Interactions and Functional Role in Learning and Memory

DISSERTATION

submitted in partial satisfaction of the requirements
for the degree of

DOCTOR OF PHILOSOPHY

in Pharmacology and Toxicology

by

Anastasia Kosenko

Dissertation Committee:
Associate Professor Naoto Hoshi, Chair
Associate Professor Geoffrey W. Abbott
Associate Professor Frederick J. Ehlert

2015

TABLE OF CONTENTS

LIST OF FIGURES

LIST OF TABLES

ACKNOWLEDGEMENTS

I would like to express my deepest appreciation to my mentor and committee chair, Professor Naoto Hoshi, for providing his guidance and continuous support and for sharing his exemplary wisdom and perseverance. Without his help this dissertation would not have been possible. I would also like to thank my committee members, Professor Geoff W. Abbott and Professor Frederick J. Ehlert, for their support and insightful comments in both scientific matters and in regards to my future career.

I would like to thank all members of the Hoshi lab, past and present, who were not only great colleagues but also great friends, genuine, kind, and patient. I would like to thank Professors Marcelo A. Wood and Norbert J. Fortin as well as their lab members (Melissa Malvaez, Ph.D., Annie Vogel-Ciernia, Ph.D. – former graduate students in Dr. Marcelo Wood's lab, and Leila M. Feinberg, M.S. – Dr. Norbert Fortin's Lab). I would also like to extend a special acknowledgement to my friends in the Department of Pharmacology, who provided professional advice and helped me enjoy my time at UCI, particularly Nayna Sanathara, Candice Gellner, John F Park, Soo Min Lee, and Peter Yu.

I thank European Molecular Biology Organization for permission to include portions of the paper originally published in EMBO Journal into my dissertation. The text of this dissertation is a partial reprint of the material as it appears in "Coordinated signal integration at the M-type potassium channel upon muscarinic stimulation." The co-author listed in this publication, Naoto Hoshi, directed and supervised research which forms the basis for the dissertation. I would like to thank the co-authors of the publication: Seungwoo Kang, Ida M. Smith, Derek L. Greene, Lorene K. Langeberg, and John D. Scott. Additionally, I would like to thank Public Library of Sciences for permission to include portions of the paper original published in PLOS ONE Journal. The text of this dissertation is a partial reprint of the material as it appears in "A change in configuration of the calmodulin–KCNQ channel complex underlies Ca^{2+}-dependent modulation of KCNQ channel activity." The co-author listed in this publication, Naoto Hoshi, directed and supervised research. Financial support was provided by the National Institute of Health grant NS067288 to NH.

Last but not least, a very special thank you to my family and friends for their unconditional love, support, and encouragement over the last five years. They helped me through tough times and celebrated with me times of happiness, but most importantly, they never stopped believing in me.

CURRICULUM VITAE

Anastasia Kosenko

Education

Ph.D. Pharmacology and Toxicology, University of California, Irvine 2015

B.S. Psychobiology, University of California, Los Angeles 2009

Field of Study

Neuropharmacology of voltage-gated ion channels and behavioral implications of channel dysregulation.

Research Experience

Graduate Student Researcher, Department of Pharmacology, UCI 2010-present
Laboratory of Naoto Hoshi, M.D., Ph.D.

- Discovered 2 signaling pathways of ion channel regulation by investigating molecular interactions via biochemical characterization and live cell imaging (FRET/TIRF)
- Designed and engineered proteins with site specific mutations in mammalian cells and E. coli, and used them to identify key sites of direct molecular interactions
- Examined functional effects of discovered protein-protein interactions in ion channel regulation by patch clamp in CHO cells and primary cultured neurons
- Established and managed behavioral testing facilities and protocols through collaborations with the Department of Neurobiology and Behavior

Research Associate, Department of Psychiatry, UCLA 2009-2010
Laboratory of George Bartzokis, M.D.

- Investigated the effect of common genetic variants on brain iron levels using genetic testing and Magnetic Resonance Imaging (MRI)
- Demonstrated proper use of MRI equipment, oversaw safety of MRI scanning procedure, and addressed instrument related questions
- Improved protocols of image analysis to minimize sample to sample variation

Additional Research Experience

Work-Study Research Assistant, Consortium for Neuropsychiatric Phenomics 2008-2009
(Robert Bilder, Ph.D.) Neuropsychiatric Institute, UCLA

Volunteer Research Assistant, Laboratory of Neuroimaging (LONI) 2007-2008
(Scott Fears, M.D., Ph.D.) Department of Neurology, UCLA

Volunteer Research Assistant, Stimulant Abuse and Addiction group 2006-2007
(Thomas Newton, M.D.) David Geffen School of Medicine, UCLA

Professional Development

NIH-sponsored short course in Integrative and Organ Systems Pharmacology, 2012
Omaha, NE

Publications

Kosenko A, Hoshi N (2013) A change in configuration of the calmodulin-KCNQ channel underlies Ca^{2+}-dependent modulation of KCNQ channel activity. *PLoS ONE* 8(12): e82290

Kosenko A, Kang S, Smith IM, Greene DL, Langeberg LK, Scott JD, Hoshi N (2012) Coordinated signal integration at the M-type potassium channel upon muscarinic stimulation. *The EMBO Journal*, 31(14):3147-56

Greene D, Kang S, **Kosenko A**, Hoshi N (2012) Adrenergic regulation of HCN4 channel requires protein association with β2-adrenergic receptor. *The Journal of Biological Chemistry*, 287(28):23690-7

Bartzokis G, Lu PH, Tishler TA, Peters DG, **Kosenko A**, Barrall KA, Finn JP, Villablanca P, Laub G, Altshuler LL, Geschwind DH, Mintz J, Neely E, Connor JR (2010) Prevalent iron metabolism gene variants associated with increased brain ferritin iron in healthy older men. *The Journal of Alzheimer's Disease*, 20(1):333-41

Oral Presentations

Using the novel knock-in mouse model, KCNQ2(S559A), to investigate the physiological role of M-current suppression in learning and memory — October 2014

KCNQ2 channel: mechanism of regulation and behavioral implications. — September 2013
7th Annual Research Day, Department of Pharmacology, UCI, Irvine, CA

Cardiac beta-adrenergic regulation via channel-receptor complexes. — September 2011
5th Annual Research Day, Department of Pharmacology, UCI, Irvine, CA

Abstracts

Kosenko A, Moftakhar S, Greene D, Hoshi N (2014) Deficits in M-channel regulation lead to impaired consolidation of recognition memory in mice. — November 2014
Society for Neuroscience, Washington DC

Kosenko A, Hoshi N (2012) Coordinated signal integration at the M-type potassium channel upon muscarinic stimulation. — November 2012
Cell Symposia: Neuromodulatory Mechanisms, New Orleans, LA

Kosenko A, Hoshi N (2012) The KCNQ2 channel integrates multiple signaling pathways by rearrangement of the channel complex. — March 2012
Annual EpiCenter Symposium, Irvine, CA

Kang S, **Kosenko A**, Greene D, Hoshi N (2012) Modulation of M-channel via Phosphorylated calmodulin by protein kinase CK2. — November 2012
Society for Neuroscience, New Orleans, LA

Noam Y, Regev L, Koh A, **Kosenko A**, Hoshi N, Baram TZ (2012) Visualizing heteromeric HCN channels on the cell membrane: new insight from FRET/TIRF imaging. — November 2012
Society for Neuroscience, New Orleans, LA

Awards and Honors

Henry Wood Elliot Memorial Award, Department of Pharmacology, UCI	2014
Travel Grant, Associated Graduate Students, UCI	2014
Travel Award, Graduate Division, UCI	2014
Travel Award, School of Medicine, UCI	2014
F1000 recommended article	2012

Laboratory Skills

patch-clamp electrophysiology (whole cell patch on stable mammalian cells and primary neurons, perforated patch on primary neurons), live cell imaging FRET/TIRF, fluorescent microscopy, immunofluorescent imaging, immunohistochemistry, co-immunoprecipitation, Western blot, protein purification, biochemical assay development, binding assays, biotinylation, cell culture, primary neuronal culture preparation and maintenance, DNA/RNA isolation and purification, PCR, cloning, primer design, plasmid design and preparation, mutagenesis, gene expression and silencing, transfection, in vivo murine experimentation, intracardiac perfusion

Software

Adobe (Photoshop, Acrobat), ImageJ, pCLAMP 10 (Clampex, Clampfit), GraphPad (Prism), MetaMorph, EndNote, Microsoft Office (PowerPoint, Word, Excel), CLC Main Workbench

Leadership Experience

Student Representative, Department of Pharmacology, UCI	Since 2014
Appointed voting member, Student Fees Advisory Committee, UCI	2013 - 2014
Arts Education Outreach Director, Do Art Foundation, Los Angeles	Since 2013
Undergraduate student mentor (5 students), UCI	Since 2012
Student mentor, Neuroimaging Laboratory of Aging, UCLA	Summer 2010
Appointed Assistant Project Director for reorganization of Student Research Program, Undergraduate Students Association Council, UCLA	2007-2008

Professional Affiliations

Society for Neuroscience, student member	Since 2012

Language

English: fluent
Russian: fluent (native)

ABSTRACT OF THE DISSERTATION

KCNQ2 Channels: Dynamic Molecular Interactions and
Functional Role in Learning and Memory

By

Anastasia Kosenko

Doctor of Philosophy in Pharmacology and Toxicology

University of California, Irvine, 2015

Professor Naoto Hoshi, Chair

Voltage-gated ion channels encoded by the members of KCNQ gene family (KCNQ2–5) conduct the M-type potassium current. Several neurotransmitters and signaling events have been shown to regulate the activity of the M-channel, including Ca^{2+} and muscarinic receptor-mediated suppression. We found that a change in the configuration of the KCNQ2 channel complex triggered by elevated intracellular Ca^{2+} lowers channel sensitivity to an essential co-factor, phosphatidylinositol 4,5-bisphosphate, which shuts down the channel. We also identified that a classical mechanism of M-current regulation mediated by muscarinic receptor activation requires KCNQ2 phosphorylation by PKC and dissociation of calmodulin, an auxiliary subunit of KCNQ2 channel complex. Based on these findings, we generated a knock-in mouse line that carries an alanine mutation at the key phosphorylation site of KCNQ2, KCNQ2(S559A). These mice show attenuated response to muscarinic-mediated M-current suppression, which enables us to address the role of physiological M-current suppression *in vivo*. Functionally, the M-current is one of the key modulators of synaptic plasticity with a proposed role in learning and memory.

Thus, we aimed to identify the effects of M-current inhibition on memory processing. To discriminate between the memory processes mediated by different brain regions, we conducted perirhinal cortex-dependent and hippocampus-dependent memory tasks. KCNQ2(S559A) mice showed normal spatial memory as evidenced by successful performance with a 24 h retention interval. However, we observed a significant long-term recognition memory impairment in KCNQ2(S559A) mice with a 24 h retention interval. Inhibition of the M-current with XE991 during memory consolidation phase rescued memory deficit in KCNQ2(S559A) mice. Our mutant mice also showed deficits in long-term social odor memory, while maintaining normal olfactory responses, further implicating the M-current in memory processes mediated by perirhinal cortex. Finally, our behavioral findings were mirrored by a lower level of neuronal activation in perirhinal cortex of KCNQ2(S559A) mice compared to the wild-type during memory consolidation, as measured by c-fos expression 2 h after novel object recognition training. Our findings provide evidence for the proposed importance of M-current suppression during memory processing and offer a novel perspective on its role in recognition memory consolidation.

Chapter One

KCNQ potassium channels

The KCNQ family – introduction

The KCNQ gene family encodes a subclass of Kv α subunits that form voltage-gated potassium channels by homo- or hetero-tetramerization. These subunits consist of six transmembrane domains (TMD), a single pore loop (P-loop) and the voltage-sensing domain. This modular structure is the standard for all voltage-gated potassium channels. The S4 transmembrane domain serves as a voltage sensor[1], while the P-loop makes up the extracellular part of the channel pore, which contains the signature sequence TxxTxGYG and forms a selectivity filter for K^+ ions (Figure 1.1). All KCNQ channel subtypes conduct outwardly rectifying voltage-dependent K^+ currents that activate at voltage potentials positive to -60 mV and exhibit slow activation and deactivation kinetics in the range of 100-600 ms, with little or no inactivation[2]. It is important to note that KCNQ channels are activated at more negative voltages than other voltage-gated potassium channels, and recent evidence suggests KCNQ channels can be open at the resting membrane potential.

There are five known subtypes in the KCNQ gene family (KCNQ 1-5). The subunits share between 30 and 65% of amino acid sequence homology, which is particularly high in the TMD regions[3,4] as well as the channel assembly domain, "A-domain", within the intracellular C-terminal tail [3,5]. The length of the C-terminus varies considerably among the subtypes, which may explain differences in channel regulation, while the N-terminus is similar in size and is

around 100 amino acids. A uniformly spaced distribution of positively charged amino acids is observed in the S4 TMD region, suggesting its role in voltage sensing. Six positively charged amino acid residues are located in the S4 region of KCNQ 2-5 proteins but only four are found in KCNQ1.

KCNQ1 subunits, well known for their role in cardiac function, have been shown to form functional heteromeric channels with β subunits encoded by the KCNE gene family[2]. The electrophysiological effects of such co-assembly vary and depend on the identity of the KCNE subunit. On the other hand, KCNQ1 subunits do not co-assemble with other members of the KCNQ family[3,4,6–8]. KCNQ1 mRNA expression has been found in many tissue types including crypt cells of the colon, kidney, lung, placenta, pancreas, and, most recently, the brain[9–11]. KCNQ1 and KCNE1 mRNA co-expression pattern includes cardiac tissue, where these KCNE1 containing channels conduct a slow delayed rectifier current, the I_{Ks} current, which plays an important role in the repolarization of cardiac action potentials[12,13]. Similarly to its functional expression in the heart, KCNQ1 channels have been shown to co-assemble with KCNE1 in the inner ear to form functional tonically active channels[14]. Mutations in both KCNQ1 and KCNE1 can, therefore, lead to hearing loss and vestibular imbalance. KCNQ1 co-assembly with KCNE2 is also observed in multiple tissues, and contributes to constitutive activation of the channels at hyperpolarized potentials in the heart as well as a variety of epithelial cell types including gastric, thyroid, and choroid plexus epithelia[11]. KCNQ1 heteromerization with KCNE3 in the colonic crypt cells is thought to conduct a K^+ current important for the intestinal Cl^- homeostasis implicated in conditions such as cystic fibrosis and cholera[2]. Evidently, the co-assembly with the members of the KCNE family, as well as its functionality, varies depending on the KCNE subtype and correlates with the expression patterns of KCNE subunits. Importantly, mutations in

the KCNQ1 channel have been linked to the most common form of long QT syndrome, LQT1, which is a potentially fatal inherited cardiac arrhythmia accounting for over 50% of LQT incidences. At least 35 different LQT related mutations have been identified in KCNQ1 to date[2].

KCNQ2 subunits are predominantly expressed in neurons. This channel subunit is of particular interest to the work reported here and is its primary focus. KCNQ2 and KCNQ3 subunits are the main molecular constituents of a slow voltage-gated channel known as the M-channel[15], although native homomeric KCNQ2 channels conducting the M-current have also been reported[16,17]. Other KCNQ subtypes may co-assemble with KCNQ2 to conduct M-like currents as well[18]. There are several known splice variants of the C-terminus of KCNQ2, although it is unclear how they are functionally different. In a heterologous expression system using *Xenopus* oocytes, injection of KCNQ2 mRNA results in expression of a slowly activating and deactivating K^+ current, whose properties are practically identical to those describing the M-channel, while injection of KCNQ3 alone does not result in the expression of a current[15]. Interestingly, a co-injection of KCNQ2 and KCNQ3 mRNA results in a current that is 11-fold larger than that of KCNQ2 alone, suggesting that KCNQ3 facilitates functional expression of KCNQ2 channels by forming heteromeric channels.

The M-channel was initially described in the bullfrog sympathetic ganglia as a K^+ conducting channel with slow depolarization-induced activation, slow deactivation, and no inactivation[19]. Soon thereafter the mammalian counterpart of this channel was characterized in the rat superior cervical ganglion (SCG) neurons[20]. However, identification of the genes responsible for the M-current took considerable amount of time, mainly due to the lack of selective pharmacological agents to block the channel. This became possible with the discovery of selective KCNQ blockers, linopirdine[21] and its later analog XE991 (Figure 1.2). Using these

compounds, in combination with characterization of biophysical properties and mRNA expression profiling, KCNQ2 and KCNQ3 subunits were concluded to be the molecular constituents of the M-channel in neurons[15,22]. Recently, KCNQ2 subunit has been identified as the dominant subunit for the expression of the M-current in the pyramidal neurons of the hippocampus[23]. Considering that, as well as the fact that homomeric KCNQ2 channels are able to conduct the M-current, in our studies we frequently use homomeric KCNQ2 channels in heterologous expression systems.

KCNQ4 subunits have been shown to be selectively expressed in the auditory system[8,24]. In heterologous expression systems, homomeric KCNQ4 channels can conduct K^+ current. KCNQ4 subunits do not co-assemble with KCNQ1. On the other hand, an increase in current amplitude by co-expression of KCNQ4 and KCNQ3, as well as its reduction in a dominant negative KCNQ3 mutant, suggests their heteromerization[8]. *In vivo*, KCNQ4 mRNA expression pattern is much more restricted than that of other KCNQ family members. It has a rather distinct distribution localized to the areas of the brain associated with the central auditory pathway such as outer hair cells of the cochlea[8,24]. The kinetics of the dominant K^+ current expressed in the outer hair cells, the $I_{K,n}$ current, are similar to those of the KCNQ4 current. Its developmental expression also overlaps with the expression of KCNQ4. However, KCNQ4 and $I_{K,n}$ currents exhibit differences in their sensitivity to pharmacological inhibition by linopirdine, with $I_{K,n}$ showing higher sensitivity to the drug. This suggests that some other K^+ channels may contribute to $I_{K,n}$ as well. Similarly to the expression of the large voltage-gated K^+ current, $I_{K,L}$, KCNQ4 subunits are only present in the Type I cells in the cochlea[25]. Moreover, $I_{K,L}$ is upregulated during postnatal development in the vestibular apparatus, which correlates with KCNQ4 expression[24]. Notably, the expression pattern of KCNQ4 in the cochlea is different from that of KCNQ1,

which is expressed together with KCNE1 in the marginal cells of the stria viscularis. KCNQ4 expression has also been confirmed in many nuclei and tracts of central auditory pathway in the brainstem[24]. Mutations in the KCNQ4 gene are observed in people affected by nonsyndromic sensorineural deafness type 2 (DFNA2), whose hearing loss progresses throughout life. This suggests that a reduction in functional KCNQ4 currents causes slow degeneration, and that KCNQ4 currents may not be critical for the hearing process *per se*.

Homomeric KCNQ5 channels can also conduct K^+ current but activate very slowly and require several seconds to activate fully upon depolarization. Similarly to KCNQ4, KCNQ5 subunits appear to co-assemble with KCNQ3 but not KCNQ1 or KCNE β subunits[3,4]. Co-expression with KCNQ3 changes the kinetic properties of KCNQ5 current slightly and increases current amplitudes. Currents expressed by homomeric KCNQ5 channels have voltage dependency and inhibitor sensitivity common to the M-current, and can also be suppressed by the activation of muscarinic m1 receptors. The expression pattern of KCNQ5 includes blood vessels, skeletal muscle as well as several brain regions such as cerebral cortex, occipital pole, frontal and temporal lobes, the putamen, and the hippocampus. Unlike other KCNQ subunits, KCNQ5 has not been mapped to a locus associated with a human disease yet. However, it was recently identified as an important modulator of synaptic inhibition in the CA3 area of the hippocampus, contributing to fast hippocampal oscillations and gamma-rhythmic discharge of pyramidal neurons[26].

KCNQ2/3 expression in heterologous systems

KCNQ2 homomeric channels can be successfully expressed as functional channels conducting K^+ current in many cell types including *Xenopus* oocytes, chinese hamster ovary (CHO), human embryonic kidney (HEK), and fibroblast-like COS cells to name a few. On the

other hand, the expression of functional homomeric KCNQ3 channels varies considerably among different groups. In most cases, transiently expressed homomeric KCNQ3 channels conduct very small K^+ currents, if any. In the reported cases of successful expression of functional homomeric KCNQ3 channels, the currents activated at voltages positive to -60 mV, showed sigmoidal activation, and became inwardly rectifying at voltages positive to 0 mV[27,28]. In most transient expression systems, co-expression of KCNQ2 and KCNQ3 leads to a significant increase in current amplitude, which correlates with an increase in the expression of functional channel at the plasma membrane[5].

Modulation of neuronal KCNQ2/3 potassium channels

KCNQ2/3 channels, or M-channels, can be suppressed by a number of metabotropic receptors, and particularly by $G\alpha_q$-protein coupled receptors. In fact, the M-channel received its name after muscarinic receptor stimulation was demonstrated to close the channel. G_q coupled receptor stimulation activates phospholipase-Cβ, which triggers a cascade of signaling events including hydrolysis of membrane-associated phosphatidylinositol-4,5-bisphospate (PIP_2) into inositol-1,4,5-trisphosphate (IP_3) and diacylglycerol (DAG). IP_3 then triggers the release of Ca^{2+} ions from intracellular sources, while DAG activates protein kinase C (PKC) (Figure 1.3). All of these second messengers were eventually identified to contribute to M-channel closure[29,30]. The first important finding in the understanding of M-channel regulation was that, similarly to several other ion channels, the opening of KCNQ2/3 channels requires certain levels of membrane-associated PIP_2. Moreover, a proposed mechanism for M-current suppression, demonstrated by Winks et al.[31], established that PIP_2 depletion, rather than the accumulation of its hydrolysis products, underlies the principle mechanism of M-channel suppression induced by G_q coupled receptor activation. Stimulation of muscarinic or bradykinin receptors leads to substantial PIP_2

depletion (~75% and ~35% respectively) in neuroblastoma cells in a relatively short time range of 30 to 60 s[32,33]. Simultaneous recordings of current and the translocation of PIP_2-binding peptide from the plasma membrane demonstrate that PIP_2 hydrolysis correlates with muscarinic-mediated inhibition of both transiently expressed KCNQ2 channels and native M-channels in SCG neurons[31,34,35].

The second important finding was the activation of PKC. However, PKC-dependent pathway long remained a subject of great controversy, as some phorbol esters (PKC activators) were ineffective in inhibiting the M-channel. This controversy was resolved with the discovery of KCNQ2 protein complexes with A-kinase anchoring protein (AKAP79/150) (79 – human ortholog, 150 – murine ortholog)[36]. AKAP79/150 also binds PKC, and the expression of PKC binding site deficient AKAP79/150 largely attenuates muscarinic receptor-induced M-channel suppression. Furthermore, AKAP79/150 synchronizes the activation of PKC and the inhibition of KCNQ2 currents. The interaction between AKAP79/150 and PKC also explains why some ATP-competitive PKC inhibitors are unable to inhibit KCNQ2 channels, as AKAP79/150 bound PKC becomes inaccessible to these compounds[37]. Additionally, while some ATP-competitive inhibitors target quiescent PKC, others prefer its activated form, which leads to changes in the PKC activation kinetics and stabilizes it in a certain confirmation, resulting in variable effects on KCNQ2 channels[38]. Importantly, Hoshi et al. identified two key PKC phosphorylation sites on KCNQ2 subunit, S534 and S541 (rat), which are required for muscarinic receptor-induced inhibition of the M-channel[36].

The third key finding was the involvement of a Ca^{2+} sensing molecule, calmodulin (CaM). A primary consequence of PLC activation is Ca^{2+} release from intracellular sources. Accordingly, M-channels show great sensitivity to changes in cytosolic Ca^{2+} levels. In fact, Ca^{2+}

levels only fractionally exceeding the resting Ca^{2+} concentration of 70-80 nM can suppress native M-channels in sympathetic neurons with an IC_{50} ~100 nM[30]. CaM plays an important role in Ca^{2+}-mediated M-current suppression and also serves as an auxiliary subunit of KCNQ2/3 channels[39,40]. The requirement for CaM in functional M-channels was investigated by overexpression of the CaM-binding domain of the KCNQ2 subunit, which showed decreased M-current density in rat primary hippocampal neurons[41]. However, the role of CaM in M-current regulation is not limited to calcium sensing. CaM has been shown to control KCNQ2 trafficking, particularly KCNQ2 exit from the endoplasmic reticulum[42,43]. Together, these findings provide evidence for CaM to play a central role in the regulation of the M-channel activity. A substantial portion of this dissertation focuses on the role of CaM in KCNQ2 channel regulation, particularly in the context of its dynamic and activity-dependent association with KCNQ2 subunit.

KCNQ2/3 potassium channel expression in the brain

Tissue distribution and functional expression of KCNQ2/KCNQ3 channels have been studied and described extensively. Although the work reported here is focused primarily on the events associated with KCNQ2 subunit, it is important to recognize that most of the M-channels *in vivo* contain both KCNQ2 and KCNQ3 subunits, and the expression profiles of these two subunits in the central nervous system (CNS) are rather similar. Tinel et al.[44] compared the distribution of KCNQ2 and KCNQ3 mRNA in different human tissues by Northern blot. They found that both genes are expressed almost exclusively in the brain, with some KCNQ2 expression in the testis and KCNQ3 in the spleen. In the mouse brain, KCNQ2 expression is already prominent at post-natal day 3 (P3) and further increased by a factor of 2.5 by P7. This level of expression then remains stable until the adult stage, identified as P90. On the other hand,

very low expression of KCNQ3 is observed at P3, which increases continuously until the adult stage. A two-fold increase in expression is observed from P7 to P30. By P30 the difference in mRNA expression of KCNQ2 and KCNQ3 reaches insignificant level and remains such into the adult stage. Within the mouse brain, KCNQ2 mRNA is highly expressed in several regions including neocortex, the hippocampus, and the granular layer of the cerebellum. *In situ* hybridization signals are also apparent in the olfactory bulb, caudate putamen, lateral septal nucleus, and several thalamic and brainstem nuclei[44]. Additionally, the hybridization signals of KCNQ2 and KCNQ3 in the mouse brain largely overlap. Similar expression pattern of KCNQ2 and KCNQ3 is also observed in the human brain[27]. The sizes of the major transcripts found in human brain are 8.5 kilobases for KCNQ2 and 10.5 kilobases for KCNQ3. Particularly high expression of human KCNQ2 is observed in the hippocampus, cerebral cortex, caudate nucleus, and amygdala. Human KCNQ2 is also moderately expressed in most other regions of the brain including the putamen, temporal lobe, frontal lobe, occipital lobe, and cerebellum, while only barely detectable expression is observed in the medulla and spinal cord[27].

Neuronal localization of KCNQ2/3 potassium channels

Human brain KCNQ protein localization was first analyzed by Western blot. Although now we can successfully solubilize KCNQ2 in Triton X-100, both KCNQ2 and KCNQ3 proteins were initially found in a triton-insoluble subcellular fraction, indicating their interaction with cytoskeleton or membrane associated proteins. Indeed, tubulin and actin were found in the same fraction with KCNQ2 as well as two other proteins implicated in the regulation of KCNQ2 channel, AKAP79 and the RIIB subunit of cyclic-AMP-dependent protein kinase (PKA)[22]. In heterologous expression systems in *Xenopus* oocytes or HEK cells, activation of PKA can enhance KCNQ2/KCNQ3 currents expressed. Accordingly, this effect is eliminated by a

mutation in the single PKA binding consensus site on the N-terminus of KCNQ2 protein[45]. Cooper et al. also identified cellular and subcellular localization of KCNQ2 and KCNQ3 proteins in the human brain by immunohistochemistry on the hippocampal formation and cerebral cortex in paraffin-embedded samples, where immunostaining was detected in the somata and dendrites of polymorphic and pyramidal neurons[22]. Both cell surface and intracellular components appeared to be labeled by punctate somatodendritic staining, and both KCNQ2 and KCNQ3 were detected in most neuronal types with the exception of mossy fiber bundles spanning the dentate hilus. Localization of KCNQ2 and KCNQ3 subunits to somatodendritic membranes of hippocampal pyramidal cells was also confirmed in culture[18].

A later study analyzed subcellular localization of KCNQ2 and KCNQ3 channels in fixed and unfixed sections of sciatic nerves from adult rats[46]. This study showed that localization of KCNQ2 proteins is restricted to regularly spaced ~1μm narrow bands along myelinated axons corresponding to nodes of Ranvier. Moreover, KCNQ2 subunits demonstrate complete co-localization with α subunits of sodium channels, Na_v, and ankyrin-G, both of which are established as nodal markers. Strikingly, double labeling for KCNQ2 and KCNQ3 demonstrates no nodal co-localization. On the other hand, KCNQ3 immunoreactivity detection was reported in the paranodes in co-localization with E-cadherin[46]. While unfixed preparations result in robust staining, fixed sections yield practically no signal. This should be an important consideration for the ongoing and future studies involving immunolabeling of KCNQ2/3 channels. Accordingly, further characterization of neuronal localization of KCNQ2 was performed in the unfixed spinal cord. Similarly to the peripheral nerve staining, spinal cord KCNQ2 immunoreactivity was detected in the nodes and showed no overlap with Kv1.2 staining indicative of juxtaparanodal regions.

An important discovery in the study of the M-channel was the detection of KCNQ2 subunits at the axon initial segments (AIS) (Figure 1.4) throughout the grey matter of the spinal cord. This expression, similarly to the nodal expression in the peripheral nerves, co-localizes with Na_v channels and ankyrin-G. Interestingly, the spinal cord grey matter shows no KCNQ3 immunoreactivity in neuronal cell bodies or the AIS. On the other hand, white matter staining indicates KCNQ3 expression in the astrocytes as well as some nodes[46]. Neuronal localization patterns in the spinal cord were further characterized throughout postnatal development. At P4, 26% of ankyrin-G positive nodal clusters in white matter were reported to have detectable KCNQ2 immunoreactivity, while no KCNQ2 was detected in ankyrin-G positive regions in grey matter at that developmental stage. The number and the density of ankyrin-G positive nodes increase by P8, and KCNQ2 labeling was documented in 68% of these clusters as well as many initial segments. Nodal KCNQ2 expression continues to increase and is estimated at 81% and 91% at P12 and P15 respectively. This expression pattern indicates that temporally KCNQ2 subunits cluster in the nodes and the AIS after ankyrin-G clustering takes place.

In an unfixed mouse brain most of the ankyrin-G positive initial segments in CA1 and CA3 subfields of the hippocampus, and the polymorphic layer of the dentate gyrus, are positive for KCNQ2. Unlike the spinal cord, many of these initial segments are also positive for KCNQ3[46,47]. Particularly strong KCNQ2 labeling is observed in the axons of the mossy fiber layer with a less intense staining in the somatodendritic compartment of pyramidal neurons. Other regions with strong AIS KCNQ2 labeling include the brainstem, striatum, and neocortex. Many initial segments of temporal neocortex and striatum show immunoreactivity for KCNQ3 as well.

In the rat hippocampus, expression of both subunits is enriched in the AIS compared to the distal axons, and cell soma appear to contain intracellularly localized KCNQ2 and KCNQ3 proteins[47]. C-termini of both KCNQ2 and KCNQ3 subunits contain a conserved ankyrin-G binding motif also found in Na_v channels[48–50], which is required for the AIS localization of heteromeric KCNQ2/3 channels. Interestingly, when expressed separately, KCNQ2 and KCNQ3 proteins with mutations in the ankyrin-G binding site show same localization patterns as the wild-type homomeric channels. However, co-expression of the mutated channels abolishes their enrichment at the AIS and results in equal levels of expression in the AIS and the distal axon. Furthermore, targeting of heteromeric channels to the AIS is unaffected by the deletion of the ankyrin-G binding site in KCNQ2 subunit alone, which suggests that wild-type KCNQ3 subunits can maintain AIS localization. Conversely, co-expression of wild-type KCNQ2 and mutated KCNQ3 results in a significant reduction of AIS enrichment, though these channels are still targeted to the AIS[47]. This study confirmed that the AIS localization of KCNQ2/3 heteromeric channels is mediated by the interaction with ankyrin-G through the C-terminus ankyrin-G binding motif.

Physiological roles of neural KCNQ potassium channels

Postsynaptic KCNQ2 channels localize to proximal dendrites and somata, which allows them to regulate neuronal excitability by controlling the spreading of excitatory postsynaptic potentials and preventing the generation of repetitive action potentials. On the other hand, axonal KCNQ2 channels control neuronal excitability and neurotransmitter release. KCNQ2 localization at the AIS enables the channels to regulate neuronal excitability, as the AIS is considered to be the site of synaptic input integration and action potential initiation[47]. Indeed, many Na_v channels required for the initiation of action potentials are localized at the AIS. Thus, KCNQ2/3 channels

clustered at the AIS function as a brake for repetitive action potential firing, and M-channel inhibition converts the neurons from phasically firing to tonically firing, ultimately leading to enhanced neuronal excitability. Due to the lack of inactivation, KCNQ2/3 channels conduct a steady voltage-dependent outward current, which allows for stabilization of the membrane potential in the presence of depolarizing currents[51]. Importantly, CaM binding to native KCNQ2 subunits has been shown to play an important role in membrane excitability in rat primary hippocampal neurons[41].

Functional roles of KCNQ potassium channels

M-channels are implicated in multiple physiological conditions that require changes in neuronal excitability such as learning and memory, pain conductance, and certain types of epilepsy. M-current functions as a band-pass filter and facilitates hippocampal resonance at "exploratory" theta frequencies (2 – 7 Hz) at depolarized potentials[52], which is critical for temporal coding, and plays an important role in learning and memory as well as synaptic plasticity[53–56]. On the other hand, M-channel inhibition enhances spike afterdepolarization and converts single spikes into high-frequency bursts of spikes[57], leading to a temporary release from subcortical tonic inhibition, which allows memory coding. Indeed, selective KCNQ blockers such as linopirdine and XE991 were developed as cognition enhancers and show acute cognition enhancing properties in some animal experiments[21,58,59]. However, conditional deletion of KCNQ2 subunits in the brain leads to an impairment of spatial learning in mice[60]. Evidently, the dynamic regulation of the M-channel contributes to learning and memory processes but the fine-tuned mechanisms, as well as the types and stages of memory process they are involved in, remain to be explored in greater detail. Chapter four of this dissertation will cover the recent progress in that research direction.

KCNQ2 and KCNQ3 genes are associated with a rare autosomal dominant idiopathic epileptic syndrome termed benign familial neonatal convulsions (BFNC). BFNC is characterized by generalized seizures that occur in newborns in the first days of life and typically recede after 3 or 4 weeks. In about 15% of all BFNC cases, however, seizures reoccur later in life and may persist into adulthood. Presumably, some secondary event or presence of other epilepsy susceptibility genes accounts for reoccurring seizures in these individuals. Mapping of BFNC to human loci 20q13.3 and 8q24 corresponds to the localization of KCNQ2 to human chromosome 20q13 and KCNQ3 to 8q24, which defined KCNQ2 and KCNQ3 as attractive candidate genes for this type of epilepsy[61]. To date, many KCNQ2 mutations implicated in BNFC have been identified including frameshift, truncation, missense and splice site mutations as well as mutations in the start codon[62]. Moreover, mutations in the C-terminus of KCNQ2 appear to account for more than a half of all identified mutations associated with BFNC[62]. For instance, a frameshift mutation was found in a large pedigree of BFNC patients from Australia. This mutation causes premature termination of KCNQ2 gene translation resulting in a deletion of the C-terminus[63]. Accordingly, in a heterologous expression system using *Xenopus* oocytes, this mutation abolishes slow outward rectifying K^+ currents observed in wild-type KCNQ2 channels[61]. Heterozygous expression of mutant KCNQ2 in *Xenopus* oocytes does not lead to a dominant negative effect despite the autosomal dominant inheritance of the pathological phenotype, which is likely due to haploinsufficiency[63,64]. In fact, most of the BFNC-associated mutations in KCNQ2 and KCNQ3 genes do not lead to significant dominant negative phenotypes or alter channel gating and ion selectivity[5,45,65]. However, mutations found in the S4 TMD, essential for voltage sensing, do alter the gating properties of the M-channel by slowing down its activation, speeding up deactivation, and reducing voltage sensitivity[64,66,67]. As such, a

mutation that abolishes the third of the six positive charges of the putative voltage sensor, R207W, slows depolarization-induced activation of the channel and shifts its voltage dependence to more positive voltages. This mutation was found in a German family that displayed an unusual hyperexcitability in the neurons of the CNS as well as the periphery. Interestingly, all family members positive for this mutation, including heterozygous mutation careers, were affected by myokymia, and all but one had a history of neonatal convulsions consistent with the symptoms of BFNC[66]. Myokymia is characterized by involuntary, spontaneous, and localized contractions of a few muscles or muscle bundles, and its main symptoms include cramps, stiffness, and muscle twitching. As it is usually the case in myokymia, the muscular hyperexcitability observed in this family was caused by altered excitability of the lower motor neuron and not the muscle *per se*[66]. Thus, R207W mutation presents an intriguing case of a KCNQ2 mutation that is not restricted to the CNS and contributes to chronic pathoexcitability that persists into the adult life. Yet some KCNQ2 mutations reportedly lead to more severe phenotypes including intellectual disability. Medical records show cases of encephalopathy in four families of BFNC patients carrying KCNQ2 mutations[68–70]. In these patients multiple daily treatment-resistant seizures occurred within the first postnatal week and continued throughout the first year of life. In most cases seizures gradually diminished to sporadic tonic or tonic-clonic seizures with the seizure offset at 4 years of life or sooner. Brain MRI displayed most apparent changes during the neonatal period, although in some cases the differences persisted for the first few years of life. Characteristic changes seen in MRI included a relatively small frontal lobe, thinning of the corpus callosum, decreases in myelin and white matter volumes, ventriculomegaly, and hyperintensities in basal ganglia and thalamus[71]. These patients suffered from profound intellectual disability, axial hypotonia as well as spastic quadriplegia, and were largely

nonverbal. As a result, KCNQ2 screening is now recommended to be included in the diagnostic workup of neonatal epileptic encephalopathies.

Of particular interest in the context of this dissertation is a single point missense mutation in KCNQ2 C-terminus, R353G, found in BFNC. Richards et al., who explored the effects of this mutation, concluded that by altering the conformation of KCNQ2 C-terminus, R353G mutation prevents the channel from being able to bind CaM[62]. Accordingly, this amino acid residue is within one of the two previously identified CaM binding domains of the KCNQ2 protein[39,40]. While R353G mutation does not alter membrane targeting of KCNQ2 channels or their co-assembly with KCNQ3, it is presumed to decrease channel opening by abolishing KCNQ2 interaction with CaM. As we continue to explore the molecular pathways of M-channel regulation, a central role for the dynamic activity-dependent changes in KCNQ2-CaM interaction becomes increasingly evident.

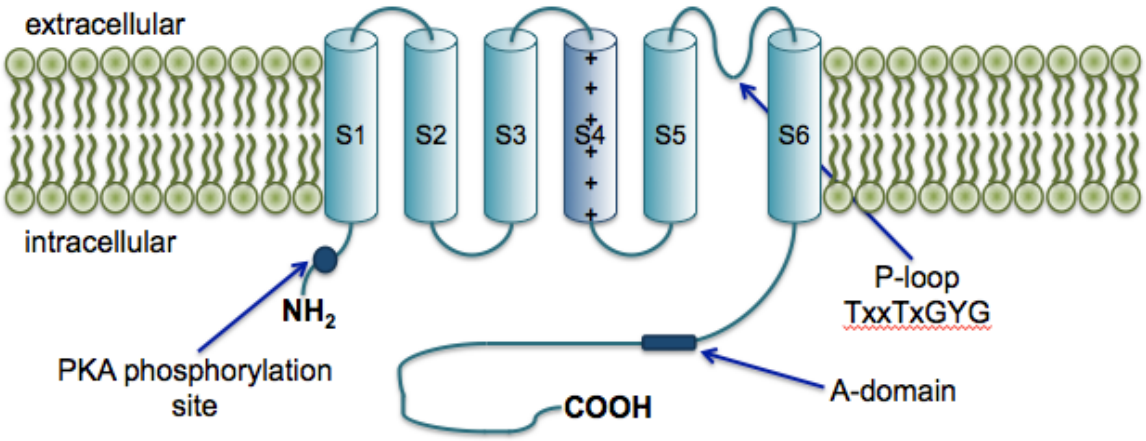

Figure 1.1 Schematic diagram of KCNQ K^+ channel structure.

Channel structure represented here reflects characteristics of KCNQ2 subunit, other KCNQ channels are structurally similar but vary in the length of C-terminus and may not contain PKA phosphorylation site. TMD are indicated as S1 – S6. PKA phosphorylation site, P-loop containing signature sequence for potassium ion selectivity (x = any amino acid), and A-domain are indicated by arrows.

A **B**

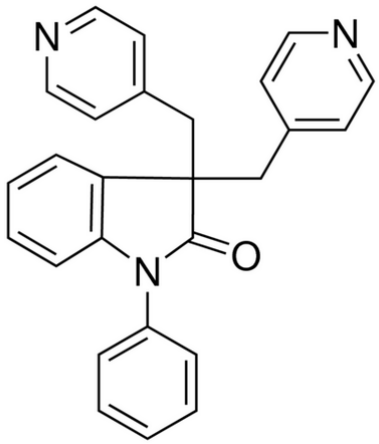

Linopirdine

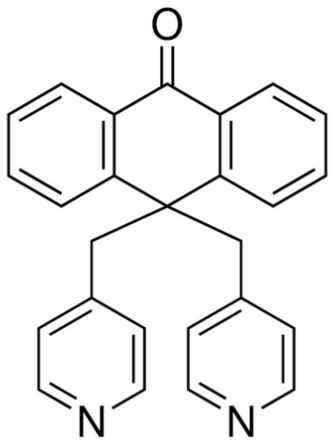

XE991

Figure 1.2 Chemical structures of selective KCNQ blockers.

A, Linopirdine.
B, XE991.

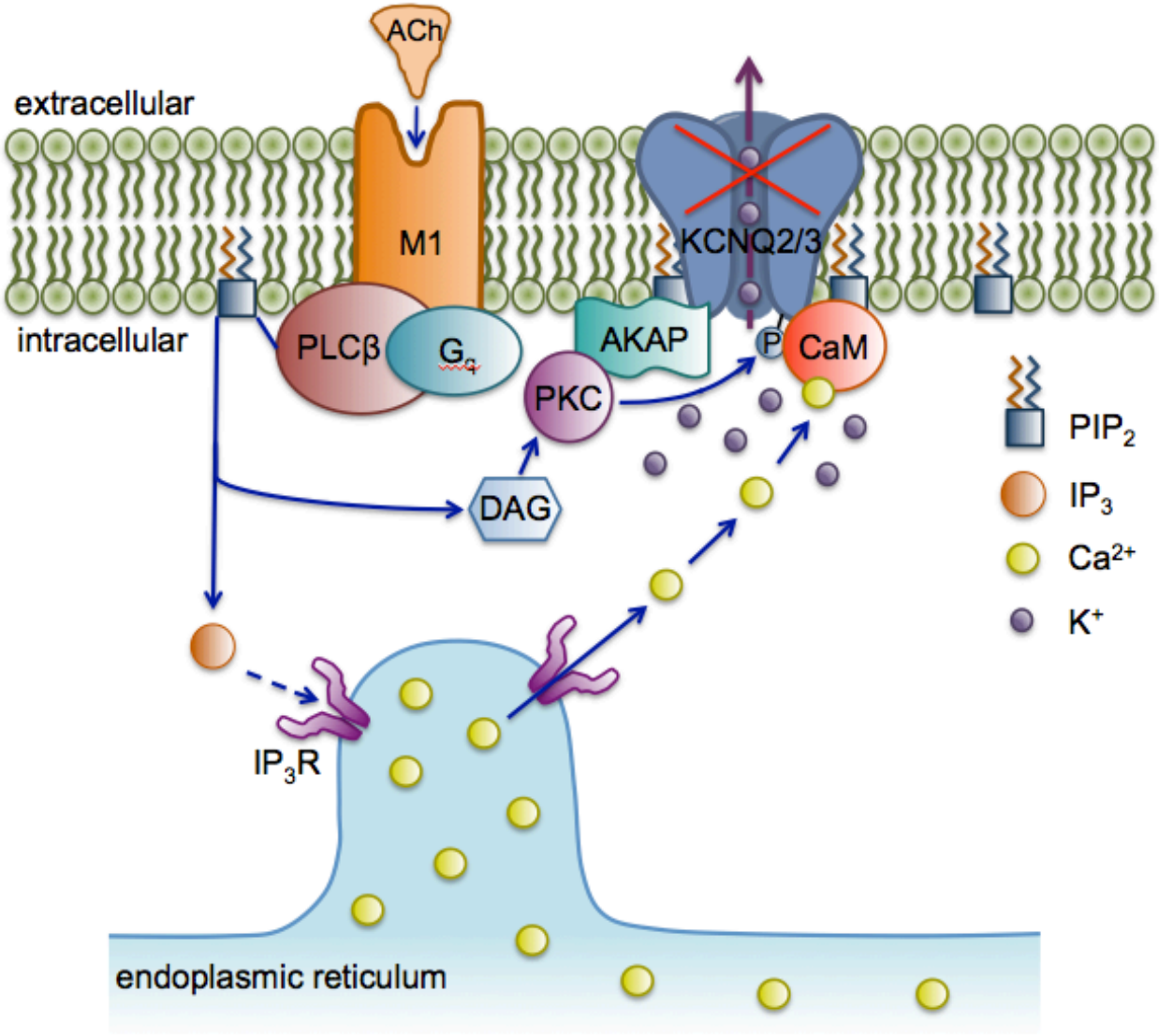

Figure 1.3 Signaling cascade of muscarinic m1 receptor activation.

Stimulation of G_q-protein coupled muscarinic m1 receptor by endogenous agonist acetylcholine (ACh) activates PLCβ, which hydrolyzes PIP_2 into IP_3 and DAG. IP_3 triggers Ca^{2+} release from intracellular stores, while DAG activates PKC, which in turn phosphorylates KCNQ2 subunits. Each of these signaling events contributes to the suppression of the M-channel.

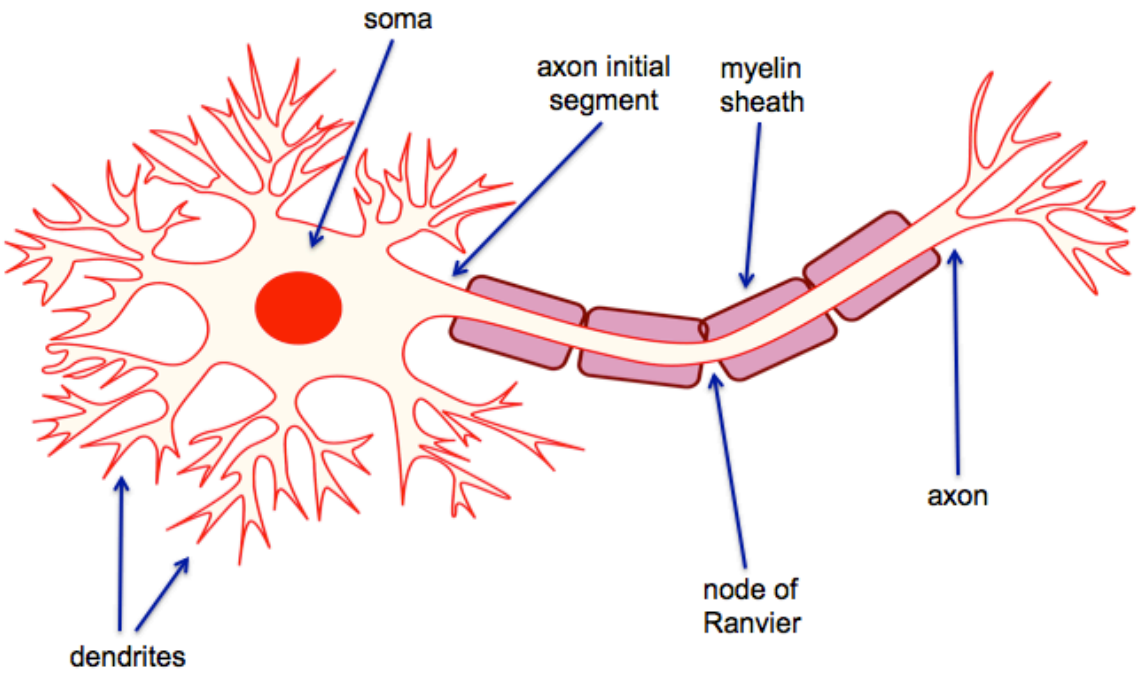

Figure 1.4 Schematic diagram of a myelinated neuron.

Arrows indicate principle cellular compartments including the AIS and nodes of Ranvier, where KCNQ2 subunits are known to cluster.

References

1. Bezanilla, F. The voltage sensor in voltage-dependent ion channels. *Physiol. Rev.* **80,** 555–592 (2000).
2. Robbins, J. KCNQ potassium channels: physiology, pathophysiology, and pharmacology. *Pharmacol. Ther.* **90,** 1–19 (2001).
3. Schroeder, B. C., Hechenberger, M., Weinreich, F., Kubisch, C. & Jentsch, T. J. KCNQ5, a novel potassium channel broadly expressed in brain, mediates M-type currents. *J. Biol. Chem.* **275,** 24089–24095 (2000).
4. Lerche, C., Scherer, C. R., Seebohm, G., Derst, C., Wei, A. D., Busch, A. E. & Steinmeyer, K. Molecular cloning and functional expression of KCNQ5, a potassium channel subunit that may contribute to neuronal M-current diversity. *J. Biol. Chem.* **275,** 22395–22400 (2000).
5. Schwake, M., Pusch, M., Kharkovets, T. & Jentsch, T. J. Surface expression and single channel properties of KCNQ2/KCNQ3, M-type K+ channels involved in epilepsy. *J. Biol. Chem.* **275,** 13343–13348 (2000).
6. Schroeder, B. C., Waldegger, S., Fehr, S., Bleich, M., Warth, R., Greger, R. & Jentsch, T. J. A constitutively open potassium channel formed by KCNQ1 and KCNE3. *Nature* **403,** 196–199 (2000).
7. Schroeder, B. C., Kubisch, C., Stein, V. & Jentsch, T. J. Moderate loss of function of cyclic-AMP-modulated KCNQ2/KCNQ3 K+ channels causes epilepsy. *Nature* **396,** 687–690 (1998).

8. Kubisch, C., Schroeder, B. C., Friedrich, T., Lütjohann, B., El-Amraoui, A., Marlin, S., Petit, C. & Jentsch, T. J. KCNQ4, a novel potassium channel expressed in sensory outer hair cells, is mutated in dominant deafness. *Cell* **96,** 437–446 (1999).

9. Wang, Q., Curran, M. E., Splawski, I., Burn, T. C., Millholland, J. M., VanRaay, T. J., Shen, J., Timothy, K. W., Vincent, G. M., de Jager, T., Schwartz, P. J., Toubin, J. A., Moss, A. J., Atkinson, D. L., Landes, G. M., Connors, T. D. & Keating, M. T. Positional cloning of a novel potassium channel gene: KVLQT1 mutations cause cardiac arrhythmias. *Nat. Genet.* **12,** 17–23 (1996).

10. Yang, W.-P., Levesque, P. C., Little, W. A., Conder, M. L., Shalaby, F. Y. & Blanar, M. A. KvLQT1, a voltage-gated potassium channel responsible for human cardiac arrhythmias. *Proc. Natl. Acad. Sci.* **94,** 4017–4021 (1997).

11. Abbott, G. W. Biology of the KCNQ1 Potassium Channel. *New J. Sci.* **2014,** 1–26 (2014).

12. Barhanin, J., Lesage, F., Guillemare, E., Fink, M., Lazdunski, M. & Romey, G. K(V)LQT1 and lsK (minK) proteins associate to form the I(Ks) cardiac potassium current. *Nature* **384,** 78–80 (1996).

13. Sanguinetti, M. C., Curran, M. E., Zou, A., Shen, J., Spector, P. S., Atkinson, D. L. & Keating, M. T. Coassembly of K(V)LQT1 and minK (IsK) proteins to form cardiac I(Ks) potassium channel. *Nature* **384,** 80–83 (1996).

14. Neyroud, N., Tesson, F., Denjoy, I., Leibovici, M., Donger, C., Barhanin, J., Fauré, S., Gary, F., Coumel, P., Petit, C., Schwartz, K. & Guicheney, P. A novel mutation in the potassium channel gene KVLQT1 causes the Jervell and Lange-Nielsen cardioauditory syndrome. *Nat. Genet.* **15,** 186–189 (1997).

15. Wang, H. S., Pan, Z., Shi, W., Brown, B. S., Wymore, R. S., Cohen, I. S., Dixon, J. E. & McKinnon, D. KCNQ2 and KCNQ3 potassium channel subunits: molecular correlates of the M-channel. *Science* **282,** 1890–1893 (1998).

16. Hadley, J. K., Passmore, G. M., Tatulian, L., Al-Qatari, M., Ye, F., Wickenden, A. D. & Brown, D. a. Stoichiometry of expressed KCNQ2/KCNQ3 potassium channels and subunit composition of native ganglionic M channels deduced from block by tetraethylammonium. *J. Neurosci.* **23,** 5012–5019 (2003).

17. Schwarz, J. R., Glassmeier, G., Cooper, E. C., Kao, T.-C., Nodera, H., Tabuena, D., Kaji, R. & Bostock, H. KCNQ channels mediate IKs, a slow K+ current regulating excitability in the rat node of Ranvier. *J. Physiol.* **573,** 17–34 (2006).

18. Shah, M. M., Mistry, M., Marsh, S. J., Brown, D. a & Delmas, P. Molecular correlates of the M-current in cultured rat hippocampal neurons. *J. Physiol.* **544,** 29–37 (2002).

19. Brown, D. A. & Adams, P. R. Muscarinic suppression of a novel voltage-sensitive K+ current in a vertebrate neurone. *Nature* **283,** 673–676 (1980).

20. Constanti, A. & Brown, D. A. M-Currents in voltage-clamped mammalian sympathetic neurones. *Neurosci. Lett.* **24,** 289–294 (1981).

21. Cook, L., Nickolson, V. J., Steinfels, G. F., Rohrbach, K. W. & DeNoble, V. J. Cognition enhancement by the acetylcholine releaser DuP996. *Drug.Dev.Res.* **19,** 301–314 (1990).

22. Cooper, E. C., Aldape, K. D., Abosch, A., Barbaro, N. M., Berger, M. S., Peacock, W. S., Jan, Y. N. & Jan, L. Y. Colocalization and coassembly of two human brain M-type potassium channel subunits that are mutated in epilepsy. *Proc. Natl. Acad. Sci.* **97,** 4914–4919 (2000).

23. Soh, H., Pant, R., Loturco, J. J. & Tzingounis, A. V. Conditional Deletions of Epilepsy-Associated KCNQ2 and KCNQ3 Channels from Cerebral Cortex Cause Differential Effects on Neuronal Excitability. *J. Neurosci.* **34,** 5311–21 (2014).

24. Kharkovets, T., Hardelin, J. P., Safieddine, S., Schweizer, M., El-Amraoui, a, Petit, C. & Jentsch, T. J. KCNQ4, a K+ channel mutated in a form of dominant deafness, is expressed in the inner ear and the central auditory pathway. *Proc. Natl. Acad. Sci.* **97,** 4333–4338 (2000).

25. Chen, J. W. & Eatock, R. A. Major potassium conductance in type I hair cells from rat semicircular canals: characterization and modulation by nitric oxide. *J. Neurophysiol.* **84,** 139–151 (2000).

26. Fidzinski, P., Korotkova, T., Heidenreich, M., Maier, N., Schuetze, S., Kobler, O., Zuschratter, W., Schmitz, D., Ponomarenko, A. & Jentsch, T. J. KCNQ5 K+ channels control hippocampal synaptic inhibition and fast network oscillations. *Nat. Commun.* **6,** 6254 (2015).

27. Yang, W. P., Levesque, P. C., Little, W. A., Conder, M. L., Ramakrishnan, P., Neubauer, M. G. & Blanar, M. A. Functional expression of two KvLQT1-related potassium channels responsible for an inherited idiopathic epilepsy. *J. Biol. Chem.* **273,** 19419–19423 (1998).

28. Selyanko, A. A., Hadley, J. K., Wood, I. C., Abogadie, F. C., Jentsch, T. J. & Brown, D. A. Inhibition of KCNQ1-4 potassium channels expressed in mammalian cells via M1 muscarinic acetylcholine receptors. *J. Physiol.* **522 Pt 3,** 349–355 (2000).

29. Marrion, N. V. Control of M-current. *Annu. Rev. Physiol.* **59,** 483–504 (1997).

30. Delmas, P. & Brown, D. A. Pathways modulating neural KCNQ/M (Kv7) potassium channels. *Nat. Rev. Neurosci.* **6,** 850–862 (2005).

31. Winks, J. S., Hughes, S., Filippov, A. K., Tatulian, L., Abogadie, F. C., Brown, D. A. & Marsh, S. J. Relationship between membrane phosphatidylinositol-4,5-bisphosphate and receptor-mediated inhibition of native neuronal M channels. *J. Neurosci.* **25,** 3400–3413 (2005).

32. Willars, G. B., Nahorski, S. R. & Challiss, R. A. J. Differential regulation of muscarinic acetylcholine receptor-sensitive polyphosphoinositide pools and consequences for signaling in human neuroblastoma cells. *J. Biol. Chem.* **273,** 5037–5046 (1998).

33. Xu, C., Watras, J. & Loew, L. M. Kinetic analysis of receptor-activated phosphoinositide turnover. *J. Cell Biol.* **161,** 779–791 (2003).

34. Suh, B.-C., Horowitz, L. F., Hirdes, W., Mackie, K. & Hille, B. Regulation of KCNQ2/KCNQ3 current by G protein cycling: the kinetics of receptor-mediated signaling by Gq. *J. Gen. Physiol.* **123,** 663–683 (2004).

35. Horowitz, L. F., Hirdes, W., Suh, B.-C., Hilgemann, D. W., Mackie, K. & Hille, B. Phospholipase C in living cells: activation, inhibition, Ca2+ requirement, and regulation of M current. *J. Gen. Physiol.* **126,** 243–262 (2005).

36. Hoshi, N., Zhang, J. S., Omaki, M., Takeuchi, T., Yokoyama, S., Wanaverbecq, N., Langeberg, L. K., Yoneda, Y., Scott, J. D., Brown, D. A. & Higashida, H. AKAP150 signaling complex promotes suppression of the M-current by muscarinic agonists. *Nat. Neurosci.* **6,** 564–571 (2003).

37. Hoshi, N., Langeberg, L. K., Gould, C. M., Newton, A. C. & Scott, J. D. Interaction with AKAP79 modifies the cellular pharmacology of PKC. *Mol. Cell* **37,** 541–550 (2010).

38. Smith, I. M. & Hoshi, N. ATP competitive protein kinase C inhibitors demonstrate distinct state-dependent inhibition. *PLoS One* **6,** (2011).

39. Wen, H. & Levitan, I. B. Calmodulin is an auxiliary subunit of KCNQ2/3 potassium channels. *J. Neurosci.* **22,** 7991–8001 (2002).

40. Yus-Nájera, E., Santana-Castro, I. & Villarroel, A. The identification and characterization of a noncontinuous calmodulin-binding site in noninactivating voltage-dependent KCNQ potassium channels. *J. Biol. Chem.* **277,** 28545–28553 (2002).

41. Shahidullah, M., Santarelli, L. C., Wen, H. & Levitan, I. B. Expression of a calmodulin-binding KCNQ2 potassium channel fragment modulates neuronal M-current and membrane excitability. *Proc. Natl. Acad. Sci.* **102,** 16454–16459 (2005).

42. Etxeberria, A., Aivar, P., Rodriguez-Alfaro, J. A., Alaimo, A., Villace, P., Gomez-Posada, J. C., Areso, P. & Villarroel, A. Calmodulin regulates the trafficking of KCNQ2 potassium channels. *FASEB J* **22,** 1135–1143 (2008).

43. Alaimo, A., Gomez-Posada, J. C., Aivar, P., Etxeberria, A., Rodriguez-Alfaro, J. A., Areso, P. & Villarroel, A. Calmodulin activation limits the rate of KCNQ2 K+ channel exit from the endoplasmic reticulum. *J. Biol. Chem.* **284,** 20668–20675 (2009).

44. Tinel, N., Lauritzen, I., Chouabe, C., Lazdunski, M. & Borsotto, M. The KCNQ2 potassium channel: Splice variants, functional and developmental expression. Brain localization and comparison with KCNQ3. *FEBS Lett.* **438,** 171–176 (1998).

45. Schroeder, B. C., Kubisch, C., Stein, V. & Jentsch, T. J. Moderate loss of function of cyclic-AMP-modulated KCNQ2/KCNQ3 K+ channels causes epilepsy. *Nature* **396,** 687–690 (1998).

46. Devaux, J. J., Kleopa, K. A., Cooper, E. C. & Scherer, S. S. KCNQ2 is a nodal K+ channel. *J. Neurosci.* **24,** 1236–1244 (2004).

47. Rasmussen, H. B., Frøkjaer-Jensen, C., Jensen, C. S., Jensen, H. S., Jørgensen, N. K., Misonou, H., Trimmer, J. S., Olesen, S.-P. & Schmitt, N. Requirement of subunit co-assembly and ankyrin-G for M-channel localization at the axon initial segment. *J. Cell Sci.* **120,** 953–963 (2007).

48. Pan, Z., Kao, T., Horvath, Z., Lemos, J., Sul, J. Y., Cranstoun, S. D., Bennett, V., Scherer, S. S. & Cooper, E. C. A common ankyrin-G-based mechanism retains KCNQ and NaV channels at electrically active domains of the axon. *J. Neurosci.* **26,** 2599–2613 (2006).

49. Garrido, J. J., Giraud, P., Carlier, E., Fernandes, F., Moussif, A., Fache, M.-P., Debanne, D. & Dargent, B. A targeting motif involved in sodium channel clustering at the axonal initial segment. *Science* **300,** 2091–2094 (2003).

50. Lemaillet, G., Walker, B. & Lambert, S. Identification of a conserved ankyrin-binding motif in the family of sodium channel ?? subunits. *J. Biol. Chem.* **278,** 27333–27339 (2003).

51. Brown, D. A. & Passmore, G. M. Neural KCNQ (Kv7) channels. *Br. J. Pharmacol.* **156,** 1185–1195 (2009).

52. Hu, H., Vervaeke, K. & Storm, J. F. Two forms of electrical resonance at theta frequencies, generated by M-current, h-current and persistent Na+ current in rat hippocampal pyramidal cells. *J. Physiol.* **545,** 783–805 (2002).

53. Winson, J. Loss of hippocampal theta rhythm results in spatial memory deficit in the rat. *Science* **201,** 160–163 (1978).

54. Huerta, P. T. & Lisman, J. E. Heightened synaptic plasticity of hippocampal CA1 neurons during a cholinergically induced rhythmic state. *Nature* **364,** 723–725 (1993).

55. Wilson, M. A. & McNaughton, B. L. Reactivation of hippocampal ensemble memories during sleep. *Science* **265,** 676–679 (1994).

56. Buzsaki, G. Theta oscillations in the hippocampus. *Neuron* **33,** 325–340 (2002).

57. Yue, C. & Yaari, Y. KCNQ/M channels control spike afterdepolarization and burst generation in hippocampal neurons. *J. Neurosci.* **24,** 4614–4624 (2004).

58. Fontana, D. J., Inouye, G. T. & Johnson, R. M. Linopirdine (DuP 996) improves performance in several tests of learning and memory by modulation of cholinergic neurotransmission. *Pharmacol. Biochem. Behav.* **49,** 1075–1082 (1994).

59. Young, M. B. & Thomas, S. a. M1-Muscarinic Receptors Promote Fear Memory Consolidation via Phospholipase C and the M-Current. *J. Neurosci.* **34,** 1570–1578 (2014).

60. Peters, H. C., Hu, H., Pongs, O., Storm, J. F. & Isbrandt, D. Conditional transgenic suppression of M channels in mouse brain reveals functions in neuronal excitability, resonance and behavior. *Nat. Neurosci.* **8,** 51–60 (2005).

61. Jentsch, T. J., Schroeder, B. C., Kubisch, C., Friedrich, T. & Stein, V. Pathophysiology of KCNQ channels: neonatal epilepsy and progressive deafness. *Epilepsia* **41,** 1068–1069 (2000).

62. Richards, M. C., Heron, S. E., Spendlove, H. E., Scheffer, I. E., Grinton, B., Berkovic, S. F., Mulley, J. C. & Davy, a. Novel mutations in the KCNQ2 gene link epilepsy to a dysfunction of the KCNQ2-calmodulin interaction. *J. Med. Genet.* **41,** e35 (2004).

63. Biervert, C., Schroeder, B. C., Kubisch, C., Berkovic, S. F., Propping, P., Jentsch, T. J. & Steinlein, O. K. A potassium channel mutation in neonatal human epilepsy. *Science* **279,** 403–406 (1998).

64. Rogawski, M. A. KCNQ2/KCNQ3 K+ channels and the molecular pathogenesis of epilepsy: Implications for therapy. *Trends Neurosci.* **23,** 393–398 (2000).

65. Lerche, H., Biervert, C., Alekov, A. K., Schleithoff, L., Lindner, M., Klingler, W., Bretschneider, F., Mitrovic, N., Jurkat-Rott, K., Bode, H., Lehmann-Horn, F. & Steinlein, O. K. A reduced K+ current due to a novel mutation in KCNQ2 causes neonatal convulsions. *Ann. Neurol.* **46,** 305–312 (1999).

66. Dedek, K., Kunath, B., Kananura, C., Reuner, U., Jentsch, T. J. & Steinlein, O. K. Myokymia and neonatal epilepsy caused by a mutation in the voltage sensor of the KCNQ2 K+ channel. *Proc. Natl. Acad. Sci.* **98,** 12272–12277 (2001).

67. Castaldo, P., del Giudice, E. M., Coppola, G., Pascotto, A., Annunziato, L. & Taglialatela, M. Benign familial neonatal convulsions caused by altered gating of KCNQ2/KCNQ3 potassium channels. *J. Neurosci.* **22,** RC199 (2002).

68. Dedek, K., Fusco, L., Teloy, N. & Steinlein, O. K. Neonatal convulsions and epileptic encephalopathy in an Italian family with a missense mutation in the fifth transmembrane region of KCNQ2. *Epilepsy Res.* **54,** 21–27 (2003).

69. Borgatti, R., Zucca, C., Cavallini, A., Ferrario, M., Panzeri, C., Castaldo, P., Soldovieri, M. V, Baschirotto, C., Bresolin, N., Dalla Bernardina, B., Taglialatela, M. & Bassi, M. T. *A novel mutation in KCNQ2 associated with BFNC, drug resistant epilepsy, and mental retardation. Neurology* **63,** 57–65 (2004).

70. Steinlein, O. K., Conrad, C. & Weidner, B. Benign familial neonatal convulsions: Always benign? *Epilepsy Res.* **73,** 245–249 (2007).

71. Weckhuysen, S., Mandelstam, S., Suls, A., Audenaert, D., Deconinck, T., Claes, L. R. F., Deprez, L., Smets, K., Hristova, D., Yordanova, I., Jordanova, A., Ceulemans, B., Jansen,

A., Hasaerts, D., Roelens, F., Lagae, L., Yendle, S., Stanley, T., Heron, S. E., Mulley, J. C., Berkovic, S. F., Scheffer, I. E. & De Jonghe, P. KCNQ2 encephalopathy: Emerging phenotype of a neonatal epileptic encephalopathy. *Ann. Neurol.* **71,** 15–25 (2012).

Chapter Two

Dynamic Activity-Dependent Changes in KCNQ2-Calmodulin Complex

Introduction

The KCNQ2 subunit has been widely used as a prototypical subunit to investigate the regulatory mechanisms of the M-type channel. Accordingly, CaM was initially identified as a co-factor of the KCNQ2 subunit[1,2] and revealed to be a common co-factor for all KCNQ subtypes. In fact, CaM also plays critical roles in KCNQ channel trafficking[3] and channel function[4], and calcium (Ca^{2+}) bound CaM, holoCaM, mediates bradykinin-induced suppression of KCNQ2/3 currents[5]. However, despite the established role of CaM as a Ca^{2+} sensor, the molecular mechanism of KCNQ2 current suppression mediated by holoCaM is not well understood. In contrast to the general consensus regarding the stable association between Ca^{2+} free CaM, apoCaM, and the KCNQ2 subunit, contradicting results have been reported by several groups regarding the association of holoCaM with KCNQ2 and other KCNQ channel subunits[1,2,5–7]. Recently, the crystal structure of holoCaM and the distal CaM binding domain (Helix B) of KCNQ4 was solved[8]. This clearly shows that Ca^{2+}-bound CaM can bind KCNQ channels in certain conditions. Since the dissociation of CaM from the KCNQ2 channel complex leads to reduced M-currents[1,4], the understanding of the stimulus-dependent changes in KCNQ2-CaM interaction is crucial to elucidate the molecular mechanisms of M-channel regulation. Therefore, we sought out to investigate how molecular interactions between KCNQ2 and CaM are altered by increased intracellular Ca^{2+} as well as by muscarinic stimulation.

Another essential co-factor for KCNQ channels is phosphatidylinositol 4,5-bisphosphate (PIP_2)[9,10]. Various ion channels and transporters have been shown to require PIP_2 in order to function properly[11]. Not surprisingly, PIP_2 has been proposed to be a signal mediator in muscarinic suppression of the M-current[12,13], and PIP_2 hydrolysis had long been considered the principal mechanism for the M-current inhibition. We hypothesized that Ca^{2+} increase may induce changes in the channel sensitivity to PIP_2, which would modulate the M-current without altering PIP_2 levels.

We examined Ca^{2+} effects on CaM-KCNQ2 channel interaction and channel activity. We found that holoCaM dissociates from the KCNQ2 channel due to a unique cysteine residue in the KCNQ2 subunit. A scaffold protein AKAP79/150, anchored to KCNQ2[14], selectively binds holoCaM, functioning as an acceptor for CaM dissociated from the KCNQ2 subunit after Ca^{2+} increase. We also found that elevation of intracellular Ca^{2+} reduces KCNQ2 affinity toward PIP_2, as evaluated by a voltage sensitive PIP_2 depleting phosphatase, Ci-VSP[15]. These results suggest that an increase in intracellular Ca^{2+} induces a change in CaM-KCNQ2 configuration, which reduces the channel affinity for PIP_2 and leads to the suppression of the KCNQ2 current.

Additionally, we found that muscarinic suppression of the M-current is facilitated by a cascade of signaling events that involves CaM dissociation from the KCNQ2 subunit. We used engineered KCNQ2 proteins with a single-point mutation at the key PKC phosphorylation site (S541 – rat) that either mimicked a state of constitutive phosphorylation of KCNQ2, S541D, or removed the phosphoacceptor residue, S541A. These experiments showed that PKC phosphorylation of the KCNQ2 subunits induced by muscarinic stimulation leads to the dissociation of CaM from KCNQ2, which suppresses the M-current in a mechanism parallel and complementary to the PIP_2 depletion pathway. Consistently, the currents from KCNQ2 mutants

that mimic constitutive phosphorylation show attenuated responses to both muscarinic stimulation and elevated Ca^{2+}.

Experimental Procedures

Reagents and Expression Plasmids.

Anti-FLAG antibody-conjugated resin and horseradish peroxidase (HRP) conjugated anti-FLAG antibody were purchased from Sigma-Aldrich (St Louis, MO, USA). Anti-AKAP150 antibody was obtained from Dr. John D. Scott (University of Washington). Anti-V5 epitope monoclonal antibody and mammalian expression vectors (pZeoSV, pcDNA3.1, pcDNA3.1/V5) were purchased from Life Technologies (Carlsbad, CA, USA). Mammalian expression constructs for the FLAG-tagged AKAP79, 3xFLAG-tagged rat KCNQ2[14], and V5-tagged CaM[16] have been described. For the AKAP150-HIS6 construct expressed in *E. coli*, the coding sequence of AKAP150 was subcloned into pET-30b expression vector (Merck, Whitehouse Station, NJ, USA). The CFP-PH construct was obtained from Dr. Tobias Meyer (Stanford University) through Addgene. Ci-VSP was obtained from Dr. Yasushi Okamura (Osaka University, Japan). CaM(4DA) mutant (D20A/D56A/D93A/D129A)[5] and KCNQ2(C527R) constructs were generated by QuikChange II XL site-directed mutagenesis (Agilent Technologies, San Diego, CA, USA). All PCR derived constructs were verified by sequencing.

Cell Cultures and Transfections.

Human embryonic kidney (HEK) 293A cells (Life Technologies, Carlsbad, CA, USA) were grown in Dulbecco's modified Eagle medium with 10% fetal bovine serum. CHO cells stably expressing human muscarinic m1 receptor (CHO hm1)[17] were grown in alpha minimum essential medium with 5% fetal bovine serum and 500 μg/ml G418 sulfate. TransIT-LT1 reagent (Mirus Bio, Madison, WI, USA) and expression plasmids were used for transient transfections.

Immunoprecipitation and *In Vitro* Binding Assay.

HEK293A cells were co-transfected with FLAG-tagged KCNQ2 and V5-epitope tagged CaM, and used for immunoprecipitation as described[16]. Briefly, 36 h following transfection, the cells were harvested and lysed in 500 μL HTE buffer containing Ca^{2+} or Ca^{2+} chelating reagents according to the experimental condition (150 mM NaCl, 20 mM HEPES (pH 7.4), 50 mM NaF, 1 mM Na_3VO_4, 1% Triton X-100 and 5 mM EDTA + 5 mM EGTA or 100 μM $CaCl_2$ and complete protease inhibitor cocktail (Roche Applied Science)). After centrifugation at 18,000 x g for 15 min, the supernatants were further precleared by incubation with protein G resin. KCNQ2-FLAG protein was purified using 10 μL anti-FLAG antibody-conjugated resin. Following incubation at 4°C, the immunoprecipitates were washed with 750 μL of corresponding HTE buffer. Protein binding was analyzed by SDS–PAGE and immunoblotting with HRP-conjugated anti-FLAG and anti-V5 antibodies. For the AKAP150 *in vitro* binding assay, AKAP150-His6 protein was purified from *E. coli* BL21 (DE3) using Ni-NTA resin. Protein purification was confirmed by Coomassie staining. 1 μg AKAP150-His6 protein was added to the HEK293A cell lysate transiently expressing KCNQ2-FLAG and CaM-V5 immediately after the preclearance step, and followed by the immunoprecipitation procedure described above. KCNQ2 binding proteins were analyzed by immunoblotting with anti-AKAP150 antibody, anti-V5 and anti-FLAG antibodies. Data were quantified with ImageJ software (NIH).

***In-vitro* Phosphorylation and Binding Assay.**

FLAG-tagged KCNQ2 channels were purified from transiently transfected HEK 293A cells by immunoprecipitation combined with high-salt/Ca^{2+} wash. Cells were lysed in a lysis buffer (150 mM NaCl, 5 mM EDTA, 5 mM EGTA, 10 mM HEPES (pH 7.4), 1% CHAPS, and complete protease inhibitor cocktail) and incubated with anti-FLAG-conjugated resin. KCNQ2-

bound resin was washed twice with lysis buffer, twice with 650 mM NaCl, 500 μM $CaCl_2$, 1% CHAPS, and 10mM HEPES (pH 7.4), and twice with 150 mM NaCl, 500 μM $CaCl_2$, 1% CHAPS, and 10mM HEPES (pH 7.4). Ca^{2+} washes reduced KCNQ2-bound CaM to an undetectable level. KCNQ2-resin was then phosphorylated with PKCα in a phosphorylation buffer (150 mM NaCl, 500 μM $CaCl_2$, 100 nM PDBu, 200 μM ATP (7.4 MBq [γ^{32}P]-ATP), 10 mM HEPES (pH 7.4)). After washes with the phosphorylation buffer, purified CaM-V5 was added. CaM-V5 was purified from transiently transfected HEK 293A cells using Ni-NTA resin. CaM-resin was washed with the lysis buffer without EDTA or EGTA, and eluted by lysis buffer with 50 mM NaF, 1mM $NaVO_4$, and 100 nM microcystin.

Surface Labeling.

FLAG-tagged KCNQ2 channels were transiently expressed in CHO hm1 cells. Cells were washed twice with ice-cold phosphate-buffered saline solution (PBS) followed by incubation with sulfo-NHS-LC-biotin for 30 min at 4°C. The treated cells were further washed twice with PBS containing 100 mM glycine. Cells were then lysed in HSE buffer with complete protease inhibitor cocktail. Biotinylated proteins were purified by neutravidin resin and detected by immunoblotting using anti-FLAG antibody.

Electrophysiological Measurements.

Patch-clamp recordings were performed at room temperature on isolated CHO hm1 cells using an Axopatch 200B patch-clamp amplifier (Molecular Devices, Sunnyvale, CA, USA) as described[16]. Series resistance compensation was set to 75-86%. Signals were sampled at 2 kHz, filtered at 1 kHz, and acquired using pCLAMP software (Version 7, Molecular Devices). For Ci-VSP experiments, sampling frequency was 500 Hz. Cells were perfused with a solution

containing 144 mM NaCl, 5 mM KCl, 2 mM $CaCl_2$, 0.5 mM $MgCl_2$, 10 mM glucose and 10 mM HEPES (pH 7.4). Patch pipettes (3 - 4 MΩ) were filled with intracellular solution containing 135 mM potassium aspartate, 2 mM $MgCl_2$, 1 mM EGTA, 0.1 mM $CaCl_2$, 4 mM ATP, 0.1 mM GTP and 10 mM HEPES (pH 7.2). Other EGTA concentrations were used as indicated in experiments shown in Figures 2.4A and 2.7. Cells were held at -70 mV and KCNQ2 channels were activated by two-step test pulses to 0 mV followed by -60 mV, with 500 ms duration for each step. KCNQ2 currents were measured at the end of the 0 mV step. To obtain a voltage-current relationship in Ci-VSP experiments, cells were held at -70 mV and 10 s step depolarizations were applied in 10 mV steps from -10 to +40 mV with 2 min inter-step intervals to allow PIP2 regeneration. To measure Ca^{2+} effect on PIP2 affinity, 1 μM ionomycin was applied one minute following the 10 s step depolarization to +10 mV, and another trace was recorded at +10 mV one minute later. In control experiments, current decay was measured with two 10-s step depolarizations to +10 mV recorded with 2-minute intervals. P-values for statistical analyses were calculated using Prism 6 (GraphPad software, La Jolla, CA, USA) and Excel (Microsoft, Redmond, WA, USA).

Live Cell Imaging.

Transiently transfected CHO hm1 cells were plated onto 18-mm glass coverslips 24 hours after transfection. FRET imaging and TIRF signals were measured as described previously[16,17]. Briefly, images were acquired with an inverted microscope IX-81 (Olympus, Tokyo, Japan) and an ImageEM CCD camera (Hamamatsu Photonics, Shizuoka, Japan), and processed with MetaMorph 7.6.3 (Molecular Devices, Sunnyvale, CA, USA). The excitation light for TIRF experiments, a 445-nm diode laser (Coherent, Santa Clara, CA, USA), and a 515-nm diode-pumped solid-state lazer (Cobolt, Stockholm, Sweden) with an acousto-optical tunable filter

were used with a TIRF module (Olympus, Tokyo, Japan). Dual-emission images were obtained simultaneously through a dual-view module (Photometrics, Tuscon, AZ, USA) with ET535/30m, ET480/40m emission filters and a T505lpxr dichroic mirror (Chroma Technology, Bellows Falls, VT, USA). Exposure time was 100 ms and images were acquired every 10 s. Low light intensity was used to minimize photobleaching. Apparent FRET efficiency was calculated from the three fluorescent channels as described (van Rheenen et al 2004, Saneyoshi et al 2008). Parameters for calculating sensitized FRET were updated every 3 h using CHO hm1 cells expressing either mCitrine or mCerulean alone.

Results

Calcium-mediated regulation of KCNQ2-CaM complex.

Whether Ca^{2+} disturbs the interaction between calmodulin (CaM) and KCNQ channels has been controversial among several labs[1,2,5,8]. To resolve this controversy, we compared KCNQ co-immunoprecipitated CaM from transiently transfected HEK293A cells in Ca^{2+} (+) and Ca^{2+} (–) conditions. In the KCNQ2 channel immunoprecipitates, we detected a reduced amount of CaM in the presence of 100 μM Ca^{2+} (Figure 2.1A). In contrast, immunoprecipitation of homomeric rat KCNQ3 channel protein indicated facilitated CaM binding in the presence of Ca^{2+} (Figure 2.1A). However, the overall signal of CaM that co-precipitated with the FLAG-tagged KCNQ3 channel was weaker than that of the FLAG-tagged KCNQ2 co-precipitate in either Ca^{2+} (+) or Ca^{2+} (–) conditions. When heteromeric KCNQ2/KCNQ3 channels were used for immunoprecipitation, Ca^{2+} reduced CaM co-immunoprecipitation (Figure 2.1A). However, the overall retention of CaM in the presence of Ca^{2+} was higher in heteromeric KCNQ2/KCNQ3 channels compared to homomeric KCNQ2 channels. These results suggest that holoCaM shows distinct binding profiles among KCNQ subtypes.

To further characterize the effect of Ca^{2+} on the interaction between CaM and KCNQ2 channel, we examined the time course of Ca^{2+}-induced dissociation of CaM from KCNQ2 protein (Figure 2.1B). After the KCNQ2-CaM complex was purified by immunoprecipitation in Ca^{2+} (–) condition, dissociation of CaM from KCNQ2 protein was examined by exposing KCNQ2-CaM resin to Ca^{2+} (Figure 2.1B). The observed decrease in CaM co-immunoprecipitation occurred rather slowly, with an estimated time constant of 20.7 $\pm$ 3.5 s (n = 3). This is much slower than the Ca^{2+}-induced conformational change of CaM that has been shown to have micro- to milli-second scale kinetics[18].

Recently, the crystal structure of a protein complex formed by hKCNQ4 and holoCaM has been reported[8]. The solved structure indicates that holoCaM stably binds to Helix B of the channel protein. In contrast, stable association with apoCaM requires two CaM binding sites on the KCNQ2 channel, Helix A and Helix B[1,2]. The reported holoCaM-KCNQ4 channel structure indicates a salt bridge between R538 of hKCNQ4 channel and E88 of CaM, which caught our attention (Figure 2.1C). Interestingly, this arginine residue in the KCNQ4 channel, R538, is conserved in all KCNQ subtypes except KCNQ2. At the corresponding position in rat KCNQ2, the channel contains cysteine, KCNQ2(C527) (Figure 2.1D). Therefore, we suspected that the arginine residue at this position determines the stable binding of holoCaM. To test this idea, we examined CaM binding to the KCNQ2(C527R) mutant channel. CaM was able to bind KCNQ2(C527R) protein in the Ca^{2+} (–) condition (Figure 2.1E). However, in contrast to the wild-type KCNQ2 subunit, addition of 100 μM Ca^{2+} further increased binding of CaM to KCNQ2(C527R) (Figure 2.1E). These results suggest that the conserved arginine residue at this position plays a critical role in holoCaM retention.

KCNQ2 subunit associates with another CaM binding protein as a constituent of the channel complex: AKAP79/150, a scaffold protein critical for KCNQ2 channel regulation[14,19]. It has been demonstrated that AKAP79/150 binds holoCaM but not apoCaM[20,21]. Our immunoprecipitation experiments confirmed that CaM binds to AKAP79 only in the presence of Ca^{2+} (Figure 2.2A). To test the overall effect of the AKAP150/KCNQ2 channel complex on CaM retention, we conducted *in vitro* binding experiments using CaM and KCNQ2 proteins with or without AKAP150 protein (Figure 2.2B). In control experiments in the absence of AKAP150, the binding of holoCaM to KCNQ2 protein was significantly lower than that of apoCaM, as shown in Figures 2.1 & 2.2B. However, when AKAP150 was present, holoCaM was retained in

the KCNQ2 channel complex (Figures 2.2B & 2.2C). In addition, the binding between KCNQ2 and AKAP150 was also augmented in the presence of Ca^{2+}, which may have contributed to an increase in CaM retention (Figure 2.2C). Collectively, our *in vitro* binding and immunoprecipitation data suggest that holoCaM dissociates from the KCNQ2 subunit. However, AKAP150 can stabilize the KCNQ2 channel complex in the presence of Ca^{2+}, as evidenced by strong CaM binding in the immunoprecipitates containing AKAP150. Alternatively, the dissociation of holoCaM from the KCNQ2 subunit can be attenuated by the KCNQ3 subunit.

Our results indicate that KCNQ3 and KCNQ2(C527R) channels show drastic differences in regards to holoCaM binding compared to the wild-type KCNQ2. We next focused on the functional consequences of such a change in holoCaM binding. We selected ionomycin (Figure 2.9A), a Ca^{2+} ionophore, as a means of elevating intracellular Ca^{2+} levels since it would not require the activation of cellular signaling mechanisms to raise Ca^{2+}. However, it has been shown that ionomycin can activate phospholipase C δ (PLCδ)[22,23], which would deplete PIP_2 and suppress KCNQ current. To evaluate ionomycin effects on PLCδ in our experimental conditions, PIP_2 levels in CHO cells were assessed by a PIP_2 probe carrying the PIP_2 binding site of PLCδ and CFP, CFP-PH[9,22,23]. Plasma membrane localization of CFP-PH was monitored by TIRF microscopy. Indeed, 10 μM ionomycin induced PIP_2 depletion as indicated by the translocation of CFP-PH as described[22,23] (Figure 2.3). However, we found that ionomycin concentrations of up to 3 μM did not alter plasma membrane localization of CFP-PH (Figure 2.3). Thus, we examined the functional effect of 1 μM ionomycin on the KCNQ2 current. Application of 1 μM ionomycin induced KCNQ2 current suppression. The level of current suppression was dependent on the concentration of EGTA in the patch pipette solution (Figure 2.4A), confirming that the suppression was due to the rise in intracellular Ca^{2+} levels. In addition, this Ca^{2+}-induced

KCNQ2 current suppression was prevented by co-expression of a dominant negative CaM, CaM(4DA), which contains alanine mutations in all four EF hand motifs, as reported by Gamper et al.[5] (Figure 2.4B). These data indicate that the increase in intracellular Ca^{2+} sensed by CaM is responsible for the KCNQ2 current suppression.

Since holoCaM gradually dissociates from the KCNQ2 channel as shown in Figure 2.1, we questioned whether a KCNQ2 mutant with impaired CaM binding would be more susceptible to ionomycin stimulation. To test this, we examined the KCNQ2(R353G) mutant. This mutation causes impaired CaM binding and is found in epilepsy patients[3,16]. As expected, application of 1 μM ionomycin resulted in augmented and almost complete suppression of the KCNQ2(R353G) current (Figure 2.4C). These results support the hypothesis that changes in Ca^{2+} levels alter KCNQ2-CaM binding, which leads to the suppression of the current.

As we showed in Figure 2.1, the KCNQ3 subunit showed facilitated binding to holoCaM, which suggests a change in the configuration of the protein-protein interaction. Thus, we examined whether the change in CaM binding configuration rather than its dissociation from the channel is sufficient to modulate the current. We measured responses of heteromeric KCNQ2/KCNQ3 and homomeric KCNQ2(C527R) channels to ionomycin treatment. Interestingly, even though the KCNQ2(C527R) mutation resulted in a drastic change in CaM binding, KCNQ2(C527) channels showed normal functional expression at basal conditions (25.4 $\pm$ 4.7 pA/pF at 500 ms, 0 mV, n = 11, $P > 0.05$). In addition, both KCNQ2/3 and KCNQ2(C527R) channels showed equivalent ionomycin-induced suppression compared to the homomeric wild-type KCNQ2 channels (Figures 2.4D, E and F). These results suggest that the Ca^{2+}-induced change in CaM binding configuration is sufficient for the KCNQ2 current suppression.

We then asked how holoCaM suppresses the KCNQ2 current. We suspected that a Ca^{2+}-induced change in CaM binding configuration might lower the PIP_2 affinity of KCNQ channels. To test this, a voltage-sensitive phosphatase, Ci-VSP, which catalyzes PIP_2[15], was co-expressed with the KCNQ2 channel. Activation of Ci-VSP has been demonstrated to deplete PIP_2 and suppress KCNQ2 currents upon depolarization to voltages more positive than 0 mV[24,25]. Since the KCNQ2 current *per se* does not inactivate, we measured the depolarization-induced current decay caused by the Ci-VSP-mediated PIP2 depletion. In the cells co-expressing Ci-VSP and KCNQ2, KCNQ2 currents exerted a current decay during the 10-s depolarization step at voltages more positive than 0 mV (Figure 2.5A). We then compared current decay at +10 mV in the control condition and after 1 μM ionomycin application (Figures 2.5B, C and E). Ionomycin treatment further facilitated Ci-VSP-mediated KCNQ2 current decay (Figure 2.5C), suggesting that after Ca^{2+} exposure, KCNQ2 channels were more susceptible to PIP_2 depletion. Next, we examined the effect of Ci-VSP on the KCNQ2(C527R) channel, in which CaM binding is facilitated by Ca^{2+} (Figure 2.5D). When co-expressed with Ci-VSP, a 10-s depolarization step to +10 mV induced a current decay, which was equivalent to that of the wild-type KCNQ2 channel at basal conditions (Figure 2.5E). The application of ionomycin further facilitated the current decay to an extent comparable to that of the wild-type KCNQ2 current (Figures 2.5D and E). These results suggest that a change in the configuration of CaM–KCNQ2 binding induced by elevated intracellular Ca^{2+} leads to the reduction in PIP_2 affinity of the KCNQ2 channel. Furthermore, this Ci-VSP-mediated current rundown occurred in both wild-type and KCNQ2(C527R) channels despite the observed differences in Ca^{2+} preference of the two constructs for CaM interaction (Figure 2.5E). These results suggest that the change in CaM

binding configuration rather than CaM dissociation from the KCNQ channel is key for this modulation.

Muscarinic-mediated regulation of KCNQ2-CaM complex.

In regards to the changes in KCNQ2-CaM complex by muscarinic stimulation, we observed that the location of the key PKC phosphorylation residue on KCNQ2, S541, coincides with the distal segment of the two CaM binding sites[1]. Thus, we suspected that phosphorylation of KCNQ2(S541) may influence CaM binding. To test this hypothesis, we performed immunoprecipitation of FLAG epitope-tagged wild-type and mutant KCNQ2 from HEK cells co-transfected with V5 epitope-tagged CaM in a Ca^{2+} (–) condition (Figure 2.6A). Immunoblot detection revealed that equivalent amounts of CaM co-precipitated with wild-type and KCNQ2(S541A) proteins (Figure 2.6, lanes 2 and 3). Conversely, a negligible amount of CaM was detected in KCNQ2(S541D) immune complexes (Figure 2.6, lane 4). This suggests that phosphorylation of S541 may interfere with CaM binding. To test this directly, we performed an *in vitro* phosphorylation using purified PKC and KCNQ2 prior to the CaM-binding assay (Figure 2.6B). KCNQ2-FLAG subunits were pulled down using anti-FLAG-conjugated beads and washed at high stringency. These KCNQ2-beads were then either left untreated, phosphorylated by purified PKC, or dephosphorylated by λ protein phosphatase. The incorporation of ^{32}P confirmed phosphorylation of the KCNQ2 protein (Figure 2.6B, middle blot, lane 2). The treated KCNQ2-beads were tested for CaM binding. CaM-V5 was used for this binding assay since it avoided the detection of residual endogenous CaM that could remain during the KCNQ2 purification procedure. The PKC phosphorylated KCNQ2 subunits bound negligible amounts of CaM (Figure 2.6B, lane 3). Thus, PKC phosphorylation disrupts the KCNQ2-CaM interaction.

Next, we examined whether the release of CaM from KCNQ2 subunits can be induced upon muscarinic receptor stimulation. CHO hm1 cells co-expressing KCNQ2-FLAG and CaM-V5 were treated with 3 μM oxo-M for 3 min. The KCNQ2 immune complexes were tested for CaM binding by immunoblot with V5 antibodies. As expected, oxo-M treatment decreased the co-precipitation of CaM (Figure 2.6C).

To further examine whether muscarinic stimulation favors the dissociation of CaM from KCNQ2 channels in living cells, we performed intermolecular fluorescent resonance energy transfer (FRET) analyses (Figure 2.7). The FRET donor was CaM tagged with monomeric cerulean, a brighter version of CFP[26], CaM-CFP. The FRET acceptor was monomeric citrine, a brighter version of YFP[26], fused to KCNQ2, KCNQ2-YFP. Fluorescent signals in the vicinity of the plasma membrane were detected by total internal reflection fluorescence (TIRF) microscopy[27]. These measurements revealed a higher FRET efficiency from the wild-type KCNQ2(wt)-YFP and CaM-CFP pair over the control pair of KCNQ2(wt)-YFP and CFP alone (Figure 2.7A and B). KCNQ2(S541A) and CaM-CFP pair showed equivalent FRET signals to those of the wild-type pair (Figure 2.7A, middle). Importantly, a lower FRET efficiency was measured with the KCNQ2(S541D)-YFP and CaM-CFP pair compared to the wild-type KCNQ2-CaM (Figure 2.7A, right). However, KCNQ2(S541D) mutation weakened but not completely eliminated the KCNQ2-CaM association, since FRET efficiency with the CaM-CFP donor was elevated over that with the CFP donor alone (Figure 2.7A, right).

Application of the muscarinic agonist oxo-M (Figure 2.9B) also lowered the FRET efficiency of the KCNQ2-YFP – CaM-CFP pair (Figures 2.7B – F). Since our co-immunoprecipitation experiments indicated less KCNQ2-CaM binding after oxo-M treatment (Figure 2.6C), we reasoned that the oxo-M-induced decrease in FRET signal was due to the

dissociation of CaM rather than a change in dipole orientation. We next examined PKC involvement in CaM dissociation by abolishing PKC phosphorylation of KCNQ2 either by treating cells with a PKC inhibitor bisindolylmaleimide IV (BIS IV) or by using KCNQ2(S541A). Oxo-M-induced drop in FRET efficiency was attenuated to a similar degree in both KCNQ2(S541A)-YFP – CaM-CFP (Figure 2.7F, green circles) and BIS IV treated KCNQ2(wt)-YFP – CaM-CFP (Figure 2.7F, black circles) compared to the control responses (Figure 2.7F). These results imply that PKC phosphorylation of KCNQ2 induces the dissociation of CaM in living cells.

The analysis of mutant KCNQ2(S541A) and KCNQ2(S541D) currents provided further support for the functional importance of the PKC-dependent KCNQ2 phosphorylation. Cells expressing KCNQ2(S541A) channels showed an increased current density when compared to the wild-type (Figure 2.8A). In contrast, the current density of KCNQ2(S541D) channels was reduced (Figure 2.8A). Since some KCNQ2 mutants undergo abnormal membrane trafficking[3,28], the surface protein amounts of these KCNQ2 mutants were validated by extracellular biotin labeling assays. All three versions of KCNQ2 channels showed equivalent biotinylation when expressed in CHO hm1 cells (Figure 2.8B). Immunoblots of KCNQ2 typically show two bands, a sharp and faint 75 kDa band and a fuzzy 100 kDa band, which would correspond to unglycosylated and glycosylated KCNQ2 proteins respectively. The absence of biotinylation on a cytosolic marker protein, GFP, confirmed specificity of this surface labeling (Figure 2.8B, lower panel). Thus, the difference in current densities of these KCNQ2 mutants in CHO hm1 cells can be attributed to the channel activity rather than the differences in trafficking rates of the mutant channels. The oxo-M responses in these mutant KCNQ2 channels confirmed the postulated functional role of PKC phosphorylation. The KCNQ2(S541A) channels exhibited a

reduced response to oxo-M stimulation (Figure 2.8C), consistent with the removal of a functionally relevant target substrate for PKC. In contrast, recordings from KCNQ2(S541D) mutant channels exhibited a more pronounced suppression compared to the wild-type (Figure 2.8C). These results support the hypothesis that PKC phosphorylation sensitizes muscarinic suppression. Additionally, ionomycin responses were reduced in KCNQ2(S541A) channel compared to the wild-type (Figure 2.8D), which suggests that this residue is important for multiple signaling pathways of M-channel suppression.

Discussion

Here we demonstrate that KCNQ2-CaM binding is an important regulatory mechanism for the M-current. We show that Ca^{2+}-mediated KCNQ2 current suppression involves a change in the molecular interaction of CaM with the KCNQ2 channel complex and the reduction in the affinity of the KCNQ2 channel for PIP_2. We confirm that CaM is the Ca^{2+} sensor for the KCNQ2 channel as previously described[6]. We also demonstrate that a CaM deficient mutant channel, KCNQ2(R353G), shows augmented ionomycin-induced current suppression, which suggests that a change in the KCNQ2-CaM interaction is critical for the suppression. We further show that ionomycin increases the vulnerability of KCNQ2 channels to PIP_2 depletion. Additionally, we show that PKC phosphorylation of KCNQ2 at S541, activated by muscarinic stimulation, causes CaM dissociation from the channel complex in Ca^{2+}-independent manner and also leads to current suppression. The inability to phosphorylate S541, by the means of alanine substitution, retains CaM bound to the channel and attenuates the suppression of KCNQ2 currents in response to muscarinic stimulation. Interestingly, KCNQ2(S541A) mutant channels also show attenuated responses to ionomycin suggesting the importance of this residue in multiple pathways of M-current regulation.

It has been controversial whether holoCaM can bind KCNQ subunits [1,2,5,8]. We determined that C527 of KCNQ2, which corresponds to an arginine residue in other KCNQ subunits, is responsible for the dissociation of holoCaM from KCNQ2. Accordingly, we were able to demonstrate that holoCaM binding is maintained by the KCNQ2(C527R) mutant channels, which mimic KCNQ3 subunit. We also showed that various factors such as the presence of KCNQ3 subunit or AKAP79/150 in the channel complex can alter holoCaM binding. In our experimental conditions, heteromeric KCNQ2/KCNQ3 channels showed reduced CaM

binding in the presence of Ca^{2+}. However, since different stoichiometry of subunit composition could result in inconsistent holoCaM retention, the use of heteromeric KCNQ2/KCNQ3 channels to study CaM interaction may have caused the conflicting results in the past[1,2,29]. Additionally, we observed a consistent difference in the migration of Ca^{2+}-bound and Ca^{2+}-unbound CaM through the SDS-PAGE gel, where the former moved faster than the latter. This difference in gel shift could be due to altered detergent binding induced by the exposure of hydrophobic methyl residues on CaM via Ca^{2+}-mediated conformational change.

We demonstrate that the dissociation of CaM from the KCNQ2 channel induced by PKC phosphorylation of S541 on KCNQ2 results in current suppression. However, our study suggests that not only the dissociation of CaM, but also a change in the configuration of CaM-KCNQ2 binding, can suppress KCNQ2 current. In fact, even though KCNQ2 and KCNQ3 channels showed distinct Ca^{2+}-dependent CaM binding, ionomycin responses of heteromeric KCNQ2/KCNQ3 channels were equivalent to those of homomeric KCNQ2 channel. Similarly, despite the facilitated holoCaM binding by the KCNQ2(C527R) mutant, KCNQ2(C527R) currents showed ionomycin-induced suppression comparable to that of the wild-type KCNQ2 currents. The observation that the KCNQ2(C527R) mutant channel has normal channel function at the basal conditions, while showing distinct holoCaM binding, suggests that the arginine residue in Helix B interacts with holoCaM but not apoCaM, which would support the recent crystal structure[8] as a physiological configuration. In addition, since apoCaM requires both Helix A and Helix B for stable binding, loss of contact with Helix A by holoCaM could be responsible for the reduced KCNQ affinity toward PIP_2.

We demonstrate that ionomycin increased the susceptibility of the channel to PIP_2 depletion induced by Ci-VSP. This suggests that ionomycin reduces the affinity of the KCNQ2

channel for PIP_2. Since the KCNQ2(R353G) channel with impaired CaM binding and low PIP_2 affinity[16] showed a stronger response to ionomycin, it would be reasonable to assume that the KCNQ2-CaM interaction regulates PIP_2 affinity of the KCNQ2 subunit. However, since Ca^{2+} can activate other signaling cascades, we cannot exclude the possibility of other mechanisms contributing to the reduction of KCNQ2 affinity toward PIP_2. For example, phosphorylation of the KCNQ2 subunit in response to Ca^{2+} rise or the overall rearrangement of the protein complex could be responsible for the decrease in PIP_2 affinity. Indeed, a large increase in intracellular Ca^{2+} would activate the PLCδ pathway and further amplify Ca^{2+}-induced KCNQ current responses. In physiological conditions, it is likely that a combination of the PLCδ pathway and the reduction in PIP_2 affinity synergistically suppress the KCNQ2 current, similarly to the muscarinic KCNQ2 current suppression, via PIP_2 depletion and PKC-mediated reduction in PIP_2 affinity[8].

In conclusion, signaling events that can change the configuration of CaM-KCNQ2 binding, such as elevation of intracellular Ca^{2+} or PKC phosphorylation, lower KCNQ2 affinity toward PIP_2. We, therefore, propose that CaM is the molecular switch for controlling PIP_2 affinity of the KCNQ channels.

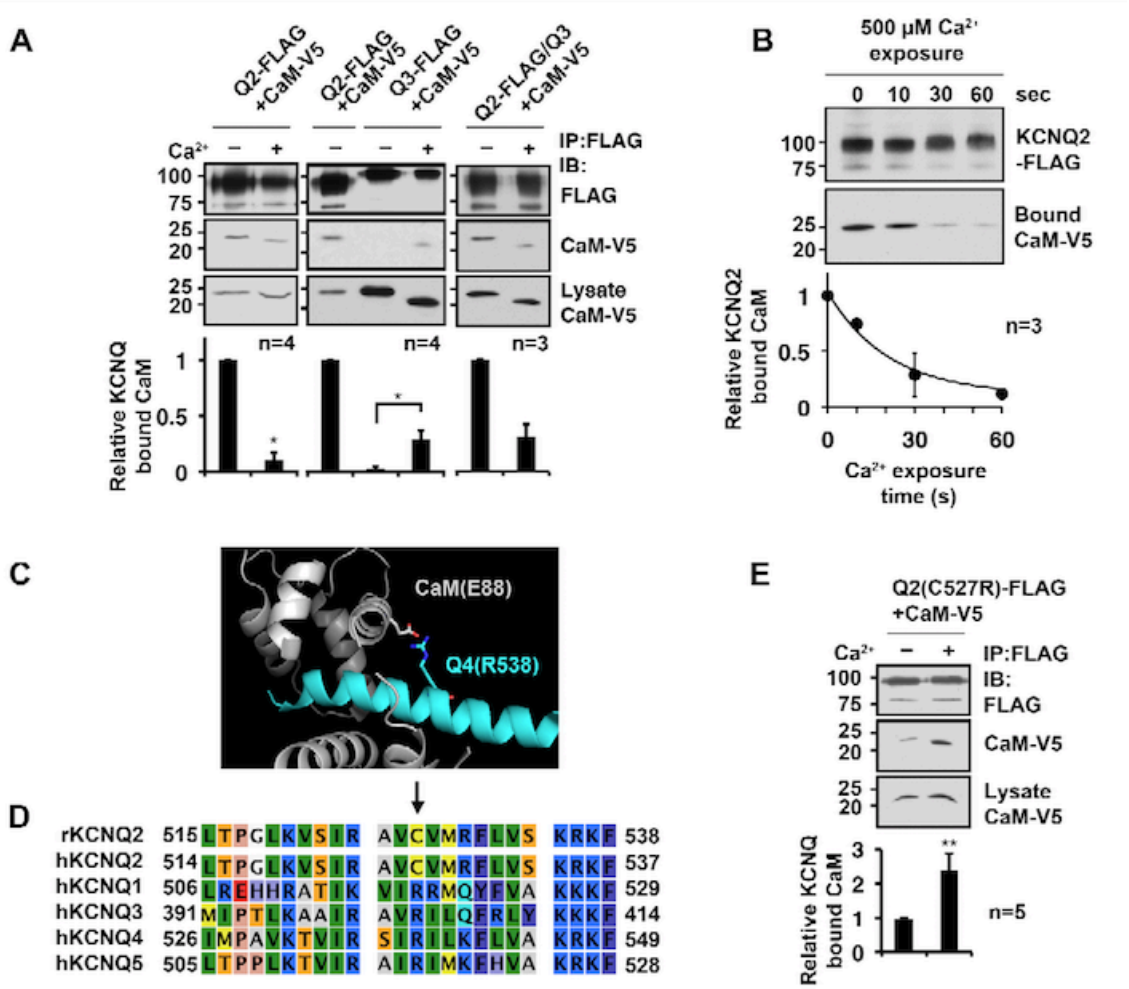

Figure 2.1 KCNQ-CaM interaction requires distinct Ca^{2+} conditions.

A, Distinct Ca^{2+} requirements for CaM binding to KCNQ2, KCNQ3, and KCNQ2/KCNQ3 channels. Representative immunoblots (top) of immunoprecipitation experiments and summary histogram (bottom) are shown. **B,** Time course of CaM dissociation from the KCNQ2 subunit upon exposure to 500 μM Ca^{2+}.
C, Molecular structure from the PDB file (4GOW) depicting the interaction between Ca^{2+}-bound CaM(E88) and KCNQ4(R538).
D, Sequence alignment of Helix B, the distal CaM binding domain, of KCNQ1-5 subunits. Arrow shows the cysteine residue on KCNQ2, rKCNQ2(C527), that corresponds to the conserved arginine residue in other KCNQ subtypes, such as KCNQ4(R538); r – rat, h – human.
E, KCNQ2(C527R) mutation retains CaM binding in the presence of Ca^{2+}.
* < 0.05, ** < 0.01 by Mann-Whitney test. Error bars show S.E.M.

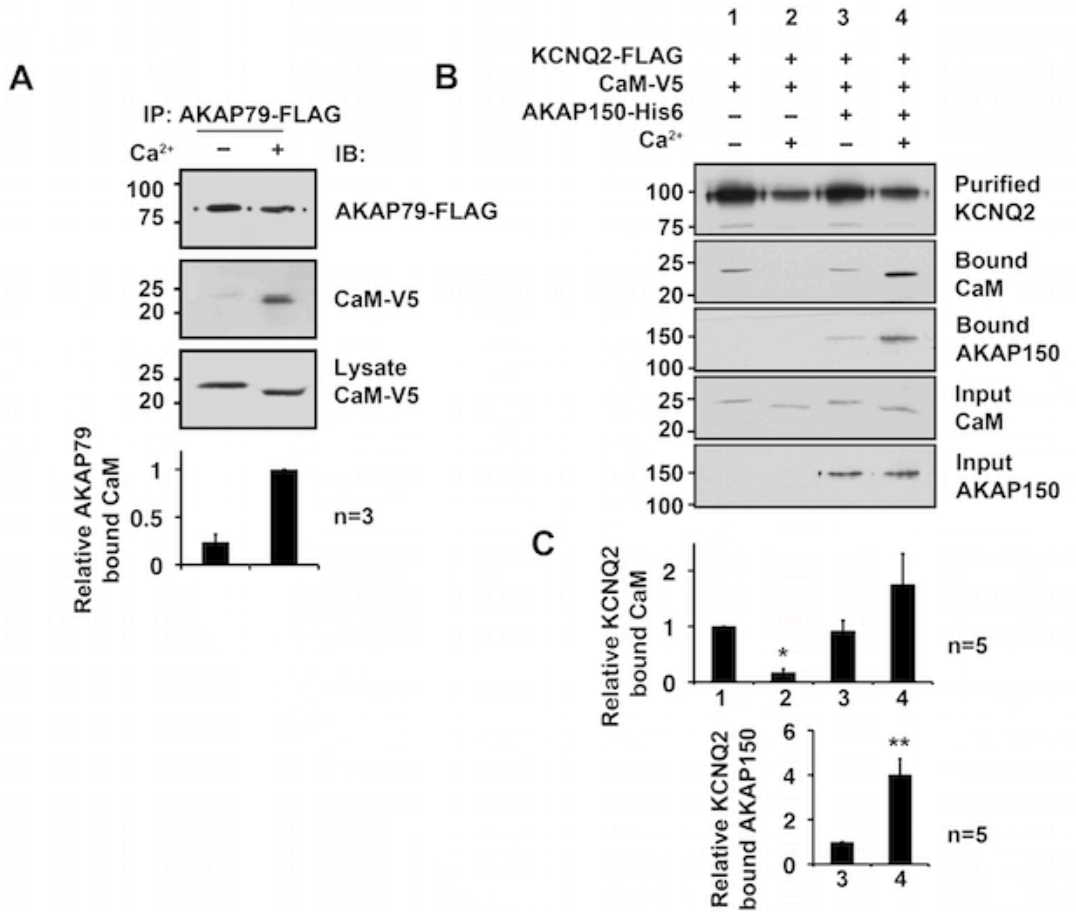

Figure 2.2. KCNQ2 channel complex retains holoCaM via AKAP150.

A, Ca^{2+} (100 μM) dependent binding of CaM to AKAP79.
B, *In vitro* binding of KCNQ2 and CaM with or without AKAP150. KCNQ2-FLAG is immunopurified by anti-FLAG conjugated resin. CaM is co-purified in Ca^{2+} (+) condition only in the presence of AKAP150.
C, Top – the summary of quantification of relative KCNQ2-bound CaM from five independent experiments shown in B**.** Bottom – the summary of quantification of relative KCNQ2-bound AKAP150 from five independent experiments shown in B. Bars are labeled corresponding to the lane numbers on the immunoblot.
*<0.05 non-parametric ANOVA followed by Dunn's multiple comparisons test,
** < 0.01 by Mann-Whitney test. Error bars show S.E.M.

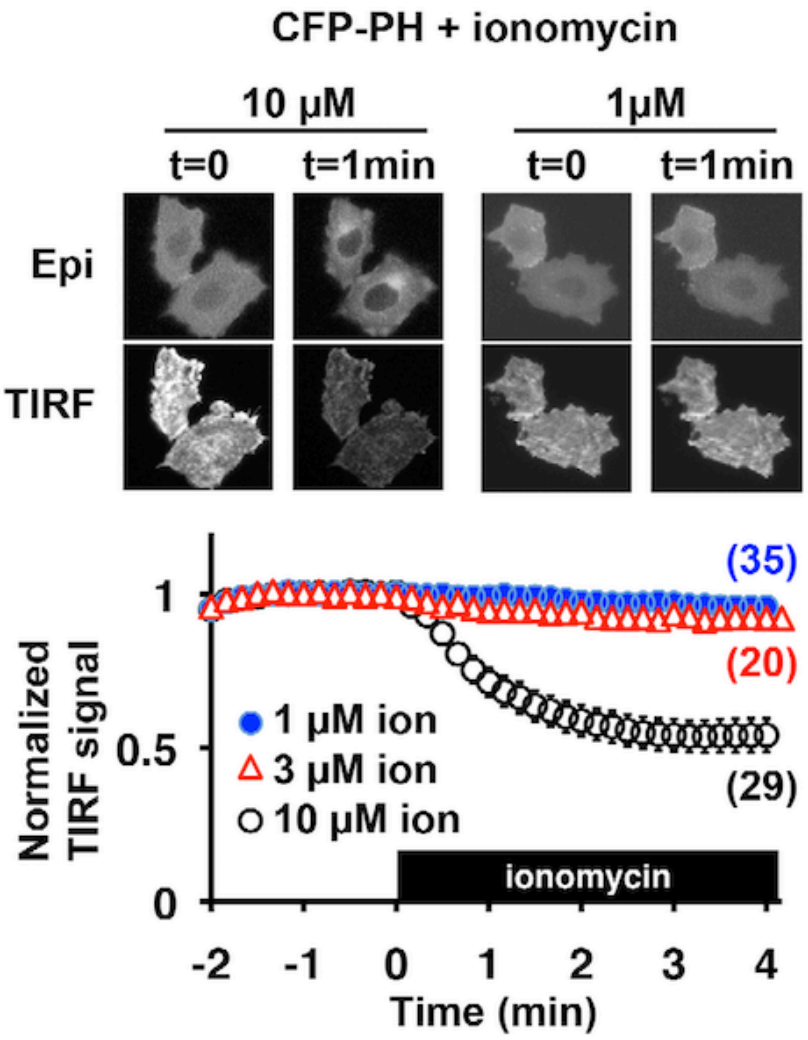

Figure 2.3. Ionomycin treatment and PIP2 depletion.

TIRF analysis indicating membrane localization of the CFP-PH probe. Top panels show epifluorescent cell images (epi) indicating total fluorescence, and TIRF images (TIRF) showing plasma membrane localization. The lower panel shows pooled data from TIRF analyses. 10 µM ionomycin induces translocation of CFP-PH, which indicates depletion of PIP2. In contrast, 1 µM or 3µM ionomycin does not alter plasma membrane localization of CFP-PH. TIRF signal is normalized to that at t = 0. Black box indicates the presence of ionomycin. Error bars show S.E.M.

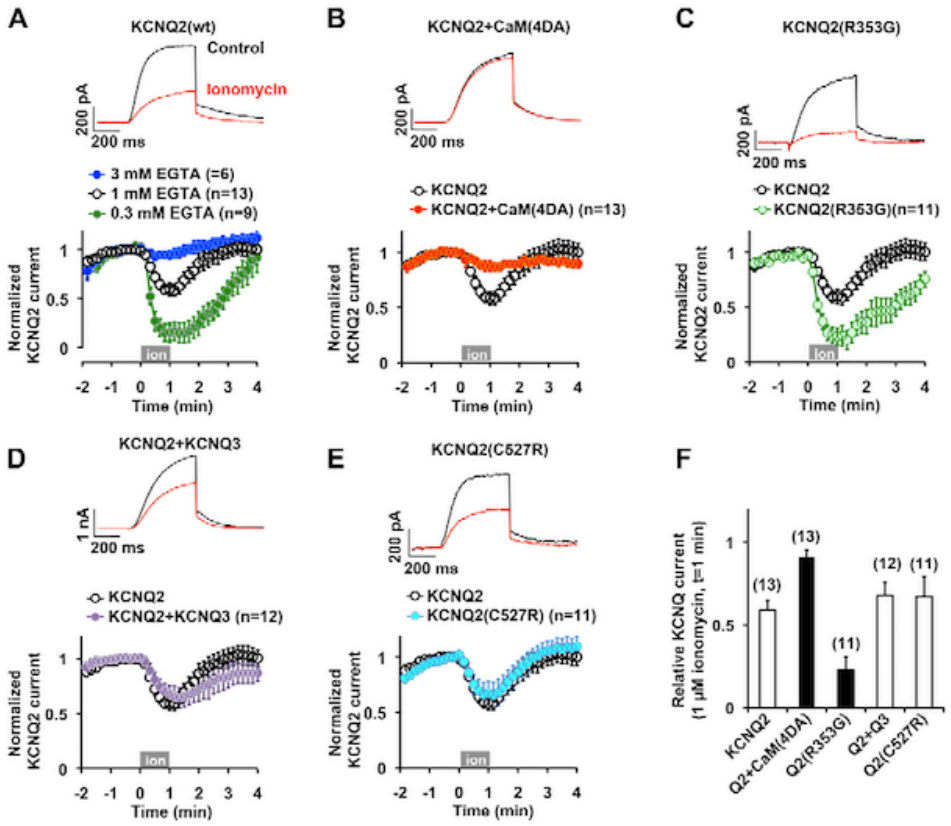

Figure 2.4. Ionomycin suppresses KCNQ currents by elevating intracellular Ca^{2+}.

A, A representative KCNQ2 current response to 1 μM ionomycin with 1 mM EGTA in the pipette solution. The lower panel summarizes ionomycin-induced suppression of the KCNQ2 current, dependent on EGTA concentration in the pipette solution. Gray box indicates the presence of 1 μM ionomycin. 1 mM EGTA was used for the rest of the experiments.
B, Ionomycin-induced KCNQ2 current suppression is prevented by co-expression of a dominant negative CaM, CaM(4DA). Control ionomycin response of KCNQ2 channel from panel A is also shown.
C, Ionomycin induces augmented suppression of the KCNQ2(R353G) current. KCNQ2 response from panel A is also shown.
D, Ionomycin response of the heteromeric KCNQ2/KCNQ3 channels is similar to that of the homomeric KCNQ2 channels.
E, Ionomycin response of the KCNQ2(C527) channel.
F, Summary of ionomycin responses. Relative KCNQ current at t = 1 min is shown. Black bars indicate responses significantly different ($p < 0.01$, nonparametric ANOVA followed by Dunnett's multiple comparisons test) from the wild-type KCNQ2 response. Error bars show S.E.M.

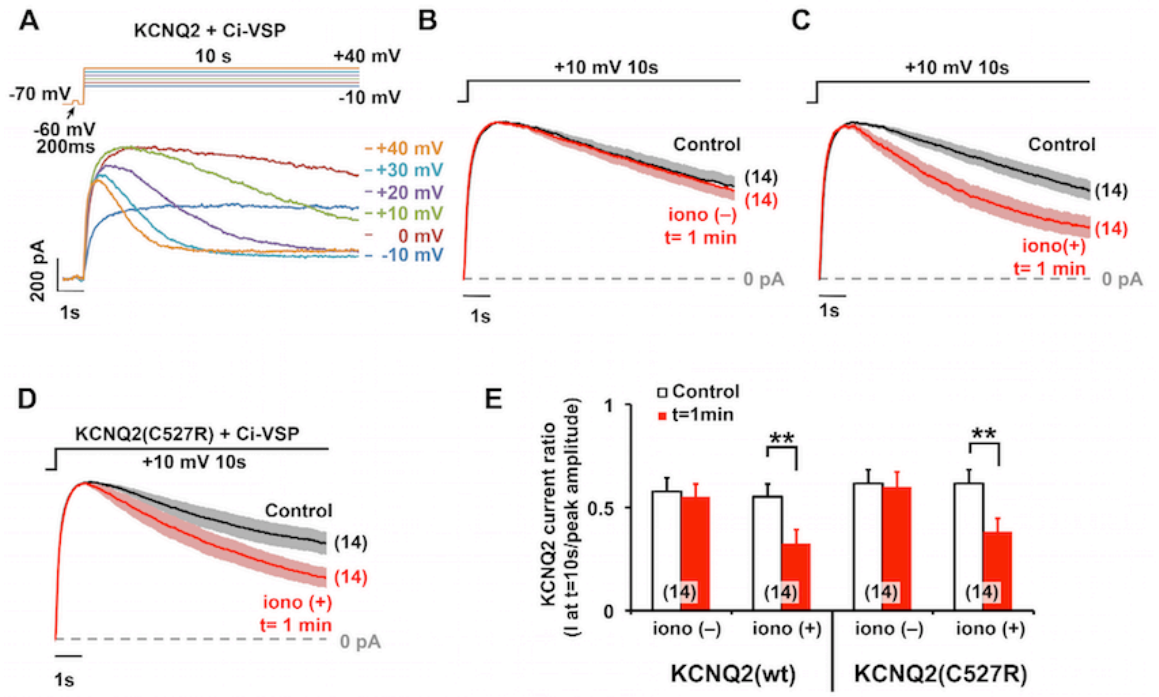

Figure 2.5. Ionomycin-induced suppression of KCNQ2 current is accompanied by a lower PIP2 affinity.

A, Representative current traces showing a voltage dependent KCNQ2 current decay due to the activation of Ci-VSP. A brief voltage step to -60 mV was applied to calculate the linear leak.
B, Scaled KCNQ2 current traces at +10 mV showing an identical Ci-VSP-mediated current decay without ionomycin at 2-min interval. Gray and shaded red areas show S.E.M.
C, Scaled KCNQ2 current traces showing the facilitation of KCNQ2 current decay 1 min after the application of 1 μM ionomycin. Control traces were obtained 1 min before ionomycin application.
D, Ci-VSP-mediated current decay of the KCNQ2(C527R) current. Scaled current traces indicate the facilitation of current decay by 1 μM ionomycin at +10 mV.
E, Summary of the Ci-VSP-induced current decay at control (t = -1 min) and t = 1 min for indicated conditions. KCNQ2(wt) and KCNQ2(C527R) show an equivalent Ci-VSP-mediated current decay both with and without 1μM ionomycin. **<0.01 by paired t-test. Error bars show S.E.M.

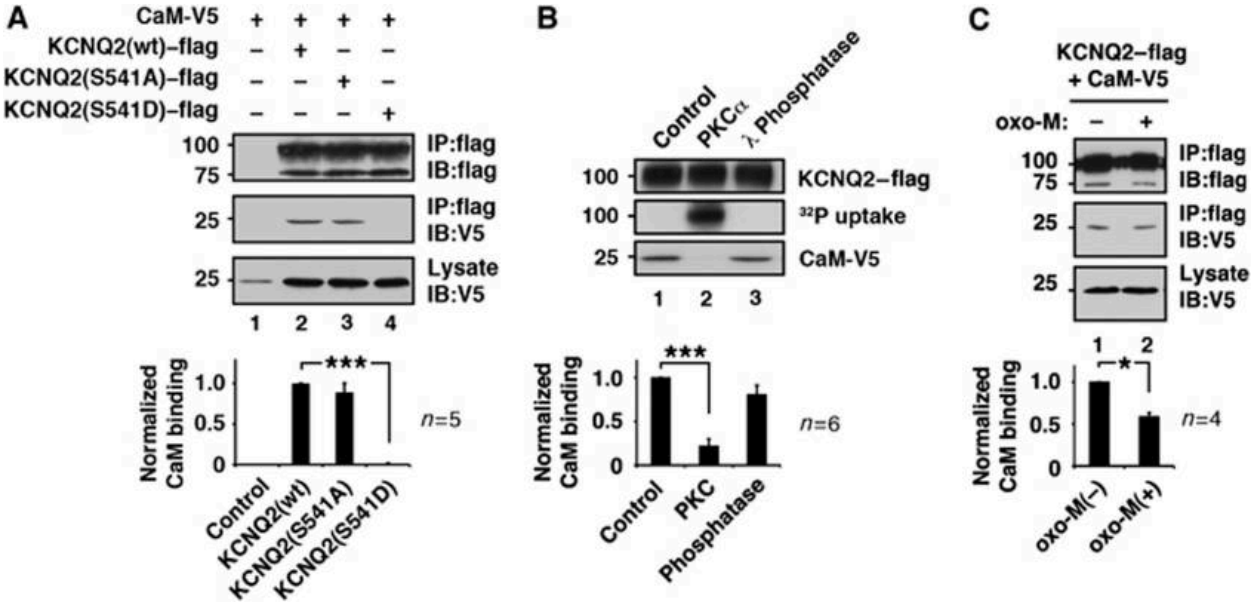

Figure 2.6. PKC phosphorylation interferes with KCNQ2-CaM interaction.

A, CaM binding to KCNQ2 protein and its PKC site mutants.
B, *In vitro* phosphorylation of KCNQ2 protein by purified PKCα and its CaM binding capability. Phosphorylated KCNQ2 protein cannot bind CaM. CaM binding of untreated control and dephosphorylated KCNQ2 are also shown.
C, Oxo-M treatment reduced CaM binding to KCNQ2.
***<0.001 by non-parametric ANOVA followed by Dunn's multiple comparisons test.
*<0.05 by paired t-test. Error bars indicate S.E.M.

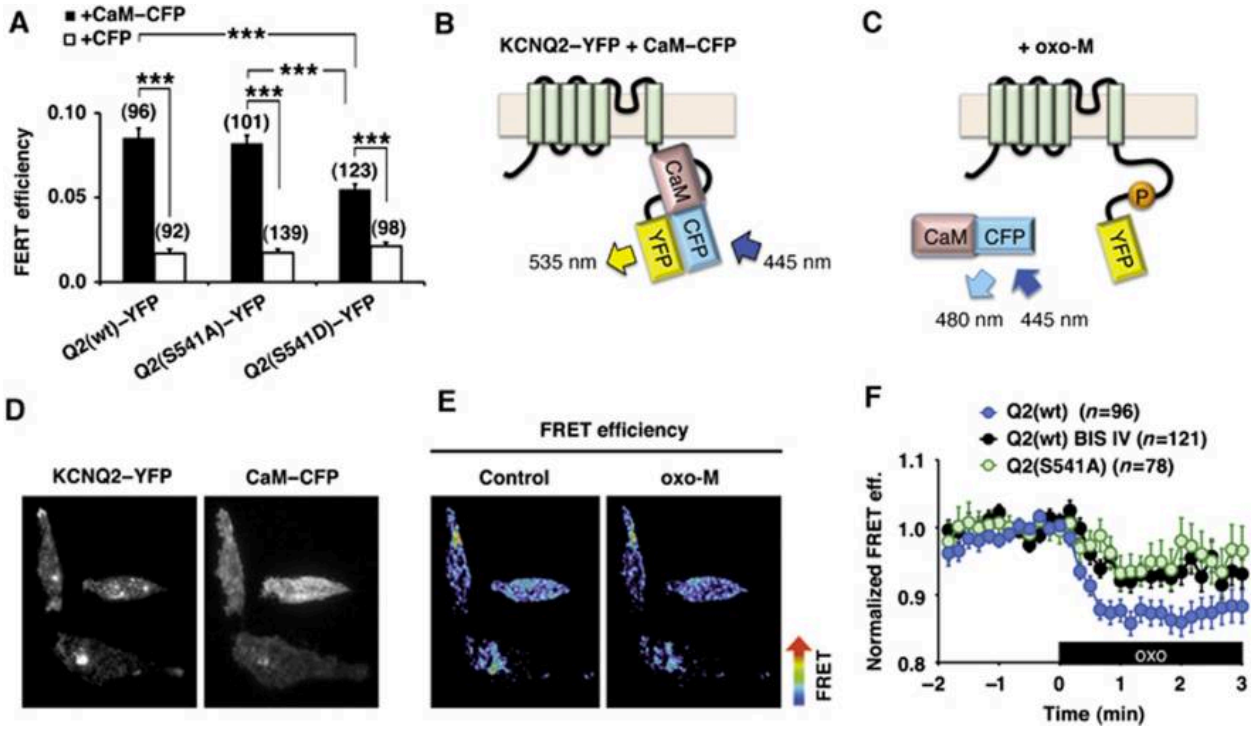

Figure 2.7. Muscarinic stimulation induces dissociation of CaM from KCNQ2 channel complex in living cells.

A, Pooled FRET efficiencies. Increased FRET efficiencies are observed in the wild-type KCNQ2-YFP (Q2(wt) –YFP) and CaM-CFP pair over the control pair, KCNQ2-YFP and CFP alone. KCNQ2(S541A)-YFP (Q2(S541A) –YFP) and CaM-CFP pair show equivalent FRET efficiency to the wild-type pair. KCNQ2(S541D)-YFP (Q2(S541D) – YFP) and CaM-CFP show reduced FRET efficiency compared to the wild-type pair, but significant FRET efficiency over the CFP control. Number of cells observed is reported in parentheses. ***<0.001 by non-parametric ANOVA followed by t-test.
B,C, Schematic representation of KCNQ2-YFP and CaM-CFP interactions in control (**B**) and oxo-M treated (**C**) conditions.
D, Fluorescent images from CHO hm1 cells co-expressing KCNQ2-YFP and CaM-CFP.
E, Pseudocolor images of the cells shown in (D) showing a decrease in FRET efficiency after application of 3μM oxo-M.
F, Changes in FRET efficiency of KCNQ2-YFP and CaM-CFP after 3μM oxo-M application. FRET efficiency of the wild-type KCNQ2-YFP – CaM-CFP (Q2(wt), blue circles) is decreased by stimulation with oxo-M. Pretreatment with BIS IV attenuates oxo-M response (Q2(wt) BIS IV, black circles). KCNQ2 (S541A)-YFP – CaM-CFP pair shows similar attenuated responses (Q2(S541A), green circles). The black box indicates the presence of oxo-M. Error bars indicate S.E.M.

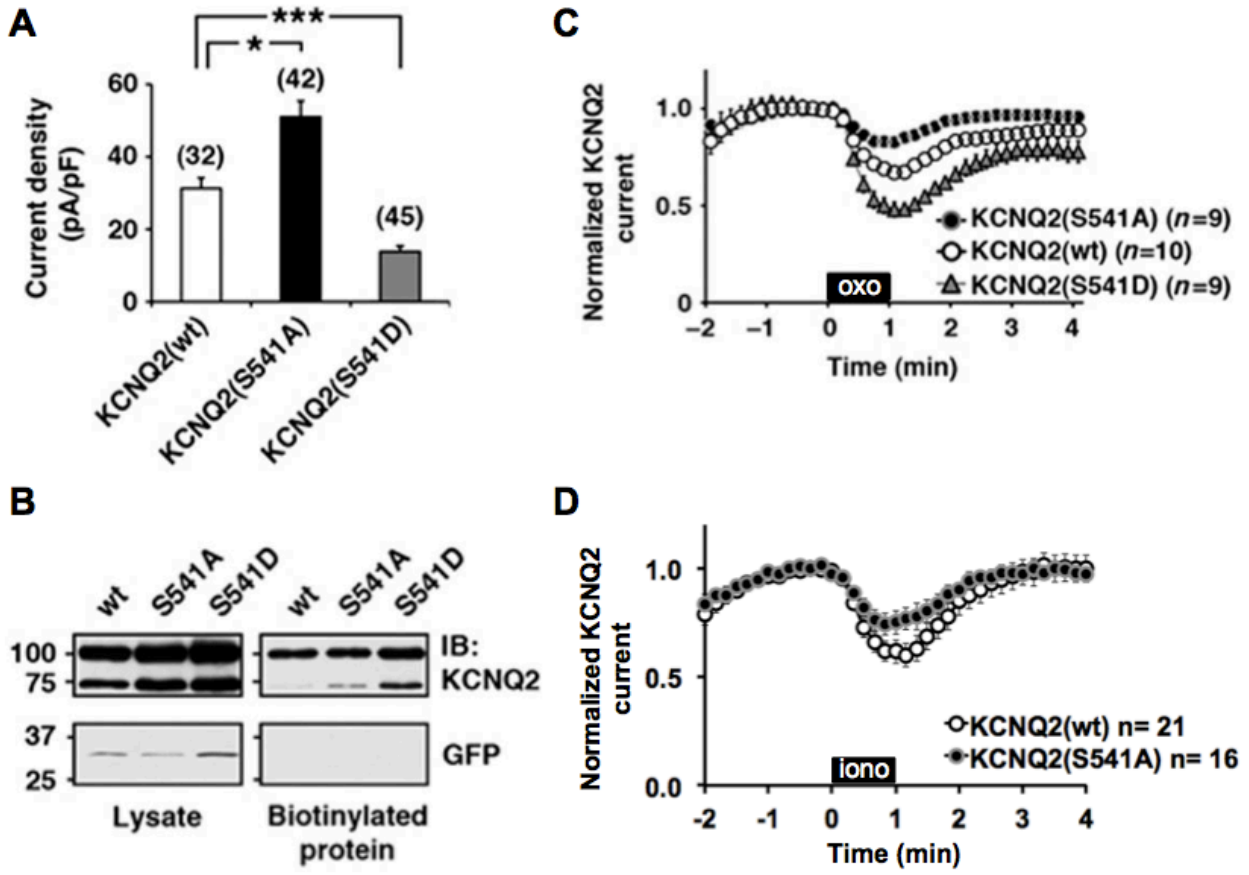

Figure 2.8. Mutations in KCNQ2 (S541) alter responses of KCNQ2 channels to muscarinic receptor activation and intracellular Ca^{2+} elevation.

A, Current densities of wild-type KCNQ2, KCNQ2(S541A), and KCNQ2(S541D). Amplitudes of the KCNQ2 currents are normalized to those at $t = 0$. *<0.05, ***<0.001 calculated by non-parametric ANOVA followed by t-test.
B, Cell surface biotin labeling of wild-type KCNQ2, KCNQ2(S541A), and KCNQ2(S541D) (top panels), and of cytosolic GFP (lower panels). A representative blot from four independent experiments is shown.
C, Pooled data from whole-cell patch-clamp recordings from CHO hm1 cells showing responses of wild-type KCNQ2, KCNQ2(S541A), and KCNQ2(S541D) to 3 μM oxo-M. Amplitudes of the KCNQ2 currents are normalized to those at $t = 0$.
D, Pooled data from whole-cell patch-clamp recordings from CHO hm1 cells showing responses of wild-type KCNQ2 and KCNQ2(S541A) to 1 μM ionomycin. Amplitudes of the KCNQ2 currents are normalized to those at $t = 0$.
Error bars indicate S.E.M.

A **B**

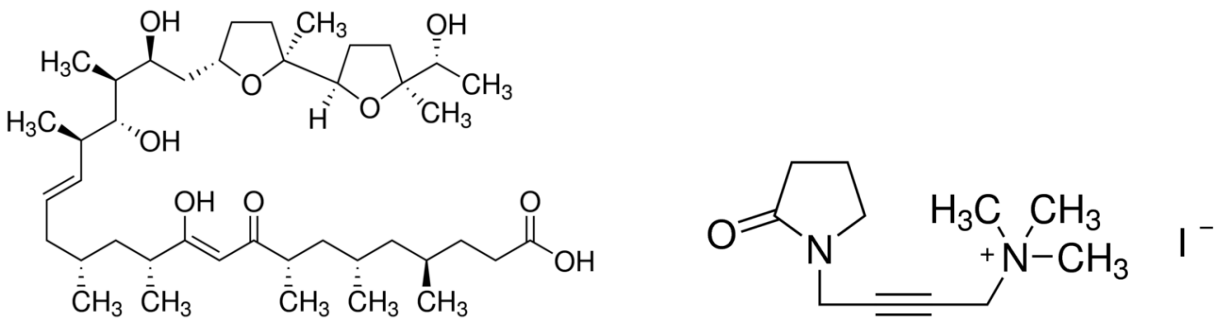

ionomycin oxotremorine M (oxo-M)

Figure 2.9. Chemical structures of compounds used.

A, Ionomycin, Ca2+ ionophore, used to elevate intracellular Ca2+ levels.
B, Oxotremorine M (oxo-M), a muscarinic receptor agonist.

References

1. Yus-Najera, E., Santana-Castro, I. & Villarroel, A. The identification and characterization of a noncontinuous calmodulin-binding site in noninactivating voltage-dependent KCNQ potassium channels. *J. Biol. Chem.* **277,** 28545–28553 (2002).
2. Wen, H. & Levitan, I. B. Calmodulin is an auxiliary subunit of KCNQ2/3 potassium channels. *J. Neurosci.* **22,** 7991–8001 (2002).
3. Etxeberria, A., Aivar, P., Rodriguez-Alfaro, J. A., Alaimo, A., Villace, P., Gomez-Posada, J. C., Areso, P. & Villarroel, A. Calmodulin regulates the trafficking of KCNQ2 potassium channels. *FASEB J* **22,** 1135–1143 (2008).
4. Shahidullah, M., Santarelli, L. C., Wen, H. & Levitan, I. B. Expression of a calmodulin-binding KCNQ2 potassium channel fragment modulates neuronal M-current and membrane excitability. *Proc. Natl. Acad. Sci.* **102,** 16454–16459 (2005).
5. Gamper, N. & Shapiro, M. S. Calmodulin Mediates Ca2+-dependent Modulation of M-type K+ Channels. *J. Gen. Physiol.* **122,** 17–31 (2003).
6. Bal, M., Zaika, O., Martin, P. & Shapiro, M. S. Calmodulin binding to M-type K+ channels assayed by TIRF/FRET in living cells. *J. Physiol.* **586,** 2307–2320 (2008).
7. Bal, M., Zhang, J., Hernandez, C. C., Zaika, O. & Shapiro, M. S. Ca2+/calmodulin disrupts AKAP79/150 interactions with KCNQ (M-Type) K+ channels. *J. Neurosci.* **30,** 2311–2323
8. Xu, Q., Chang, A., Tolia, A. & Minor Jr., D. L. Structure of a Ca(2+)/CaM:Kv7.4 (KCNQ4) B-helix complex provides insight into M current modulation. *J. Mol. Biol.* **425,** 378–394 (2013).

9. Suh, B.-C., Inoue, T., Meyer, T. & Hille, B. Rapid chemically induced changes of PtdIns(4,5)P2 gate KCNQ ion channels. *Science* **314,** 1454–1457 (2006).

10. Zhang, H., Craciun, L. C., Mirshahi, T., Rohács, T., Lopes, C. M. B., Jin, T. & Logothetis, D. E. PIP2 activates KCNQ channels, and its hydrolysis underlies receptor-mediated inhibition of M currents. *Neuron* **37,** 963–975 (2003).

11. Suh, B. C. & Hille, B. PIP2 is a necessary cofactor for ion channel function: how and why? *Annu. Rev. Biophys.* **37,** 175–195 (2008).

12. Suh, B. C. & Hille, B. Recovery from muscarinic modulation of M current channels requires phosphatidylinositol 4,5-bisphosphate synthesis. *Neuron* **35,** 507–520 (2002).

13. Winks, J. S., Hughes, S., Filippov, A. K., Tatulian, L., Abogadie, F. C., Brown, D. A. & Marsh, S. J. Relationship between membrane phosphatidylinositol-4,5-bisphosphate and receptor-mediated inhibition of native neuronal M channels. *J. Neurosci.* **25,** 3400–3413 (2005).

14. Hoshi, N., Zhang, J. S., Omaki, M., Takeuchi, T., Yokoyama, S., Wanaverbecq, N., Langeberg, L. K., Yoneda, Y., Scott, J. D., Brown, D. A. & Higashida, H. AKAP150 signaling complex promotes suppression of the M-current by muscarinic agonists. *Nat. Neurosci.* **6,** 564–571 (2003).

15. Murata, Y., Iwasaki, H., Sasaki, M., Inaba, K. & Okamura, Y. Phosphoinositide phosphatase activity coupled to an intrinsic voltage sensor. *Nature* **435,** 1239–1243 (2005).

16. Kosenko, A., Kang, S., Smith, I. M., Greene, D. L., Langeberg, L. K., Scott, J. D. & Hoshi, N. Coordinated signal integration at the M-type potassium channel upon muscarinic stimulation. *EMBO J* **31,** 3147–3156 (2012).

17. Smith, I. M. & Hoshi, N. ATP competitive protein kinase C inhibitors demonstrate distinct state-dependent inhibition. *PLoS One* **6,** (2011).

18. Park, H. Y., Kim, S. A., Korlach, J., Rhoades, E., Kwok, L. W., Zipfel, W. R., Waxham, M. N., Webb, W. W. & Pollack, L. Conformational changes of calmodulin upon Ca2+ binding studied with a microfluidic mixer. *Proc. Natl. Acad. Sci.* **105,** 542–547 (2008).

19. Hoshi, N., Langeberg, L. K. & Scott, J. D. Distinct enzyme combinations in AKAP signalling complexes permit functional diversity. *Nat. Cell Biol.* **7,** 1066–1073 (2005).

20. Faux, M. C. & Scott, J. D. Regulation of the AKAP79-protein kinase C interaction by Ca2+/Calmodulin. *J. Biol. Chem.* **272,** 17038–17044 (1997).

21. Dell'Acqua, M. L., Faux, M. C., Thorburn, J., Thorburn, A. & Scott, J. D. Membrane-targeting sequences on AKAP79 bind phosphatidylinositol-4,5-bisphosphate. *EMBO J.* **17,** 2246–2260 (1998).

22. Aharonovitz, O., Zaun, H. C., Balla, T., York, J. D., Orlowski, J. & Grinstein, S. Intracellular pH regulation by Na(+)/H(+) exchange requires phosphatidylinositol 4,5-bisphosphate. *J. Cell Biol.* **150,** 213–224 (2000).

23. Várnai, P., Lin, X., Lee, S. B., Tuymetova, G., Bondeva, T., Spät, A., Rhee, S. G., Czky, G. H. & Balla, T. Inositol lipid binding and membrane localization of isolated pleckstrin homology (PH) domains. Studies on the PH domains of phospholipase C δ1 and p130. *J. Biol. Chem.* **277,** 27412–27422 (2002).

24. Murata, Y. & Okamura, Y. Depolarization activates the phosphoinositide phosphatase Ci-VSP, as detected in Xenopus oocytes coexpressing sensors of PIP2. *J. Physiol.* **583,** 875–889 (2007).

25. Villalba-Galea, C. A., Miceli, F., Taglialatela, M. & Bezanilla, F. Coupling between the voltage-sensing and phosphatase domains of Ci-VSP. *J. Gen. Physiol.* **134,** 5–14 (2009).

26. Shaner, N. C., Steinbach, P. a & Tsien, R. Y. A guide to choosing fluorescent proteins. *Nat. Methods* **2,** 905–909 (2005).

27. Steyer, J. a & Almers, W. A real-time view of life within 100 nm of the plasma membrane. *Nat. Rev. Mol. Cell Biol.* **2,** 268–275 (2001).

28. Jentsch, T. J. Neuronal KCNQ potassium channels: physiology and role in disease. *Nat. Rev. Neurosci.* **1,** 21–30 (2000).

29. Gamper, N., Li, Y. & Shapiro, M. S. Structural requirements for differential sensitivity of KCNQ K+ channels to modulation by Ca2+/calmodulin. *Mol. Bio.l Cell* **16,** 3538–3551 (2005).

Chapter Three

Functional Role of M-current suppression in cognition:

Step 1, Generation and Basic Characterization of KCNQ2(S559A) mice

Introduction

Until recently, transgenic animals available for the study of the M-current were limited to KCNQ2 knock-out and dominant-negative mouse models, which abolish the presence of functional M-channels in neurons. Homozygous knock-out mice are neonatal lethal due to the inability to breathe. On the other hand, inducible dominant-negative mice show a distinct phenotype, which includes an impairment in spatial learning[1]. This model proved useful in investigating the physiological roles of the M-current, including its role in spatial learning. However, since these mice do not have any M-current, we cannot use them to study the functional role of transient M-current suppression induced by neurotransmitters. To investigate the physiological relevance of the suppression of the M-current, we need an animal model that would be resistant to neurotransmitter-induced M-channel block but maintain basal M-channel activities. Since M-channels are dynamically regulated to control neural excitability, their suppression is likely to play an important role in physiological processes that require changes in intrinsic excitability such as learning and memory. Indeed, selective KCNQ blockers such as linopirdine and XE991 were originally developed as cognition enhancers and show acute cognition enhancing properties in some animal experiments[2–4].

In our work described in chapter two, we identified a KCNQ2 mutation (KCNQ2(S541A), rat) that abolishes PKC-mediated phosphorylation of KCNQ2 subunits and resultant CaM dissociation, thereby disrupting muscarinic suppression of the M-current. KCNQ2 channels with an S541A mutation have been demonstrated to maintain basal channel activities, while attenuating the response to muscarinic stimulation in electrophysiological experiments[5,6]. Transiently expressed KCNQ2(S541A) channels also demonstrate attenuated responses to changes in cytosolic Ca^{2+} levels (Figure 2.8D). Based on these observations, we generated a mouse line carrying an alanine residue at the position of serine corresponding to the rat KCNQ2(S541A), which we designated KCNQ2(S559A) [residue position according to transcript variant 1 (NM010611.2)]. Here, we describe the biophysical characteristics of M-currents in KCNQ2(S559A) mice and their behavioral phenotype observed in a battery of basic behavioral assays.

Experimental Procedures

Generation of KCNQ2(S559A) mice.

An alanine mutation was introduced into exon 13 at the position 559 (Figure 3.1). The targeting vector was generated at BAC Recombineering Core, Duke Comprehensive Cancer Center (Duke University). The targeting vector was used for homologous recombination using a C57BL/6NTac derived ES cell line, JM8.N4, at the UC Irvine Transgenic Mouse Facility. An ES cell clone that showed homologous recombination by genomic Southern blots and the highest score for karyotyping was used to generate chimeric mice. The resultant offspring were screened by genomic PCR. This floxed KCNQ2(S559A) mouse line was then crossed with C57BL/6 background Cre mice that express Cre in oocytes, C57BL/6-Tg (Zp3-cre)93Knw/j, to generate global knock-in mice. Excision of the neo cassette was confirmed by genomic PCR. All mice were backcrossed to C57BL/6J mice (The Jackson Laboratory) 6 generations.

Primary Neuron Culture.

Neuron isolation and primary neuron culture were performed according to the protocol described previously[7] with some modifications. Briefly, four to five neonatal pups from wild-type or homozygous KCNQ2(S559A) mice were decapitated and disinfected with 70% ethanol. The forebrains were removed and placed in a 60 mm dish containing Hank's Balanced Salt Solution (HBSS) (Life Technologies, Carlsbad, CA, USA). The cerebral hemispheres were separated under a dissecting microscope, and the meninges were stripped away using forceps. The hippocampi and cortices were separated out and transferred to 60 mm dishes containing Hibernate A solution (Life Technologies, Carlsbad, CA, USA). After all brains were processed, the separated hippocampi and cortices were finely chopped into four to five equally sized pieces. Hibernate A was then aspirated and the tissue was transferred into 14 mL conical centrifuge

tubes containing a 37°C solution of Hibernate A, papain, and DNase. The cultures were incubated at 37°C for 21 min while shaking. Following the incubation, the papain solution was aspirated and ~3 mL of plating medium (85% Neurobasal A, 10% Horse serum, 2% B27, 1% Glutamax, and 20 mM HEPES) were added to the tube. The cultures were then triturated by passing the solution up and down 10 – 12 times in a fire polished glass pipette. After trituration the tissue was allowed to set to the bottom of the tube and the supernatant was transferred to a new tube. The trituration procedure was repeated three more times, until the tissue was resuspended in a total of ~9 mL of plating medium. The cells were counted with a hemocytometer and plated onto poly-D-lysine coated 35 mm dishes containing plating medium at 8 x 10^5 to 1 x 10^6 cells per plate. The plating medium was replaced two to three hours after plating with growth medium (97% Neurobasal A, 2% B27, and 1% Glutamax). On the third day after plating, growth medium was replaced with feeding medium (96.9% Neurobasal A, 2% B27, 1% Glutamax, and 0.1% AraC), and fresh feeding medium continued to be added or replaced every 3 days for the duration of the culturing period.

Electrophysiological Measurements.

Perforated patch-clamp recordings were performed at room temperature on isolated primary hippocampal and cortical neurons from wild-type and homozygous KCNQ2(S559A) mice using an Axopatch 200B patch-clamp amplifier (Molecular Devices, Sunnyvale, CA, USA). Signals were sampled at 2 kHz, filtered at 1 kHz, and acquired using pClamp software (version 7, Molecular Devices). The perforated patch-clamp method was used to record macroscopic currents as described previously[8]. Briefly, patch pipettes (1–2 MΩ) were filled with the intracellular solution containing 130 mM potassium acetate, 15 mM KCl, 3 mM $MgCl_2$, 6 mM NaCl, and 10 mM HEPES (adjusted to pH = 7.2 by NaOH), in which amphotericin B (0.1–

0.2 mg/ml) was dissolved. The extracellular solution consisted of 130 mM NaCl, 3 mM KCl, 1 mM $MgCl_2$, 0.1 mM $CaCl_2$, 11 mM glucose, and 10 mM HEPES (adjusted to pH = 7.4 with NaOH). Amplitudes of the M-currents were measured as deactivating currents during a 500-ms test pulse to -50 mV from a holding potential of -30 mV.

Nissl Staining.

Brains were removed from the mice, flash frozen with Isopentane, and cryosectioned into 30 μm coronal slices. Brain slices were then mounted onto premium frosted microscope slides (Fisher Scientific, Waltham, MA, USA). Nissl staining of brain tissue was performed essentially as follows: microscope slides containing brain slices were inserted into the slide racks and passed through the following sequence of treatments: 95% ethanol for 15 min, 70% ethanol for 1 min, 50% ethanol for 1 min, distilled water for 2 min, distilled water for 1 min, Cresyl Violet Stain for 5 min, distilled water for 1 min, 95% ethanol for 2 min, followed by a few more dips into 95% ethanol, and 1 min in 100% ethanol. Following this procedure, the slides were allowed to air dry before glass cover slips were permanently mounted.

Behavioral Assays.

Mice.

All mice used in the behavioral experiments were between 8 and 15 weeks old at the time of testing. All mice had *ad libitum* access to food and water, unless stated otherwise. The lights were maintained on a 12 h : 12 h light/dark cycle, and all behavioral experiments were performed during the light cycle with a starting time consistent between the groups. All mice were group housed, with a maximum of one week of single housing if required by the experimental protocol. All experiments were conducted according to US National Institute of

Health guidelines for animal care and use and were approved by the Institutional Animal Care and Use Committee of the University of California, Irvine.

Locomotion and Open Field Tests.

Locomotion was monitored in an automated activity system (50 × 50 × 40 cm) equipped with IR sensors for both horizontal and vertical activity measurements (VersaMax, AccuScan Instruments, Inc., Columbus, OH, USA). For the open field test, the center zone was defined as a 30 × 30 cm imaginary square in the middle of the observation area, and mice were monitored for up to 15 min without prior habituation to the testing arena. Wild-type and KCNQ2(S559A) mice were placed into the lower left or the upper right quadrant of the arena at random. Activity was measured over 30 min by 18 × 12 infrared sensors placed 2 cm above the floor. Horizontal activity represents IR beam breaks in the *x* and *y* dimensions. A second set of sensors 8 cm above the floor was used to record rearing events (*z* dimension). Stereotypic behavior is defined as repetitive breaks of a single beam that is not followed by a consecutive beam break of an adjacent sensor. Arousal is defined as horizontal and vertical activity during the first 10 min of exposure to the unfamiliar area. The automated system does not allow for differentiation of individual stereotypic behaviors, such as grooming or sniffing. Data were collected using VersaMax software (AccuScan, Inc.). Number of beam breaks, total distance traveled, vertical activity and episodes of stereotypic behavior were recorded and analyzed as described[9,10].

Rotarod Test.

Mice were placed on a rotarod (TSE Systems, Bad Homburg, Germany) at an initial speed of 6 rpm. A single session consisted of a 5 min interval during which the rotarod accelerated linearly from 6 to 60 rpm as described[11]. The latency and rotation speed, at which the mice fell off the rod, were recorded automatically by an infrared beam located below the rotating

rod. Each mouse was given three trials with intertrial intervals of 20 min. A trained experimenter blind to the genotypes of the mice was present in the room.

Results and Discussion

Generation of mice.

As shown in Figure 3.1, transfected ES cells generated cell colonies that underwent homologous recombination, as evaluated by Southern blotts using 3' and 5' probes. These ES cells with floxed Neo cassette were used to generate founder chimeric mice.

General characterization of KCNQ2(S559A) mice.

Unlike homozygous KCNQ2 knockout mice or Szt1 mice that have spontaneous deletions in the KCNQ2 C-terminus, both of which are neonatal lethal for the homozygotes due to pulmonary atelectasis[12,13], our heterozygous and homozygous KCNQ2(S559A) mice are born without any apparent defects. Consistent with our pilot experiments that KCNQ2(S54A) channel maintains basal M-current, KCNQ2(S559A) mutation does not cause spontaneous seizures characteristic of BFNC phenotype associated with multiple mutations in the KCNQ2 gene. Both heterozygous and homozygous KCNQ2(S559A) mice breed normally and give birth to healthy offspring, and the mothers carrying the mutation nurture their pups equally as good as the wild-type mothers. KCNQ2(S559A) pups are born with normal body weight comparable to the wild-type, and show no abnormalities in the rate of weight gain and general growth throughout development (Figure 3.2). Additionally, by performing Nissl staining on unfixed flash frozen brains from adult wild-type and homozygous KCNQ2(S559A) mice, we confirmed that our genetic manipulations did not affect gross brain morphology (Figure 3.3). Importantly, no apparent malformations were observed in the hippocampus, cortex, and corpus callosum, all of which can be implicated in physiological functions that rely on changes in neuronal excitability.

As a prerequisite for examining the physiological implications of the KCNQ2(S559A) mutation, we needed to ensure that our knock-in mice are able to move freely, balance, and

coordinate their movements. Additionally, we wanted to confirm that the mutation had no effect on the arousal and exploration levels in our mice, as these parameters are essential for testing the rodent performance in behavioral assays of cognitive function. We first used a battery of behavioral tasks testing the locomotor ability. Locomotion assays were carried out in activity boxes, which represented a novel environment for the experimental mice. The activity boxes used for this test are equipped with three-directional infrared beams that enable tracking of the mouse movements and stereotypic activity. The parameters built into the activity boxes can also be modified and customized to examine other behaviors, which allows evaluation of mouse performance on open field, dark-light, and T-maze tests to name a few. Evidently, locomotion tests are a convenient tool for characterizing basic behavioral phenotypes in novel mouse models and pharmacological treatments. These tasks also provide the means for a thorough examination of mouse locomotor ability without the use of invasive and potentially confounding procedures. We first compared horizontal and vertical activity of KCNQ2(S559A) mice and their wild-type littermates in the first 10 min after introducing them to the novel environment, i.e. the activity box. We used this test to determine if our genetic manipulations had an effect on the arousal. As shown in Figure 3.4A, we observed no differences between the arousal of wild-type, heterozygous and homozygous KCNQ2(S559A) mice. We also examined stereotypic behavior of KCNQ2(S559A) mice, as repetitive stereotypy may be maladaptive and can confound behavioral experimentation. However, some level of stereotypic behavior is normal and observed in many species including primates. The most common stereotypic activity in the rodent models is grooming, which in some models can be used to investigate depression and anxiety. We did not observe any apparent differences in the level of stereotypic activity of heterozygous and homozygous KCNQ2(S559A) mice compared to their wild-type littermates (Figure 3.4B). This

suggests that KCNQ2(S559A) mutation does not cause repetitive stereotypic behavior in mice. Finally, KCNQ2(S559A) mice showed normal locomotor ability when the testing duration was increased to 30 min, with a gradual decrease in locomotion comparable to that in the wild-type (Figure 3.4C).

To examine the exploratory behavior in KCNQ2(S559A) mice, we performed an open field test. Due to the rodent innate tendency to explore novel environments, open field test measures general locomotion as well as the number of entries and the time spent in the center of the testing arena. The exploration generally subsides as the mouse gets more familiar with the environment. Thus, it is important to ensure that the animal is new to the testing arena and use the measurements acquired in the first five to ten minutes of the experiment. Since mice prefer dark and covered places to brightly lit and open areas, the amount of time spent in the center of the testing arena may also be interpreted in the context of anxiety, with more center time indicating anxiolytic effects. When we performed an open field test with our wild-type and KCNQ2(S559A) mice, we did not see any significant differences between the genotypes (Figure 3.5), which indicates that KCNQ2(S559A) mutation does not alter the exploratory behavior and anxiety levels.

Next, we decided to examine the performance of KCNQ2(S559A) mice on the rotarod test. Similarly to the locomotion tests, the advantage of rotarod is that it measures behavioral performance quantitatively and leaves little room for variation in interpretation. Rotarod is commonly used to evaluate balance, grip strength, and motor coordination in rodents. Mice instinctively try to stay on the rotating rotarod in order not to fall. Thus, we used the length of the time a mouse was able to stay on the accelerating rotarod as a measure of balance, coordination, and motor planning. Figure 3.6 shows that we observed normal performance of heterozygous and

homozygous KCNQ2(S559A) mice on the accelerating rotarod, indicating no mutation-induced defects in balance, grip strength or motor coordination.

In parallel with behavioral characterization of KCNQ2(S559A) mice, we decided to examine electrophysiological properties of the mutant neuronal M-channels. As mentioned earlier, the rationale for generating the KCNQ2(S559A) mouse model came from the discovery of rat S541 (mouse S559) as the key PKC phosphorylation site required for M-channel suppression. Activation of muscarinic Gq-protein coupled receptors, which activates PKC, is the classical way to regulate the activity of the M-channel. Additionally, we used muscarinic agonist, oxo-M, in our previous study to identify and characterize the role of S541. Therefore, we used oxo-M to investigate the effect of the KCNQ2(S559A) mutation on M-channel suppression induced by muscarinic stimulation. We found that a concentration of oxo-M (0.3 μM) that elicited a 64.7 ± 7.2% inhibitory response in isolated wild-type hippocampal neurons had only a 24 ± 6.8% response in hippocampal neurons from homozygous KCNQ2(S559A) mice (Figure 3.7A). We also observed a significant attenuation of oxo-M-induced M-channel inhibition in cortical neurons from KCNQ2(S559A) mice, where application of 0.3 μM oxo-M resulted in a 45.2 ± 8.4% suppression in the wild-type and only 10.4 ± 7.6% suppression in the homozygous mutant (Figure 3.7B). We saw a similar effect in the SCG neurons (45.8 ± 0.04% suppression in wild-type, 16.1 ± 0.04% in homozygous mutant, data not shown). This clearly indicates that KCNQ2(S559A) mutation attenuates muscarinic responses of the native M-channels in neurons both in the CNS and the periphery. Further, we performed a dose response in homozygous KCNQ2(S559A) neurons, and found that oxo-M has an estimated IC50 of about 1.6 μM in hippocampal neurons and about 2.8 μM in cortical neurons. Though these values may be slightly

off, as we only tested doses of oxo-M up to 10 μM, which may not have revealed the true saturation point. Thus, we estimated the doses of oxo-M in homozygous KCNQ2(S559A) neurons that elicited a similar response to that of 0.3 μM oxo-M in the wild-type, and found them to be approximately 2.5 μM for hippocampal, and 4 μM for cortical neurons. These results show that the sensitivity of the M-channels in KCNQ2(S559A) neurons to muscarinic suppression is about 10-fold lower than that of the wild-type. However, it is important to note that basic electrophysiological properties, as well as the amplitudes of XE991 sensitive M-like currents, in KCNQ2(S559A) hippocampal and cortical neurons were not significantly different from the wild-type. These properties are summarized in Tables 3.1 and 3.2.

Altogether, our basic behavioral characterization confirms that in generating KCNQ2(S559A) mice we were able to avoid developmental issues. Additionally, the brains of KCNQ2(S559A) mice appear normal, and the biophysical properties of hippocampal and cortical neurons from these mice are comparable to those from the wild-type. However, native neuronal M-channels from KCNQ2(S559A) mice show a distinct attenuation of muscarinic-induced suppression. This suggests that we generated a mouse model with functional M-channels that remain open after Gq-protein coupled receptor stimulation.

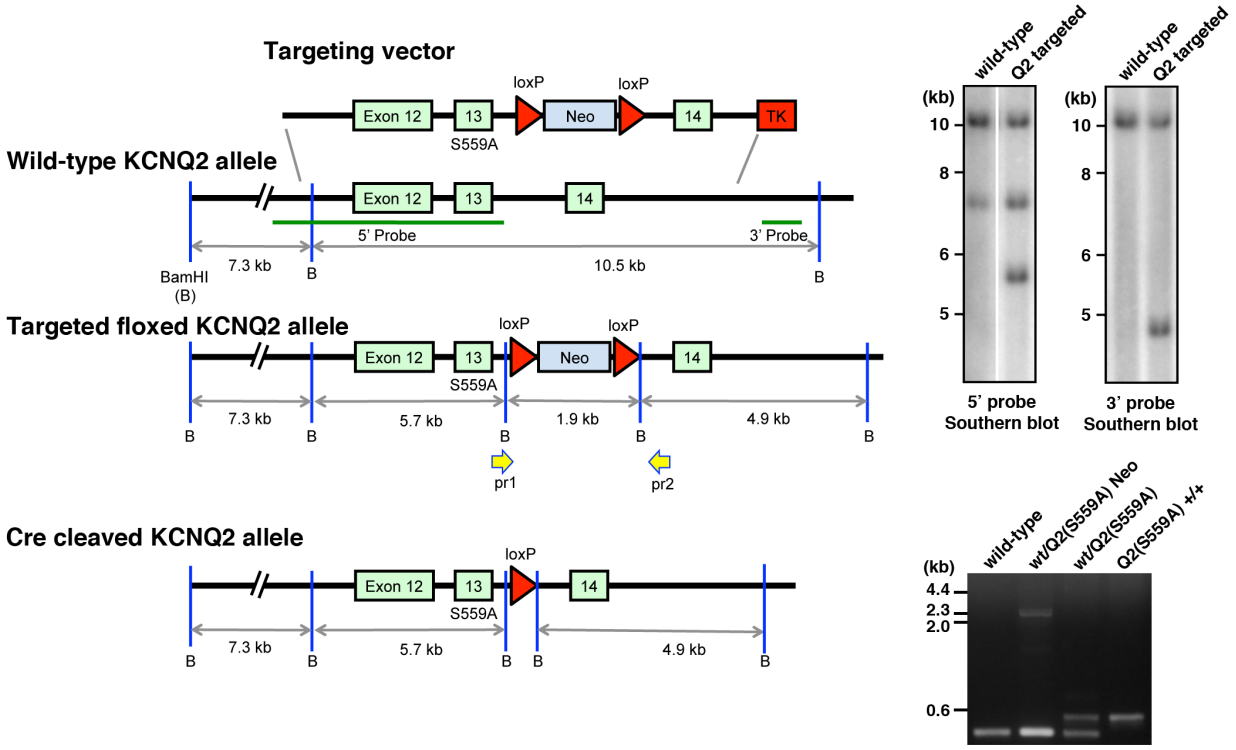

Figure 3.1. Generation of floxed and global KCNQ2(S559A) knock-in mice.

Targeting vector shows the single-point alanine substitution of serine 541 on exon 13 of KCNQ2 gene. Genomic Southern blots indicate the presence of the Neo cassette and the KCNQ2(S559A) mutation in floxed heterozygous knock-in mutants. Gel electrophoresis confirms the genotypes of generated Cre cleaved global heterozygous and homozygous KCNQ2(S559A) mutants.

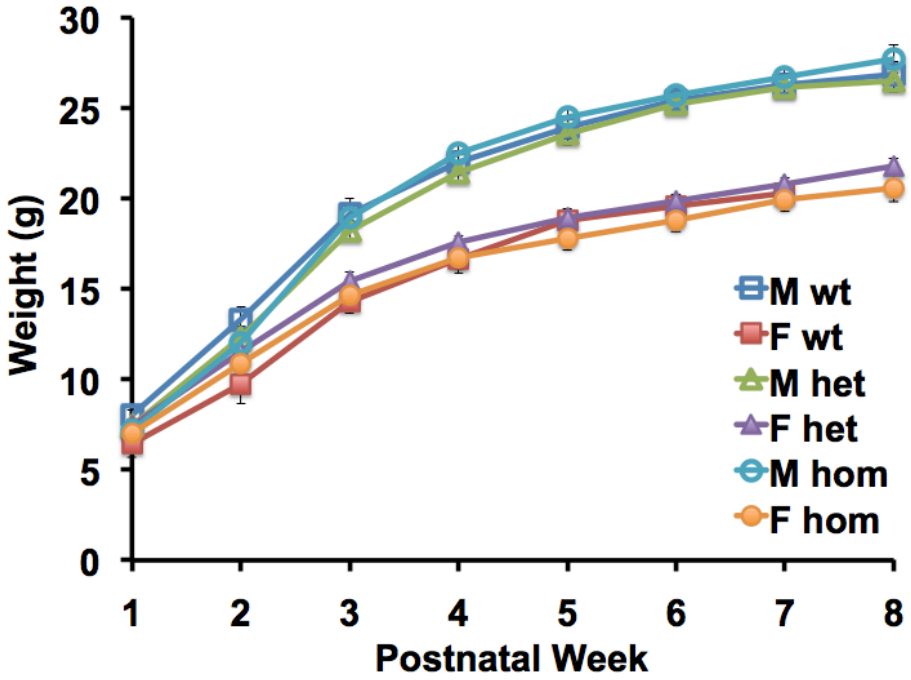

Figure 3.2. Normal body weight of KCNQ2(S559A) mice.

KCNQ2(S559A) mice are born with normal body weight comparable to the wild-type. The body mass of heterozygous and homozygous KCNQ2(S559A) mice increases at the same rate as that of the wild-type for both males and females. (Males: wt: n=10, het: n=11, hom: n=9. Females: wt: n=3, het: n=11, hom: n=5). Error bars show S.E.M. wt – wild-type, het – heterozygous, hom – homozygous

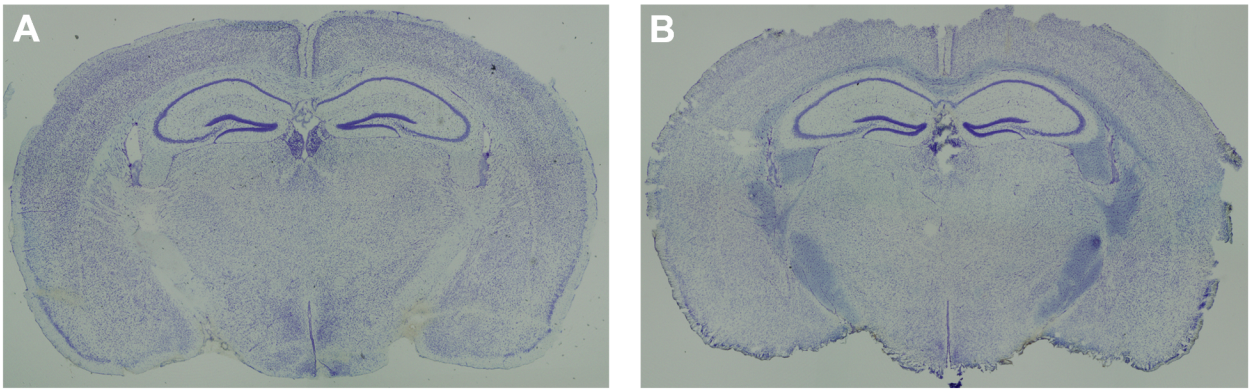

Figure 3.3. Normal brain morphology in KCNQ2(S559A) mice.

A, Nissl staining of a wild-type mouse brain slice
B, Nissl staining of a KCNQ2(S559A) mouse brain slice

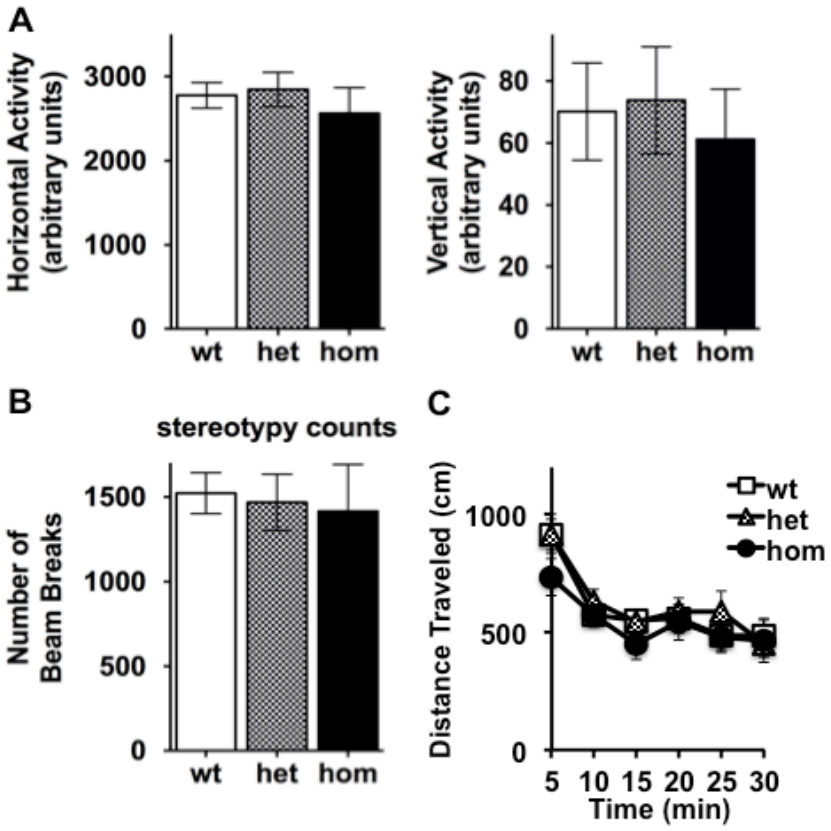

Figure 3.4. KCNQ2(S559A) mice show normal arousal, stereotypic behavior, and locomotion.

A, Arousal of wild-type, heterozygous and homozygous KCNQ2(S559A) mice measured by horizontal and vertical activity in 10 min, showing no differences between the genotypes. (Horizontal activity: wt: n=12, het: n=13, hom: n=12. Vertical activity: wt: n=12, het: n=10, hom: n=10)
B, Stereotypic behavior of heterozygous and homozygous KCNQ2(S559A) mice is comparable to the wild-type when measured for 10 min. (wt: n=12, het: n=13, hom: n=12)
C, Locomotion test showing normal locomotor ability of heterozygous and homozygous KCNQ2(S559A) mice compared to the wild-type. (wt: n=12, het: n=13, hom: n=12)
Error bars show S.E.M.
wt – wild-type, het – heterozygous, hom – homozygous

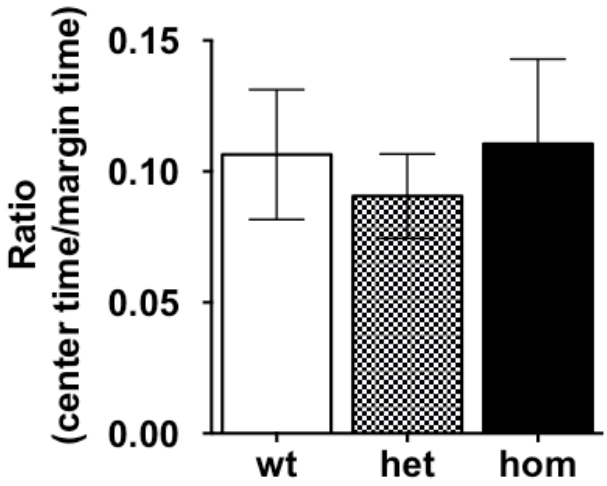

Figure 3.5. Normal performance on the open field test.

Ratio of the time spent in the center of the arena over the time spent in the margins during a 5 min period, showing no differences between wild-type, heterozygous or homozygous KCNQ2(S559A) mice. Error bars show S.E.M. wt – wild-type, het – heterozygous, hom – homozygous. (wt: n=11, het: n=11, hom: n=10)

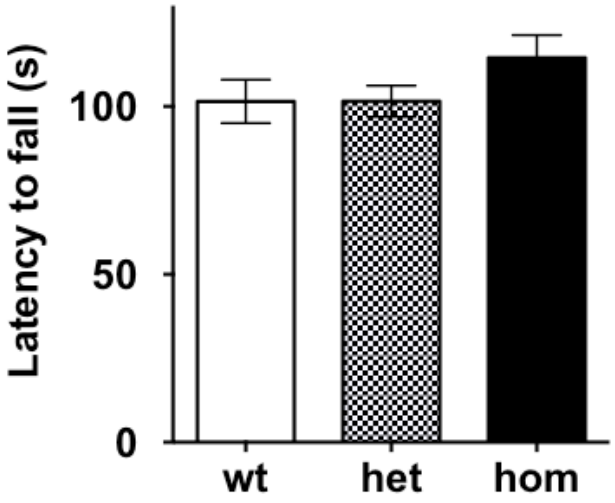

Figure 3.6. Normal performance on the rotarod test.

Average of three trials showing latency to fall from the accelerating rotarod indicating no genotypic differences in motor coordination. Maximal test duration/latency to fall was defined as 3 min. Error bars show S.E.M. wt – wild-type, het – heterozygous, hom – homozygous. (wt: n=10, het: n=10, hom: n=10)

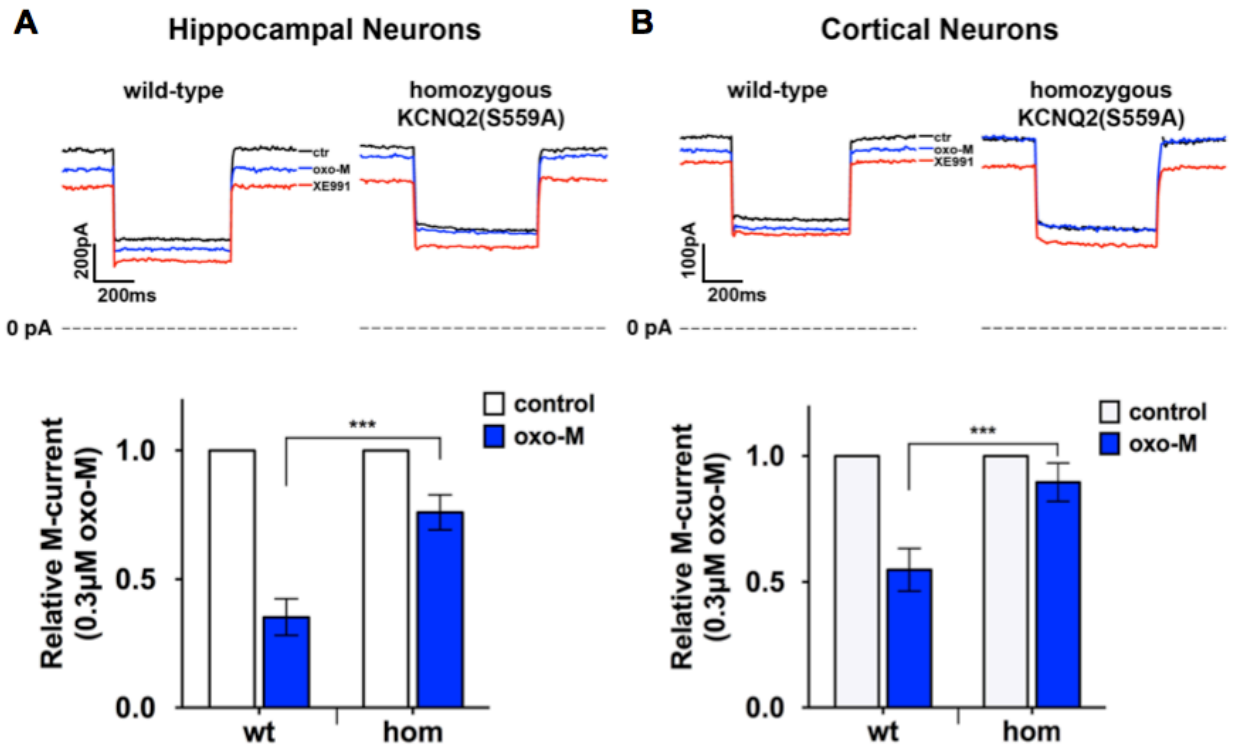

Figure 3.7. Muscarinic agonist oxo-M induces weaker M-channel suppression in hippocampal and cortical neurons from homozygous KCNQ2(S559A) mice.

A, Current traces recorded from hippocampal neurons (top panel), showing attenuated response of KCNQ2(S559A) neurons to oxo-M. Bottom panel showing quantitative histogram of current suppression induced by 0.3 μM oxo-M. (wt: n=7, hom: n=10)
B, Current traces recorded from cortical neurons (top panel) showing attenuated response of KCNQ2(S559A) neurons to oxo-M. Quantitative histogram showing a summary of responses induced by 0.3 μM oxo-M (bottom panel). (wt: n=9, hom: n=10)
Error bars show S.E.M.
wt – wild-type, hom – homozygous KCNQ2(S559A)

Table 3.1. Electrophysiological properties of hippocampal neurons from wild-type and homozygous KCNQ2(S559A) mice.

	input resistance (MΩ)	cell capacitance (pF)	standing current at -30 mV (pA) (control)	standing current at -30 mV (pA) (10 μM XE991)
wild-type (# of cells)	232.6 ± 19.1 (23)	47.2 ± 5.7 (21)	422.7 ± 114.1 (6)	321.0 ± 105.4 (6)
homozygous KCNQ2(S559A) (# of cells)	240.2 ± 21.7 (28)	45.3 ± 5.7 (28)	426.5 ± 79.4 (13)	361.8 ± 69.6 (13)

Table 3.2. Electrophysiological properties of cortical neurons from wild-type and homozygous KCNQ2(S559A) mice.

	input resistance (MΩ)	cell capacitance (pF)	standing current at -30 mV (pA) (control)	standing current at -30 mV (pA) (10 μM XE991)
wild-type (number of cells)	221.8 ± 20.1 (31)	40.3 ± 4.2 (28)	360.6 ± 49.3 (9)	292.3 ± 40.2 (9)
homozygous KCNQ2(S559A) (number of cells)	223.0 ± 27.1 (16)	36.4 ± 3.1 (16)	327.6 ± 32.2 (10)	259.0 ± 40.8 (10)

References

1. Peters, H. C., Hu, H., Pongs, O., Storm, J. F. & Isbrandt, D. Conditional transgenic suppression of M channels in mouse brain reveals functions in neuronal excitability, resonance and behavior. *Nat. Neurosci.* **8,** 51–60 (2005).
2. Cook, L., Nickolson, V. J., Steinfels, G. F., Rohrbach, K. W. & DeNoble, V. J. Cognition enhancement by the acetylcholine releaser DuP996. *Drug.Dev.Res.* **19,** 301–314 (1990).
3. Fontana, D. J., Inouye, G. T. & Johnson, R. M. Linopirdine (DuP 996) improves performance in several tests of learning and memory by modulation of cholinergic neurotransmission. *Pharmacol. Biochem. Behav.* **49,** 1075–1082 (1994).
4. Young, M. B. & Thomas, S. a. M1-Muscarinic Receptors Promote Fear Memory Consolidation via Phospholipase C and the M-Current. *J. Neurosci.* **34,** 1570–1578 (2014).
5. Hoshi, N., Zhang, J. S., Omaki, M., Takeuchi, T., Yokoyama, S., Wanaverbecq, N., Langeberg, L. K., Yoneda, Y., Scott, J. D., Brown, D. A. & Higashida, H. AKAP150 signaling complex promotes suppression of the M-current by muscarinic agonists. *Nat. Neurosci.* **6,** 564–571 (2003).
6. Kosenko, A., Kang, S., Smith, I. M., Greene, D. L., Langeberg, L. K., Scott, J. D. & Hoshi, N. Coordinated signal integration at the M-type potassium channel upon muscarinic stimulation. *EMBO J.* **31,** 3147–3156 (2012).
7. Kaech, S. & Banker, G. Culturing hippocampal neurons. *Nat. Protoc.* **1,** 2406–2415 (2006).

8. Selyanko, A. A., Stansfeld, C. E. & Brown, D. A. Closure of potassium M-channels by muscarinic acetylcholine-receptor stimulants requires a diffusible messenger. *Proc. Biol. Sci.* **250,** 119–125 (1992).

9. Xu, Y. L., Reinscheid, R. K., Huitron-Resendiz, S., Clark, S. D., Wang, Z., Lin, S. H., Brucher, F. A., Zeng, J., Ly, N. K., Henriksen, S. J., De Lecea, L. & Civelli, O. Neuropeptide S: A neuropeptide promoting arousal and anxiolytic-like effects. *Neuron* **43,** 487–497 (2004).

10. Okamura, N., Habay, S. A., Zeng, J., Chamberlin, A. R. & Reinscheid, R. K. Synthesis and pharmacological in vitro and in vivo profile of 3-oxo-1,1-diphenyl-tetrahydro-oxazolo[3,4-a]pyrazine-7-carboxylic acid 4-fluoro-benzylamide (SHA 68), a selective antagonist of the neuropeptide S receptor. *J. Pharmacol. Exp. Ther.* **325,** 893–901 (2008).

11. Duangdao, D. M., Clark, S. D., Okamura, N. & Reinscheid, R. K. Behavioral phenotyping of Neuropeptide S receptor knockout mice. *Behavioural Brain Research* **205,** 1–9 (2009).

12. Watanabe, H., Nagata, E., Kosakai, A., Nakamura, M., Yokoyama, M., Tanaka, K. & Sasai, H. Disruption of the epilepsy KCNQ2 gene results in neural hyperexcitability. *J. Neurochem.* **75,** 28–33 (2000).

13. Yang, Y., Beyer, B. J., Otto, J. F., O'Brien, T. P., Letts, V. A., White, H. S. & Frankel, W. N. Spontaneous deletion of epilepsy gene orthologs in a mutant mouse with a low eletroconvulsive threshold. *Human Molecular Genetics* **12,** 975–984 (2003).

Chapter Four

The Functional Role of M-current suppression in cognition:

Step 2, Role of M-Channel Suppression in Learning and Memory

Introduction

Learning and memory processes are classically considered to rely on synaptic plasticity such as LTP and LTD. On the other hand, the role of non-synaptic intrinsic plasticity, i.e. the changes in the intrinsic excitability of neurons, had been largely overlooked until recently. It is now widely accepted that intrinsic plasticity resulting from the dynamic regulation of ion channels in the central nervous system is essential for learning and memory[1–4]. The M-channel is one of the voltage-gated ion channels whose biophysical characteristics enable it to regulate neuronal excitability and spike-frequency adaptation[5,6]. As mentioned in Chapter One, multiple lines of evidence suggest a role for the M-channel regulation in physiological processes that require changes in neuronal excitability such as learning and memory.

To study the role of M-current suppression in learning and memory, we turned to behavioral tasks of recognition memory. Recognition memory is the capacity to know that something has been previously experienced[7,8]. This can include memories for individual stimuli, whole events as well as spatial and temporal information. The recognition process is generally thought of as a combination of two components: the judgment of item familiarity and the recollection of contextual cues for where and when the item was encountered[8,9]. Interestingly, different brain regions encode memories for these two components, with perirhinal and

entorhinal cortices being predominantly responsible for familiarity, and the hippocampus for contextual spatial information[10–16]. Available behavioral tasks such as novel object recognition (NOR), novel location recognition (NLR) or object in context recognition (OCR) allow examining region-specific memory impairment in rodent models in a relatively straightforward manner.

Memory processing consists of several phases and starts with learning, or the acquisition of information. While working memory or short-term memory is characterized by transient processing of information, long-term memory requires protein synthesis in relevant brain regions during a phase termed memory consolidation, which occurs several minutes to a few hours after the initial acquisition. Another important phase in memory processing is the retrieval, or memory recall, which identifies necessary information from memory storage when it needs to be used. The use of pharmacological agents at specific time points during memory processing can be advantageous to the study of molecular pathways regulating cognitive function. With our KCNQ2(S559A) mouse model described in Chapter Three, we can address the role of M-current suppression in learning and memory, and use specific KCNQ blockers to temporarily reverse the effects of KCNQ2(S559A) mutation during a certain phase of memory processing.

We used behavioral approaches described above in combination with pharmacology in KCNQ2(S559A) mice to demonstrate that M-current suppression regulates consolidation of object recognition memory mediated by cortical function. Further, we examined performance of KCNQ2(S559A) mice on the memory tasks that require the function of the hippocampus. Finally, we investigated genotype-specific changes in neuronal activation induced by novel object learning via immunohistochemistry for immediate early gene c-fos.

Experimental Procedures

Behavioral Assays.

Mice.

All mice used in the behavioral experiments were between 8 and 15 weeks old at the time of testing. All mice had *ad libitum* access to food and water, unless stated otherwise. The lights were maintained on a 12 h : 12 h light/dark cycle, and all behavioral experiments were performed during the light cycle with a starting time consistent between the groups. All mice were group housed, with a maximum of one week of single housing if required by the experimental protocol. All experiments were conducted according to US National Institute of Health guidelines for animal care and use and were approved by the Institutional Animal Care and Use Committee of the University of California, Irvine.

NOR, NLR, and OCR Tasks.

All mice were handled for three consecutive days for one min per day, followed by three consecutive days of habituation to the testing arena for 5 min per day. Two different testing arenas (contexts) were used for the OCR task, and mice were habituated to both contexts for three consecutive days, 5 min per day with a 90 min interval between the contexts. Training began 24 h after the last habituation session.

For the NOR task, objects similar in size (6-7 cm) but different in color and shape were used (2" x 2 ½", 3 oz spice jars and 2" x 2" square tealight candle holders). A crossover design was used in all recognition memory experiments by using different sets of objects for training in order to exclude potential confounding influences of preference for particular objects.

The NOR task consisted of two sessions: a training session followed by a retention trial 90 min or 24 h later. During the training session, two identical objects (A and A) were placed at

the predetermined locations in the arena (circular bucket, diameter 28.4 cm x height 20.5 cm with vertical silver marking strip) and surrounded by bedding. Each mouse was allowed to explore the objects for 10 min. The total time spent exploring each object was recorded by a trained observer blind to the genotype. After training, the mice were immediately transferred back to the home cage. During the retention session, a new set of objects containing one identical/familiar and one novel object (A and B) were used. The mice were allowed to explore the objects for 5 min and the time spent exploring each object was recorded.

Since absolute exploration times differ considerably between individual animals, exploration times were normalized [(time exploring object A) + (time exploring object B/C) = 100 %], and exploration of each object was expressed as percentage of total exploration time. Increased exploration of the novel object is interpreted as successful retention of memory for the familiar object.

NLR was investigated by presenting two identical objects (100 mL beakers) placed in distinct corners of the testing arena (white rectangular open field 30 x 23 x 21.5 cm with vertical silver marking strip) during the training session, and allowing 10 min exploration. Alternating corners were chosen for object presentation during training in order to exclude spatial preferences of object location. 24 h later, one of the objects was moved to a different location (identified by a mark on the arena) and the time spent exploring both objects during the 5 min period was recorded. Discrimination index was calculated as described for NOR. Increased time spent exploring the object in the novel location is interpreted as successful retention of spatial memory for the object that had not been moved[17].

The OCR task consisted of two training sessions 24 h apart, and a test 24 h following the last training session. During training mice were allowed to explore two different objects (A and

B) for 10 min in context 1. During second training session, conducted 24 h later, mice were placed into a different context (context 2) and allowed to explore two identical previously presented objects (A and A) for 10 min. On the memory test, mice were reintroduced to context 2 and allowed to explore for 5 min one copy of an object previously presented in context 2 (A) and one copy of an object previously presented in context 1 but not in context 2 (B). Discrimination index was calculated as follows: time of exploration of familiar object in novel context / (time of exploration of familiar object in familiar context + time of exploration of familiar object in novel context). A discrimination index equal to 0.5 reflects no preference, while discrimination index greater than 0.5 indicated preference for the familiar object in a novel context[16].

Social Olfactory Memory Task.

Single-housed male mice were used for the olfactory memory experiments. The social odor stimuli were presented on wooden beads (Woodworks LTD, Haltom City, TX) scented by adult male odor donor mice. During training session, mice were allowed to explore a single bead scented with a novel social odor for 2 min. 24 h following training, experimental mice were presented with two beads, one scented with the social odor presented during training and the other scented with a novel social odor. Mice were allowed to explore the beads for 2 min after the initiation of exploration. Sniffing was scored when the animal was orienting toward the bead with its nose 2 cm or closer. Social odor memory was measured according to the discrimination index equation, as described previously[23].

Test of Olfactory Function.

Mice were single housed for 3 consecutive days before the test. During this time, a piece of cookie, Teddy Grahams (Nabisco, Hanover, NJ), was placed into subjects' cages every 24 h to

familiarize the mice with the odor and flavor of the cookie. 24 h before the test, all food was removed from the food hoppers of subjects' cages. The water bottle was not removed. During the test, the mouse was placed into a clean cage with 3 cm of clean bedding and allowed to acclimate to the cage for 5 min. The mouse was then transferred into another clean cage and a food stimulus (cookie) was buried about 1 cm beneath the bedding surface, in a random corner of the cage. The observer started the stopwatch when the mouse was reintroduced into the cage and stopped it when the mouse found the buried cookie. The test was discontinued if the mouse did not find the food within 15 min. After the test, the mouse was returned to the home cage and allowed access to food and water *ad libitum*.

Odor Habituation/Dishabituation Task.

This test consists of sequential presentation of different odors and assesses the ability of mice to smell and distinguish same and different odors. The following sequence of odors was used: water – almond – banana – social odor 1 – social odor 2. Each odor was presented in 3 consecutive trials for duration of 2 min with an inter-trial interval of 1 min. Habituation is defined by a progressive in olfactory investigation after a repeated presentation of the same stimulus. Dishabituation is defined by the reinstatement of sniffing when a novel odor is presented. Odors were presented on cotton-tipped wooden applicators prepared on the day of the experiment. Non-social odors were obtained from pure natural almond and banana extracts (Frontier Natural Products, Norway, IA), and social odors were obtained from mouse cages of the same sex as the subject mouse. For non-social odors, 1:100 dilutions of extracts in ddH_2O were used. To prepare social odor, applicators were swiped across the cage bottoms in a zigzag fashion.

Subject mouse was placed into a clean cage containing bedding for 30 min, and a dry cotton-tipped applicator was inserted into the cage lid for habituation. Following the 30 min habituation, the testing trial began by inserting the applicator dipped into one of the odors into the cage lid. For each subsequent trial, the applicator was anchored to the lid at the same angle and to the same depth (about 2.5 cm). Sniffing was scored when the animal was orienting toward the applicator with its nose 2 cm or closer.

Contextual Fear Conditioning.

Mice were handled for 3 consecutive days for 1 min each day. On the training day, mice were put into a conditioning chamber. A single 2 s 0.7 mA scrambled foot-shock was delivered at time 2:28 of a 3-min training period. A 5 min testing period followed 24 h later, in which the mice were exposed to the same conditioned context in the absence of a shock. Freezing was measured every 10 s for the duration of a 5 min test trial by an observer blind to the genotype. Freezing was measured and compared between the genotypes both at the baseline, before the foot-shock, and 24 h following the foot-shock.

Neuronal Activation by Immunohistochemistry for c-fos.

Two hours after training, mice were anesthetized with isoflurane and perfused via the heart with ice-cold 4% paraformaldehyde (PFA) in 0.1 M PBS (pH 7.4). The brains were then be removed and post-fixed in 4% PFA overnight. The brains were sectioned into 30 μm thick coronal slices on a vibratome (Leica VT1200) and stored in a cryoprotectant solution at -20°C for histological analysis. Immunohistochemistry was performed according to the free-floating method as previously described[18]. Briefly, sections were fixed in 4% PFA for 10 min and incubated with 0.3% H_2O_2 for 15 min to quench endogenous peroxidase activity. The sections were placed in blocking solution containing 10% normal goat serum and 0.3% Triton X-100 in

0.01 M PBS (pH 7.2) for 30 min at 37°C, and then incubated at 4 °C for 48 h with a rabbit polyclonal antibody against c-*fos* at 1:5000 dilution (Ab-5, Calbiochem, La Jolla, CA) in blocking buffer. Following the 48-h incubation, the sections were incubated with Cy3-conjugated goat anti-rabbit IgG antibody at 1:500 dilution (Millipore, Billerica, MA, USA). Sections were mounted, dehydrated and cover slipped. As a negative control, adjacent brain sections were incubated without primary or secondary antibody to confirm specific staining. Differences in c-*fos* expression in the PRH were examined between the wild-type and KCNQ2(S559A) brains. Equal c-*fos* expression in regions unaffected by exposure to novel stimuli was used as a control. Immunofluorescent images were acquired using a fluorescent light microscope (Leica, DM4000B) equipped with a CCD camera (Optronics MicroFire, OPTMIF).

Results

M-current suppression is required for consolidation of long-term recognition memory.

To examine whether M-current suppression influences memory processes, we first tested KCNQ2(S559A) mice in both short- and long-term NOR tasks[17,19]. This task does not require the use of reinforcing or conditional stimuli. However, since memory is measured as the natural preference of mice for the object novelty, it is essential to habituate mice to the testing arena to remove its novelty factor, and provide object familiarity training (Figure 4.1A). Wild-type, heterozygous and homozygous KCNQ2(S559A) mice showed normal habituation to the testing arena (data not shown) as well as no object preference during training (Figures 4.1B & 4.1C). Additionally, there was no genotype-dependent differences in NOR performance with a 90 min delay between training and test sessions, indicating no perceptual or short-term memory deficits (Figure 4.1B). However, when the retention time was increased to 24 h, both heterozygous and homozygous KCNQ2(S559A) mice were no longer able to exhibit preference for the novel object. On the other hand, wild-type mice demonstrated normal long-term memory, as evidenced by positive discrimination indices (Figure 4.1C).

Performance on the NOR task with a long-term storage of information (24 h) requires cortical function, particularly of the perirhinal cortex (PRH)[8,20]. PRH has also been implicated in the learning of social stimuli[21,22], and a recent study linked PRH lesions to deficits in recognition memory for social odors when information storage exceeded 20 min[23]. Therefore, in order to confirm that PRH-mediated memory processes require M-current suppression, we next examined the performance of KCNQ2(S559A) mice on the social odor memory task (Figure 4.2A). The KCNQ2(S559A) mutation did not affect the overall exploration of social olfactory stimuli, but significantly impaired the ability of mice to form recognition memories for social odors with

long retention intervals (90 min – 24 h) (Figure 4.2B). As expected, wild-type littermates were able to demonstrate recognition memory for social odors following long retention times tested up to 24 h. We confirmed that the KCNQ2(S559A) mutation did not bring about olfactory deficits, as evidenced by normal performance of mutant mice on the test of olfactory function as well as odor discrimination task (Figures 4.2B &4.2C). Therefore, the inability of the mutant mice to perform on the social odor memory task indicated a memory impairment, and not an olfactory dysfunction.

Altogether, our findings from the NOR and social odor memory experiments suggest that M-current suppression is required for long-term recognition memory encoded by the perirhinal cortex and potentially other cortical regions. Moreover, since KCNQ2(S559A) mice did not show recognition memory impairments following short retention intervals, we concluded that suppression of the M-current was not critical for stimuli perception or recognition.

Pharmacological inhibition of M-current during memory consolidation rescues long-term recognition memory.

The results from our recognition memory experiments raised two important questions. First, whether the observed long-term memory impairment was in fact due to disrupted M-current regulation and not the off-target effects of genetic manipulations. Secondly, which stage of memory processing requires suppression of the M-current.

To address the first question, we used a KCNQ specific open channel inhibitor, XE991, in order to confirm that long-term recognition memory deficits observed in KCNQ2(S559A) mice were not a result of compensatory developmental mechanisms caused by genetic manipulations. In order to examine pharmacological effects of XE991 in homozygous KCNQ2(S559A) mice, we selected a maximal XE991 dose that had no effect on the memory of

the wild-type animals (Figure 4.3). When administered 15 min prior to NOR training, XE991 was able to rescue object recognition memory in KCNQ2(S559A) mice tested after a 24 h retention period (Figure 4.3A). This suggests that memory deficits seen in KCNQ2(S559A) mice are caused by the resistance of the mutant M-channels to physiological suppression induced by the activity-dependent stimulation of Gq-coupled receptors. However, administration of XE991 prior to training could affect both acquisition and consolidation of memory. To determine which step of memory processing requires M-current suppression, we administered XE991 immediately after NOR training. Pharmacological inhibition of the M-current immediately after NOR training was able to rescue the long-term object recognition memory tested with a 24 h retention delay (Figure 4.3B). Accordingly, XE991 administration did not result in any apparent differences in exploration, as measured by the open field test in either genotype (data not shown). We further tested whether M-current suppression during memory retrieval can rescue the impairment observed in KCNQ2(S559A) mice. XE991 treatment 15 min before NOR test (24 h following training) did not improve memory of the mutant mice for the familiar object (Figure 4.3C). Since memory of the wild-type littermates was unaffected by XE991 treatment (Figure 4.3C), we can conclude that the lack of rescue in KCNQ2(S559A) mice was not due to the effects of XE991 on the performance of the behavioral task. This indicates that M-current suppression is temporally critical during consolidation of long-term recognition memory. Conversely, when temporally restricted to retrieval, inhibition of M-channels is not sufficient for the rescue of memory impairment in KCNQ2(S559A) mice.

M-current suppression is not critical for long-term spatial or contextual memory.

Dominant-negative KCNQ2 mice show spatial memory deficits in the Morris water maze task[24], suggesting a role for the M-channel in processing of spatial memories. To investigate

whether M-current suppression plays a distinct role in spatial memory in our mouse model, we used NLR, a variation of the NOR task (Figure 4.4A). This task is designed to test hippocampus-dependent memory reliant on spatial cues. As such, it measures the increase in object exploration when a familiar object is moved to a novel location. KCNQ2(S559A) mice performed as successfully as the wild-type on the NLR task with a 24 h retention period, suggesting normal long-term memory for spatial cues (Figure 4.4B).

To further investigate whether M-current suppression is a critical component of consolidation of contextual memory, we explored the performance of KCNQ2(S559A) mice on the OCR task. Contextual recognition memory, which pairs associative information about item and context, has been demonstrated to require protein synthesis in the hippocampus, but not in cortical regions or basolateral amygdala[16,25–27]. In other words, despite the apparent similarities in the experimental design for NOR and OCR tasks, OCR performance does not require PRH function. Thus, by conducting this experiment, we could selectively address the role of M-current suppression in the hippocampus. As shown in Figure 4.5, we did not observe a memory deficit in KCNQ2(S559A) mice on the OCR task with a 24 h retention interval. We also confirmed this in the classical contextual fear conditioning task with a 24 h delay, which is another method to evaluate hippocampal function. In contextual fear conditioning paradigm, the context, in which a mild foot-shock is delivered to the mouse, serves as the main cue for the formation of an unpleasant memory. Here, the hippocampus mediates the freezing response to the context where a single foot-shock was received[28–30]. We found that KCNQ2(S559A) mice showed the same level of freezing as their wild-type littermates when placed into the testing chamber where they received a single 2 s 0.7 mA foot-shock 24 earlier (Figure 4.6). Normal performance of the KCNQ2(S559A) mice on both of these tasks of contextual recognition

memory indicates that their hippocampal function of memory processing is spared despite the resistance to neurotransmitter-induced M-current suppression.

Novel stimuli induce lower neuronal activation in perirhinal cortex in KCNQ2(S559A) mice.

We next focused on changes in neuronal activation after presentation of the novel objects in NOR training. Because our results from behavioral experiments with KCNQ2(S559A) mice suggest that M-current suppression is temporally critical for consolidation of recognition memory, we sought out to investigate neuronal activation during that time period. Presentation of novel objects has been shown to induce robust expression of c-fos in PRH, with the number of c-fos stained neurons significantly higher in the animals shown novel objects than the familiar ones[31,32]. Thus, we analyzed neuronal activation by counting neurons expressing c-fos protein in PRH 2 h after NOR training. We used hippocampal c-fos expression as a control as novel stimuli reportedly do not induce higher activation than the familiar ones in the hippocampus[31–33]. We focused on the CA1 subfield and the dentate gyrus when analyzing hippocampal c-fos expression. PRH c-fos counts in the brains of KCNQ2(S559A) mice were significantly lower compared to the wild-type, but hippocampal counts did not differ between the genotypes (Figure 4.7). We also compared c-fos expression in the wild-type and KCNQ2(S559A) mice that did not receive any experimental stimuli, and found no genotypic differences in the baseline c-fos expression in either PRH or the hippocampus. Additionally, we observed a NOR training-dependent increase in c-fos expression in both regions independently of the genotype. Although c-fos expression was lower in the KCNQ2(S559A) PRH compared to the wild-type, both genotypes showed robust changes in c-fos protein expression following NOR training, indicating

that the training period was sufficient to induce activity-dependent protein expression during memory consolidation.

Finally, we tested whether XE991 treatment immediately after NOR training rescued the deficit in PRH c-fos activation. Post-training XE991 treatment significantly increased KCNQ2(S559A) c-fos expression in PRH compared to the PBS group, and reached the level of expression equal to that of the wild-type (Figure 4.8). Although i.p. injections increased c-fos expression across all groups, wild-type counts were identical for both PBS and XE991 treatments, indicating that administration of 2 mg/kg XE991 did not affect neuronal activation in wild-type mice, which confirms our behavioral observations. Moreover, we did not see a XE991 treatment-mediated increase in c-fos expression in the hippocampus compared to PBS in either genotype (Figure 4.9).

Discussion

We found the NOR/NLR tasks particularly valuable for the initial evaluation of memory because these behavioral assays do not require external motivation, reward or punishment, and rely on the innate tendency of rodents to explore new objects. This eliminates a potential confound of reinforcing or aversive stimuli. The memory of a single learning episode is more vulnerable than that of repetitive associations such as reinforcing or conditional stimuli[34]. Therefore, NOR and NLR paradigms offer the means to detect memory deficits without the use of highly salient stimuli. This is important because KCNQ2(S559A) mutation attenuates, but does not completely abolish, the M-channel response to muscarinic stimulation. Neuronal hyperexcitability triggered by highly salient stimuli would likely surpass the mutation-induced threshold and lead to memory formation potentially concealing the role of M-channel regulation. Furthermore, because these tasks evaluate the ability of mice to recognize previously presented stimuli, they serve as a reliable animal model of human amnesia[35]. We found that KCNQ2(S559A) mice had intact object recognition memory on the NOR task with a 90 min retention delay, but impaired memory on the same task when the retention delay was increased to 24 h. These results are consistent with a dysfunction in PRH, which would cause a deficit in long-term object recognition memory but not in working memory or object perception. The role of M-current suppression in PRH was further confirmed by the social odor memory task, in which KCNQ2(S559A) mice were able to retain the information about social odor familiarity for 20 min but not 90 min or 24 h. These observations are in line with the study, in which PRH lesions were reported to impair social odor memory at retention intervals longer than 20 min[23]. Importantly, our findings also indicate that recognition memory requires M-current suppression independently of the sensory input, as similar effects of KCNQ2(S559A) were observed in

response to both visual and olfactory stimuli. Furthermore, by using KCNQ specific open channel blocker XE991, we were able to suppress the M-channel activity at different phases of memory processing during NOR task. This allowed us to temporally narrow down the requirement for M-current suppression to consolidation phase of recognition memory processing.

In the examination of hippocampus-dependent spatial memory in KCNQ2(S559A) mice by the NLR task we did not see any genotype-dependent differences. For further analyses, we performed the OCR task and contextual fear conditioning, both of which specifically addressed the role of the hippocampus in contextual memory formation. We observed normal long-term (24 h) memory in KCNQ2(S559A) mice on the OCR task. In contextual fear conditioning, we found that both wild-type and KCNQ2(S559A) mice demonstrated identical increase in freezing when reintroduced into the same conditioning chamber 24 h after a delivery of a mild foot-shock in the absence of any other cues. Our findings from NLR, OCR and contextual fear conditioning tasks indicate that KCNQ2(S559A)-mediated attenuation of neurotransmitter-induced M-current suppression does not elicit functional effects in relation to hippocampus-dependent memory function. Although a growing body of literature provides evidence for the role of M-channel in spatial hippocampus-dependent memory[24], from our study we cannot conclude that such memory processes require M-channel suppression. Interestingly, while we observed significantly attenuated Oxo-M responses in the homozygous KCNQ2(S559A) hippocampal neurons compared to the wild-type, same dose of Oxo-M elicited stronger suppression in hippocampal neurons than in SCG or cortical neurons in both genotypes. This suggests that hippocampal neurons express more functional KCNQ2 channels, which may have contributed to the normal performance of KCNQ2(S559A) mice on the tests of hippocampal function.

To confirm our behavioral observations, we investigated the differences in neuronal activation in KCNQ2(S559A) mice compared to the wild-type. While presentation of novel objects induces c-fos expression in PRH, an increase in c-fos expression in CA1 region of the hippocampus and the dentate gyrus has been reported in response to the novel arrangement of familiar items[36]. We observed a significant increase in c-fos expression 2 h after NOR training in PRH from both wild-type and KCNQ2(S559A) mice. However, c-fos counts from KCNQ2(S559A) were significantly lower than those from the wild-type. Post-training XE991 treatment was able to restore c-fos expression in the homozygous mice to the wild-type levels. These results correlate with our behavioral observations but do not explain why significant c-fos expression induced by NOR training was insufficient for recognition memory consolidation in KCNQ2(S559A) mice. Expression of KCNQ2 channels is reportedly not affected by NOR training[37], further supporting the idea that aberrant regulation of KCNQ2(S559A) channels resulted in the observed memory impairment.

In summary, the findings of our study suggest that M-current suppression plays a very specific and temporally restricted role in memory processing, namely consolidation of recognition memory. This knowledge may provide the basis for the optimization of therapeutic use of KCNQ inhibitors, which could unmask their previously unrealized therapeutic potential.

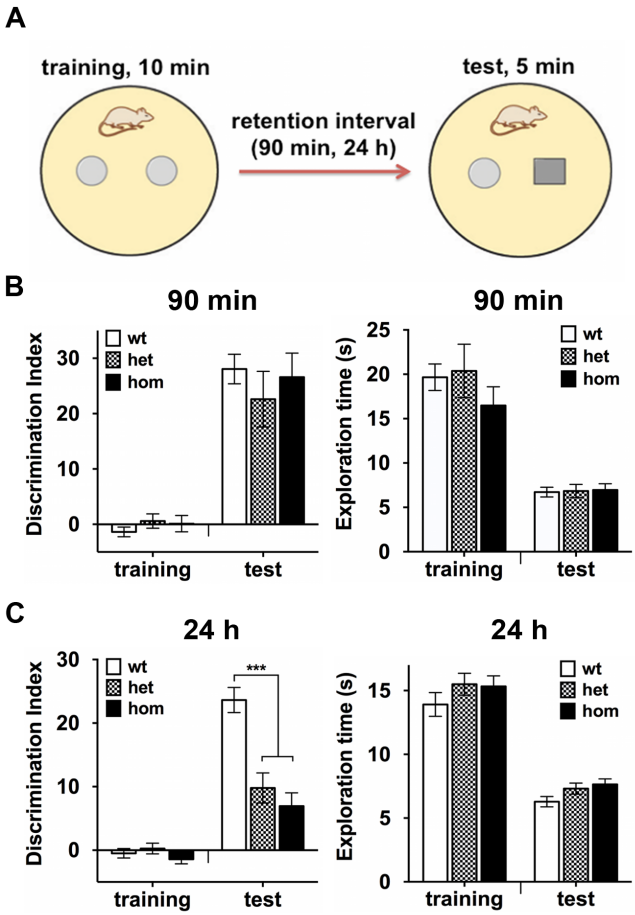

Figure 4.1. KCNQ2(S559A) mice have impaired long-term object recognition memory.

A, Schematic representation of the NOR paradigm, training and test set-ups are shown
B, Heterozygous (n=5) and homozygous (n=6) KCNQ2(S559A) mice show normal memory for the familiar object with a 90 min retention as compared to the wild-type (n=6) (left panel), (ANOVA, $F_{2,14}$=0.46, p=0.64). There were no significant differences in exploration time between genotypes (right panel) during training (ANOVA, $F_{2,14}$=0.9, p=0.43) or test (ANOVA, $F_{2,14}$=0.04, p=0.97)
C, Heterozygous (n=16) and homozygous (n=16) KCNQ2(S559A) mice exhibit significant PRH-dependent long-term memory deficits as compared to wild-type littermates (n=14) on NOR with 24 h retention (left panel), (ANOVA, $F_{2,43}$=16.21, p<0.001). There were no significant differences in exploration time between genotypes (right panel) during training (ANOVA, $F_{2,43}$=0.95, p=0.4) or test (ANOVA, $F_{2,43}$=2.66, p=0.1)
Error bars indicate S.E.M.

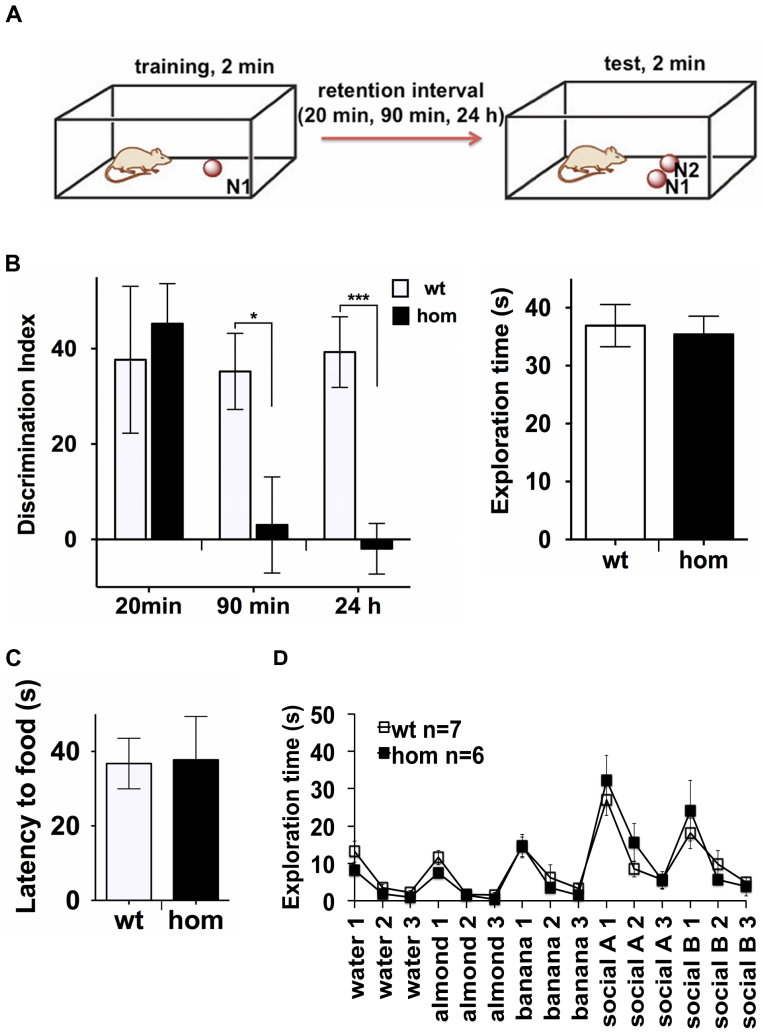

Figure 4.2. KCNQ2(S559A) mice have impaired social odor memory.

A, Schematic representation of the social odor memory paradigm, training and test sessions are shown

B, As compared to wild-type, homozygous KCNQ2(S559A) mice show normal PRH-independent memory for social odor with 20 min retention (wt: n=7, hom: n=7; t-test $t(12)=0.43$, $p=0.67$), impaired PRH-dependent social odor memory with 90 min retention (wt: n=8, hom: n=9; t-test $t(15)=2.46$, $p=0.03$), and impaired PRH-dependent social odor memory with 24 h retention (wt: n=11, hom n=12; t-test $t(21)=4.58$, $p<0.001$). There were no significant differences in exploration time between genotypes (pulled exploration times, wt: n=26, hom: n=28; t-test $t(52)=0.32$, $p=0.75$)

C, KCNQ2(S559A) mice have normal olfaction as compared to wild-type littermates (wt: n=8, hom: n=8; Mann-Whitney test, $p=0.67$)

D, KCNQ2(S559A) mice exhibit normal odor discrimination as compared to wild-type (wt: n=7, hom: n=6)

Error bars indicate S.E.M.

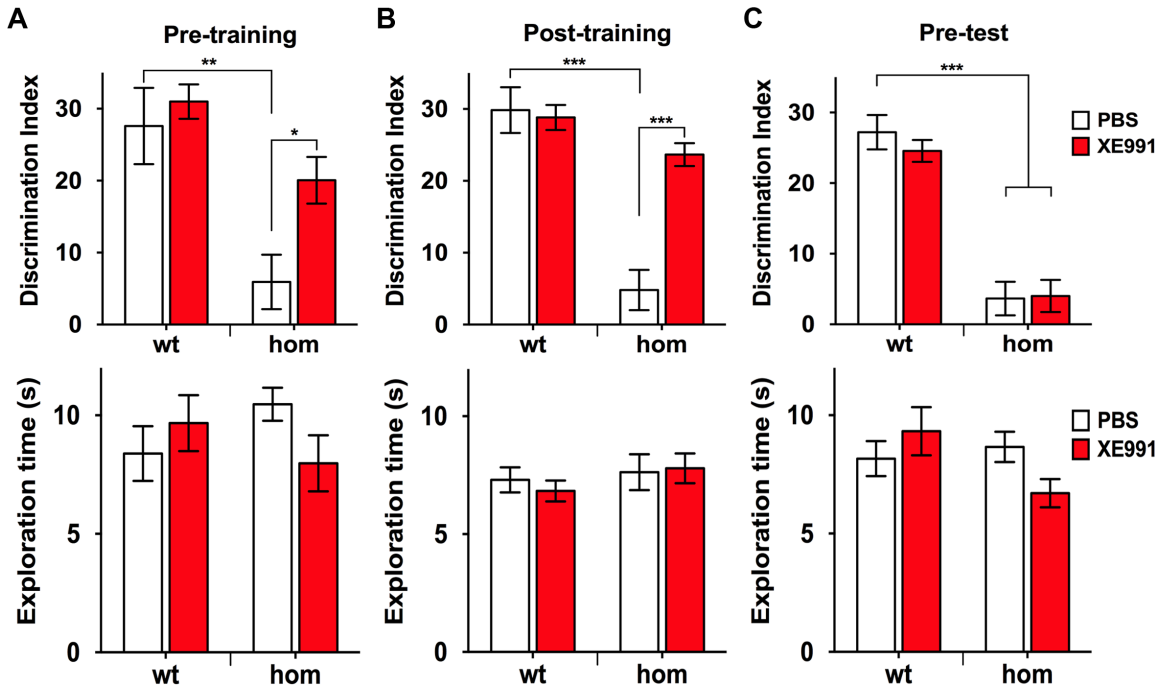

Figure 4.3. XE991 treatment during memory consolidation rescues memory deficit in KCNQ2(S559A) mice.

A, XE991 treatment 15 min prior to NOR training rescued memory deficit in KCNQ2(S559A) mice (top panel), (wt PBS: n=6, wt XE: n=7, hom PBS: n=7, hom XE: n=8; two-way ANOVA, effect of genotype $F_{1,24}$=19.45, p<0.001, effect of treatment $F_{1,24}$=5.62, p=0.03; followed by Tukey's multiple comparisons test). There were no significant differences between genotypes or treatment groups in exploration time (bottom panel), (genotype $F_{1,24}$=0.03, p=0.86, treatment $F_{1,24}$=0.31, p=0.58)

B, XE991 treatment immediately after NOR training rescued memory deficit in KCNQ2(S559A) mice (top panel), (wt PBS: n=8, wt XE: n=9, hom PBS: n=8, hom XE: n=8; two-way ANOVA, effect of genotype $F_{1,29}$=39.79, p<0.001, effect of treatment $F_{1,29}$=13.85, p<0.001; followed by Tukey's multiple comparisons test). There were no significant differences between genotypes or treatment groups in exploration time (bottom panel), (genotype $F_{1,29}$=1.17, p=0.29, treatment $F_{1,29}$=0.06, p=0.8)

C, XE991 treatment 15 min prior to NOR test did not improve memory in KCNQ2(S559A) mice (top panel), (wt PBS: n=12, wt XE: n=12, hom PBS: n=12, hom XE: n=10; two-way ANOVA, effect of genotype $F_{1,41}$=102,6, p<0.001, effect of treatment $F_{1,41}$=0.28, p=0.6; followed by Tukey's multiple comparisons test). There were no significant differences between genotypes or treatment groups in exploration time (bottom panel), (genotype $F_{1,41}$=1.88, p=0.18, treatment $F_{1,41}$=0.26, p=0.61)

Error bars indicate S.E.M.

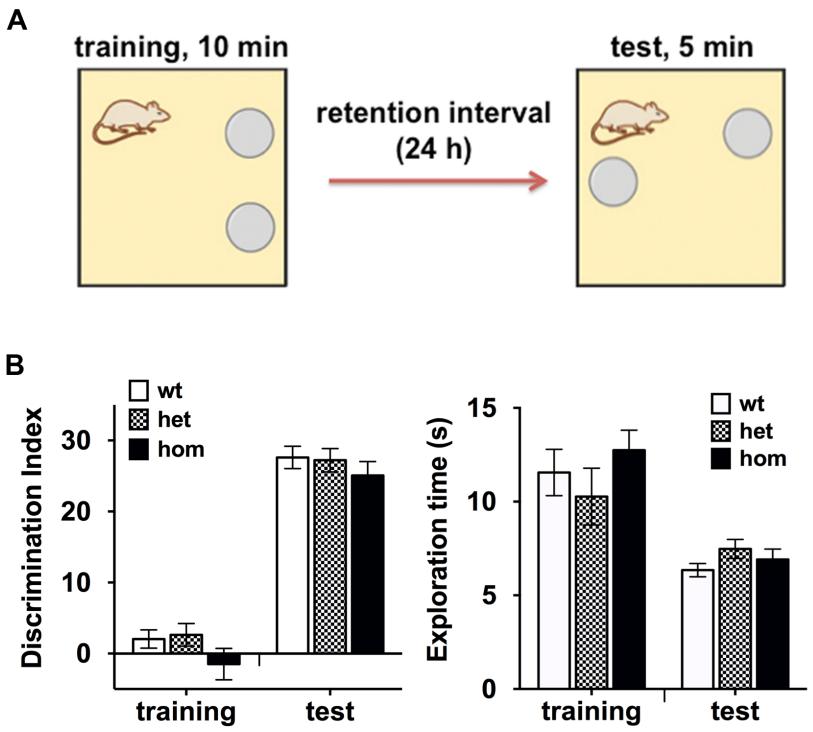

Figure 4.4. KCNQ2(S559A) mice have normal spatial memory.

A, Schematic representative of the NLR paradigm, training and test sessions are shown
B, Heterozygous (n=8) and homozygous (n=9) KCNQ2(S559A) mice exhibit normal hippocampus-dependent spatial memory on the NLR task with a 24 h retention as compared to wild-type (n=10) (left panel), (ANOVA, $F_{2,24}$=0.64, p=0.54). There were no significant differences in exploration time between genotypes (right panel) during training (ANOVA, $F_{2,24}$=0.89, p=0.43) or test (ANOVA, $F_{2,24}$=1.44, p=0.26)
Error bars indicate S.E.M.

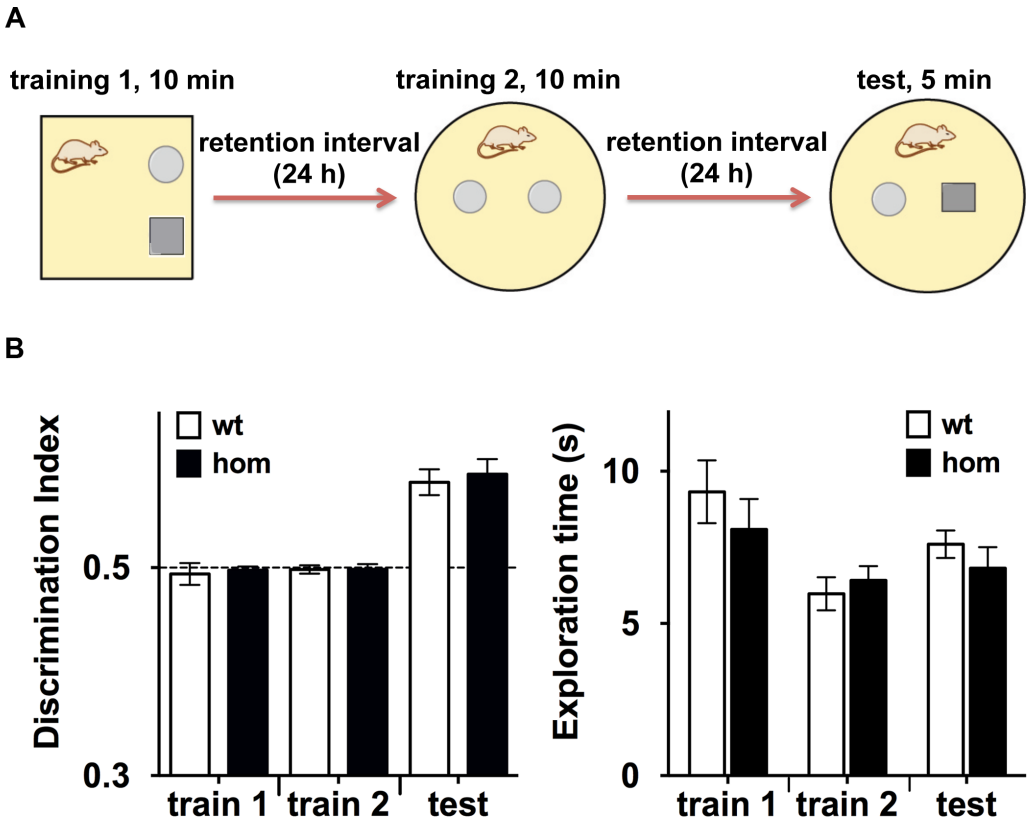

Figure 4.5. KCNQ2(S559A) mice have normal context memory.

A, Schematic representation of the OCR paradigm, set-ups for two training sessions and test are shown

B, Homozygous KCNQ2(S559A) mice (n=8) show normal hippocampus-dependent memory on the OCR task with a 24 h retention as compared to wild-type (n=8) (left panel), (t-test $t(14)=0.41$, $p=0.69$). There were no significant differences in exploration time between genotypes (right panel) during first training (t-test $t(14)=0.86$, $p=0.4$), second training or test (t-test $t(14)=0.96$, $p=0.36$). Error bars indicate S.E.M.

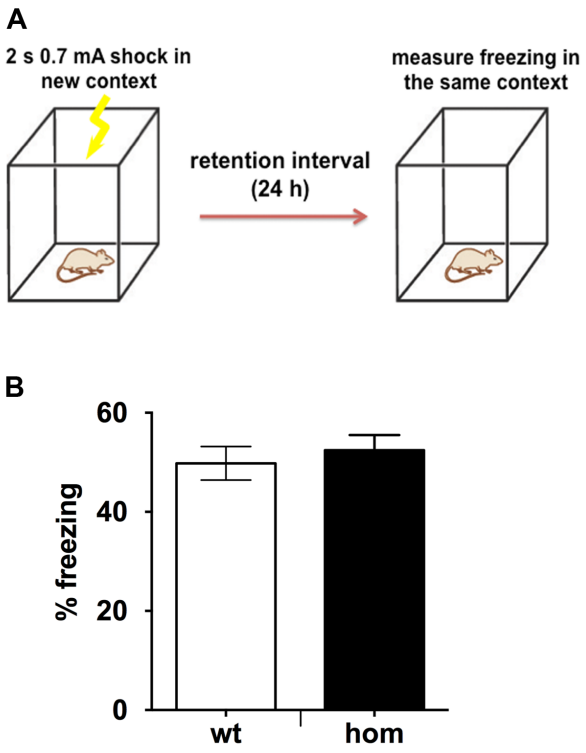

Figure 4.6. KCNQ2(S559A) mice have normal memory in contextual fear conditioning.

A, Schematic representation of contextual fear conditioning paradigm
B, Homozygous KCNQ2(S559A) mice (n=15) exhibit normal level of freezing 24 h after receiving a 0.7 mA 2 s scrambled foot-shock as compared to wild-type (n=16), indicating normal hippocampus-dependent memory for contextual cues (t-test $t(29)=0.58$, $p=0.57$). Error bars indicate S.E.M.

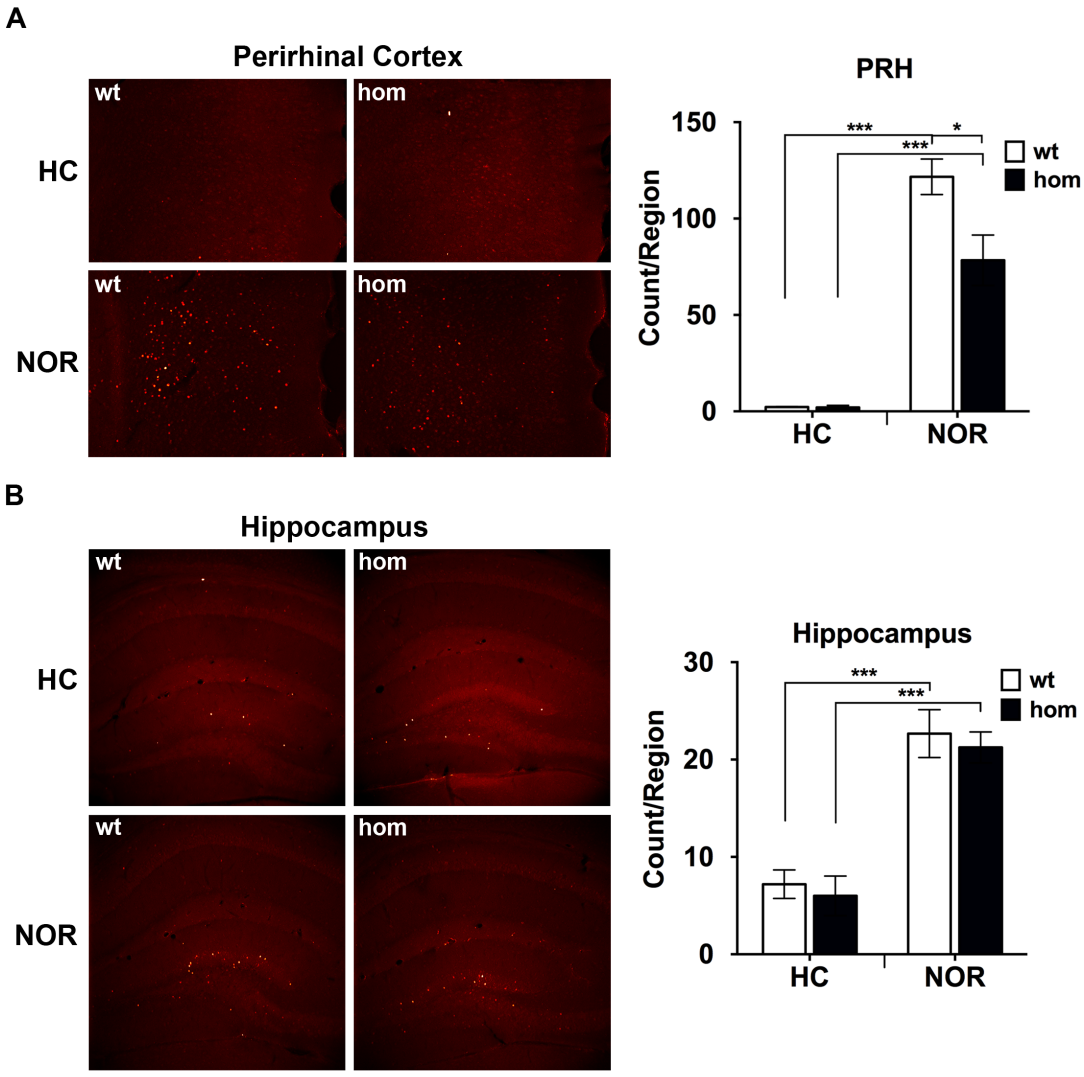

Figure 4.7. Lower NOR training-induced neuronal activation in PRH in brains from KCNQ2(S559A) mice.

A, Representative images of PRH from wild-type and homozygous KCNQ2(S559A) brain slices (left panel) and a histogram summarizing quantitative analysis of c-fos counts per region in home cage (HC) and after NOR training (NOR) conditions (right panel), (wt HC: n=5, hom HC: n=4, wt NOR: n=8, hom NOR: n=8; two-way ANOVA followed by Tukey's multiple comparisons test)
B, Representative images of the hippocampus from wild-type and homozygous KCNQ2(S559A) brain slices (left panel) and a histogram summarizing quantitative analysis of c-fos counts per region in home cage (HC) and after NOR training (NOR) conditions (right panel), (wt HC: n=5, hom HC: n=4, wt NOR: n=8, hom NOR: n=8; two-way ANOVA followed by Tukey's multiple comparisons test)
Error bars indicate S.E.M.

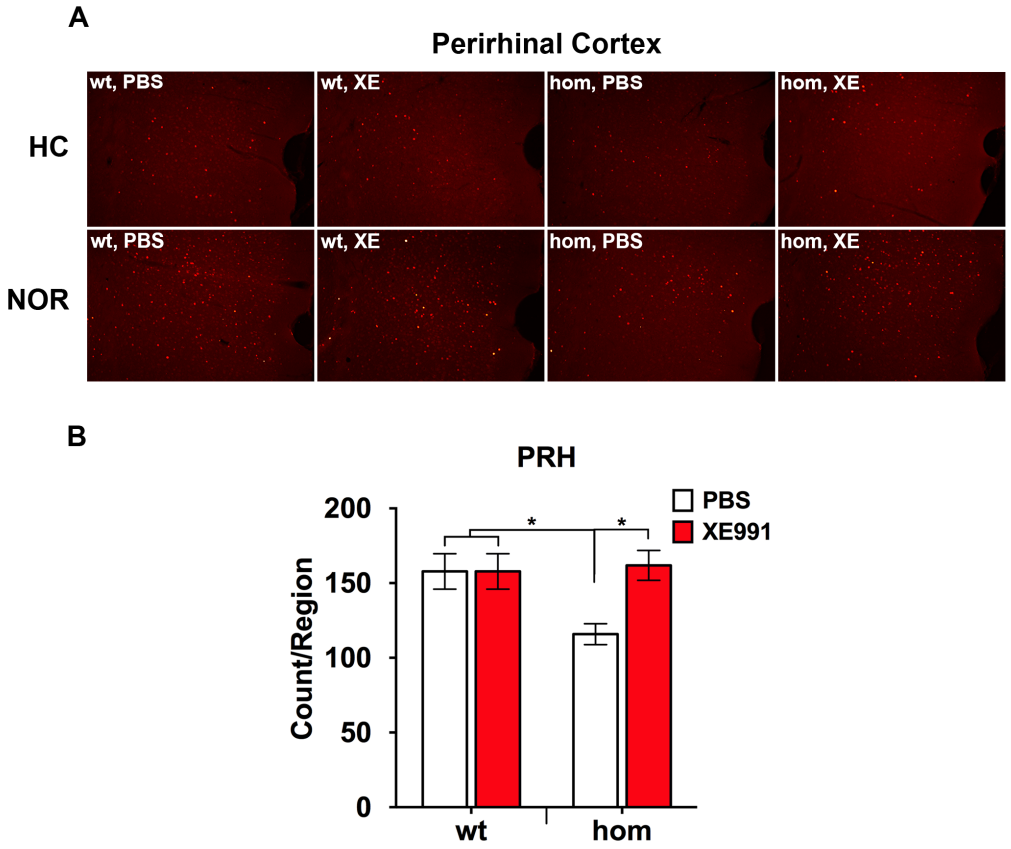

Figure 4.8. XE991 treatment after NOR training restores neuronal activation in PRH from KCNQ2(S559A) brains to wild-type level.

A, Representative images of PRH from wild-type and homozygous KCNQ2(S559A) brain slices treated with PBS or XE991 in home cage (HC) and after NOR training (NOR) conditions
B, Histogram summarizing quantitative analysis of c-fos counts per region after NOR training, showing XE991-mediated increase in PRH c-fos counts in brain slices from homozygous KCNQ2(S559A) mice (wt PBS: n=6, wt XE: n=6, hom PBS: n=6, hom XE: n=6; two-way ANOVA followed by Tukey's multiple comparisons test). Error bars indicate S.E.M.

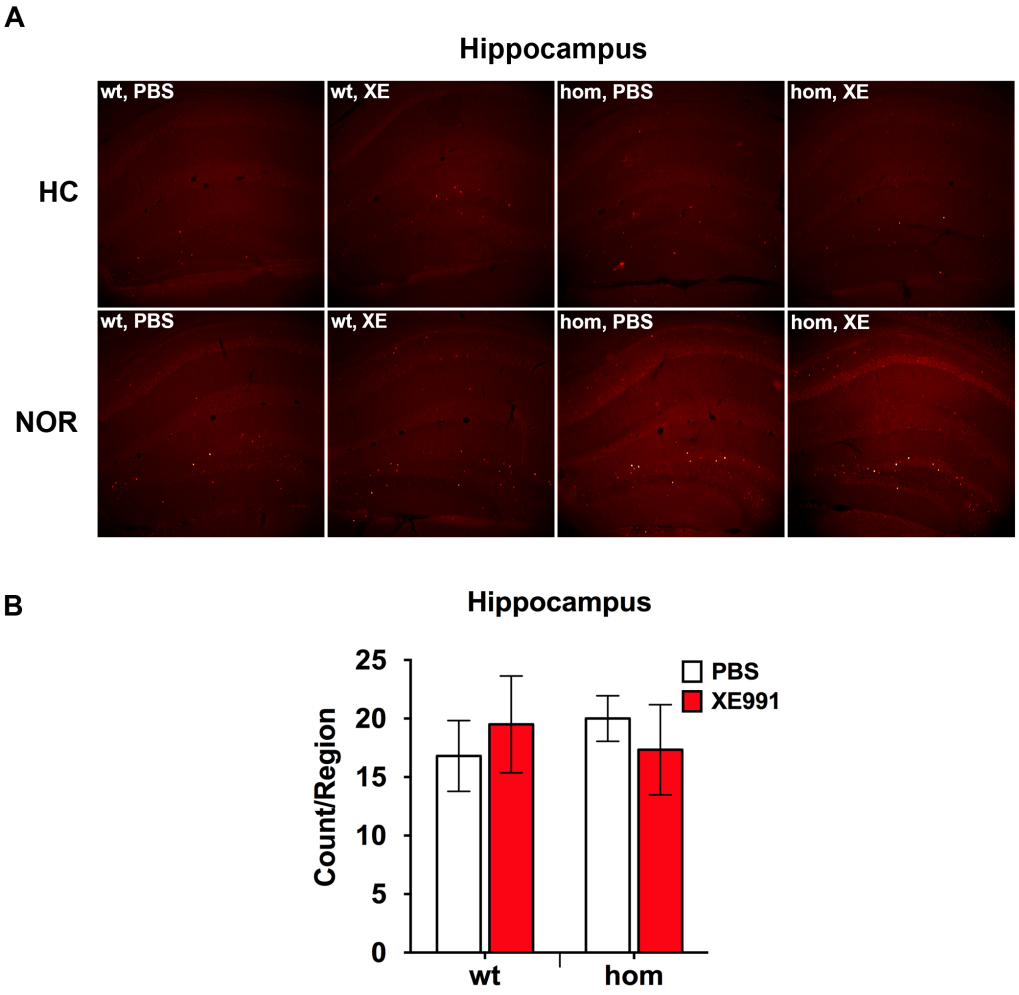

Figure 4.9. XE991 treatment after NOR training does not affect neuronal activation in the hippocampus from KCNQ2(S559A) brains.

A, Representative images of the hippocampus from wild-type and homozygous KCNQ2(S559A) brain slices treated with PBS or XE991 in home cage (HC) and after NOR training (NOR) conditions

B, Histogram summarizing quantitative analysis of c-fos counts per region after NOR training showing no effect of XE991 treatment of hippocampal c-fos counts in brain slices from wild-type or homozygous KCNQ2(S559A) mice (wt PBS: n=5, wt XE: n=6, hom PBS: n=5, hom XE: n=6; two-way ANOVA followed by Tukey's multiple comparisons test). Error bars indicate S.E.M.

References

1. Frick, A. & Johnston, D. Plasticity of dendritic excitability. *J. Neurobiol.* **64,** 100–115 (2005).
2. Song, C., Detert, J. a., Sehgal, M. & Moyer, J. R. Trace fear conditioning enhances synaptic and intrinsic plasticity in rat hippocampus. *J. Neurophysiol.* **107,** 3397–3408 (2012).
3. Zhang, W. & Linden, D. J. The other side of the engram: experience-driven changes in neuronal intrinsic excitability. *Nat. Rev. Neurosci.* **4,** 885–900 (2003).
4. Sehgal, M., Song, C., Ehlers, V. L. & Moyer, J. R. Learning to learn - Intrinsic plasticity as a metaplasticity mechanism for memory formation. *Neurobiol. Learn. Mem.* **105,** 186–199 (2013).
5. Brown, D. A. & Adams, P. R. Muscarinic suppression of a novel voltage-sensitive K+ current in a vertebrate neurone. *Nature* **283,** 673–676 (1980).
6. Brown, D. M-currents: an update. *Trends Neurosci.* **11,** 294–299 (1988).
7. Mandler, G. Recognizing: The judgment of previous occurrence. *Psychological Review* **87,** 252–271 (1980).
8. Brown, M. W. & Aggleton, J. P. Recognition memory: what are the roles of the perirhinal cortex and hippocampus? *Nat. Rev. Neurosci.* **2,** 51–61 (2001).
9. Yonelinas, A. P., Kroll, N. E. A., Quamme, J. R., Lazzara, M. M., Sauvé, M.-J., Widaman, K. F. & Knight, R. T. Effects of extensive temporal lobe damage or mild hypoxia on recollection and familiarity. *Nat. Neurosci.* **5,** 1236–1241 (2002).

10. Ennaceur, A., Neave, N. & Aggleton, J. P. Neurotoxic lesions of the perirhinal cortex do not mimic the behavioural effects of fornix transection in the rat. *Behav. Brain Res.* **80,** 9–25 (1996).

11. Ennaceur, A. & Aggleton, J. P. The effects of neurotoxic lesions of the perirhinal cortex combined to fornix transection on object recognition memory in the rat. *Behav. Brain Res.* **88,** 181–193 (1997).

12. Bussey, T. J., Muir, J. L. & Aggleton, J. P. Functionally dissociating aspects of event memory: the effects of combined perirhinal and postrhinal cortex lesions on object and place memory in the rat. *J. Neurosci.* **19,** 495–502 (1999).

13. Mumby, D. G., Gaskin, S., Glenn, M. J., Schramek, T. E. & Lehmann, H. Hippocampal Damage and Exploratory Preferences in Rats: Memory for Objects, Places, and Contexts. *Learn. Mem.* **9,** 49–57 (2002).

14. Stupien, G., Florian, C. & Roullet, P. Involvement of the hippocampal CA3-region in acquisition and in memory consolidation of spatial but not in object information in mice. *Neurobiol. Learn. Mem.* **80,** 32–41 (2003).

15. Mumby, D. G., Piterkin, P., Lecluse, V. & Lehmann, H. Perirhinal cortex damage and anterograde object-recognition in rats after long retention intervals. *Behav. Brain Res.* **185,** 82–87 (2007).

16. Balderas, I., Rodriguez-Ortiz, C. J., Salgado-Tonda, P., Chavez-Hurtado, J., McGaugh, J. L. & Bermudez-Rattoni, F. The consolidation of object and context recognition memory involve different regions of the temporal lobe. *Learn. Mem.* **15,** 618–624 (2008).

17. Vogel-Ciernia, A., Matheos, D. P., Barrett, R. M., Kramar, E. A., Azzawi, S., Chen, Y., Magnan, C. N., Zeller, M., Sylvain, A., Haettig, J., Jia, Y., Tran, A., Dang, R., Post, R. J.,

Chabrier, M., Babayan, A. H., Wu, J. I., Crabtree, G. R., Baldi, P., Baram, T. Z., Lynch, G. & Wood, M. A. The neuron-specific chromatin regulatory subunit BAF53b is necessary for synaptic plasticity and memory. *Nat. Neurosci.* **16,** 552–561 (2013).

18. Chen, C. R., Zhou, X. Z., Luo, Y. J., Huang, Z. L., Urade, Y. & Qu, W. M. Magnolol, a major bioactive constituent of the bark of Magnolia officinalis, induces sleep via the benzodiazepine site of GABA(A) receptor in mice. *Neuropharmacology* **63,** 1191–1199 (2012).

19. Antunes, M. & Biala, G. The novel object recognition memory: neurobiology, test procedure, and its modifications. *Cogn. Process* **13,** 93–110 (2011).

20. Suzuki, W. A. Untangling memory from perception in the medial temporal lobe. *Trends. Cogn. Sci.* **14,** 195–200 (2010).

21. Furtak, S. C., Allen, T. a & Brown, T. H. Single-unit firing in rat perirhinal cortex caused by fear conditioning to arbitrary and ecological stimuli. *J. Neurosci.* **27,** 12277–12291 (2007).

22. Petrulis, a. & Eichenbaum, H. The perirhinal-entorhinal cortex, but not the hippocampus, is critical for expression of individual recognition in the context of the Coolidge effect. *Neuroscience* **122,** 599–607 (2003).

23. Feinberg, L. M., Allen, T. A., Ly, D. & Fortin, N. J. Recognition memory for social and non-social odors: differential effects of neurotoxic lesions to the hippocampus and perirhinal cortex. *Neurobiol. Learn. Mem.* **97,** 7–16 (2012).

24. Peters, H. C., Hu, H., Pongs, O., Storm, J. F. & Isbrandt, D. Conditional transgenic suppression of M channels in mouse brain reveals functions in neuronal excitability, resonance and behavior. *Nat. Neurosci.* **8,** 51–60 (2005).

25. Aggleton, J. P. & Brown, M. W. Episodic memory, amnesia, and the hippocampal-anterior thalamic axis. *Behav. Brain Sci.* **22,** 425–444; discussion 444–489 (1999).

26. Diana, R. a., Yonelinas, A. P. & Ranganath, C. Imaging recollection and familiarity in the medial temporal lobe: a three-component model. *Trends Cogn. Sci.* **11,** 379–386 (2007).

27. Ranganath, C. A unified framework for the functional organization of the medial temporal lobes and the phenomenology of episodic memory. *Hippocampus* **20,** 1263–1290 (2010).

28. Wiltgen, B. J., Sanders, M. J., Anagnostaras, S. G., Sage, J. R. & Fanselow, M. S. Context fear learning in the absence of the hippocampus. *J. Neurosci.* **26,** 5484–5491 (2006).

29. Gewirtz, J. C., McNish, K. a. & Davis, M. Is the hippocampus necessary for contextual fear conditioning? *Behav. Brain Res.* **110,** 83–95 (2000).

30. Anagnostaras, S. G., Gale, G. D. & Fanselow, M. S. Hippocampus and contextual fear conditioning: Recent controversies and advances. *Hippocampus* **11,** 8–17 (2001).

31. Zhu, X. O., McCabe, B. J., Aggleton, J. P. & Brown, M. W. Mapping visual recognition memory through expression of the immediate early gene c-fos. *Neuroreport* **7,** 1871–1875 (1996).

32. Zhu, X. O., Brown, M. W., McCabe, B. J. & Aggleton, J. P. Effects of the novelty or familiarity of visual stimuli on the expression of the immediate early gene c-fos in rat brain. *Neuroscience* **69,** 821–829 (1995).

33. Aggleton, J. P. & Brown, M. W. Contrasting hippocampal and perirhinal cortex function using immediate early gene imaging. *Q. J. Exp. Psychol. B.* **58,** 218–233 (2005).

34. Ennaceur, a. & Meliani, K. A new one-trial test for neurobiological studies of memory in rats. III. Spatial vs. non-spatial working memory. *Behav. Brain Res.* **51,** 83–92 (1992).

35. Baxter, M. G. “I’ve seen it all before”: explaining age-related impairments in object recognition. Theoretical comment on Burke et al. (2010). *Behav. Neurosci.* **124,** 706–709 (2010).

36. Wan, H., Aggleton, J. P. & Brown, M. W. Different contributions of the hippocampus and perirhinal cortex to recognition memory. *J. Neurosci.* **19,** 1142–1148 (1999).

37. Fontan-Lozano, A., Suarez-Pereira, I., Delgado-Garcia, J. M. & Carrion, A. M. The M-current inhibitor XE991 decreases the stimulation threshold for long-term synaptic plasticity in healthy mice and in models of cognitive disease. *Hippocampus* **21,** 22–32

Chapter Five

Summary, Conclusions, and Future Directions

In this dissertation, I identified the molecular mechanism for KCNQ2 channel regulation, applied the gained information to generate a novel mouse model, and characterized the role of M-current suppression in learning and memory in these mice. I clarified the dynamic changes of molecular interactions that take place during M-channel signaling. This work contributed to the rationale for generating a novel knock-in mouse model, KCNQ2(S559A). I also described how I used these mice to investigate the physiological role of M-current suppression in learning and memory *in vivo*.

M-Current suppression: molecular mechanisms

I elucidated the changes in protein-protein interactions triggered by intracellular Ca^{2+} release, which leads to the suppression of the M-current. Several electrophysiological studies have concluded that increase in cytoplasmic Ca^{2+} suppresses the M-current[1–3]. However, the mechanism of such regulation had remained controversial due to discrepancies in data reported by different labs. One group argued that dissociation of CaM from KCNQ2 subunit corresponded to the loss of channel function[4], whereas others contended that conformational change of constitutively bound CaM regulated channel activity[3,5]. In Chapter Two, I provided evidence for what we believe to be the mechanism of Ca^{2+}-mediated M-current suppression. We found that the key role in this process plays a change in CaM configuration within the KCNQ2 channel complex, rather than its conformational change or dissociation from the channel. A model depicted in Figure 5.1 summarizes the signaling events triggered by the elevation of intracellular

Ca^{2+} levels. CaM acts as a Ca^{2+} sensor that binds four Ca^{2+} molecules, which alters its conformation and induces a change in the configuration of the channel complex. This change in turn leads to a decrease in PIP_2 affinity of KCNQ2 subunit, which suppresses the M-current. During this process, AKAP79/150, or KCNQ3 subunit in heteromeric channels, contributes to the retention of Ca^{2+}-bound CaM in the channel complex to allow for a fast current recovery once Ca^{2+} influx recedes. In addition to this pathway, we suspect that PKC phosphorylation of KCNQ2 subunit contributes to Ca^{2+}-mediated M-current regulation, as a phosphoacceptor-deficient KCNQ2 subunit, KCNQ2(S541A) (rat), showed attenuated response to ionomycin application in CHO hm1 cells. In conclusion, intracellular Ca^{2+} elevation appears to trigger signaling events that rearrange the configuration of KCNQ2-CaM complex, which leads to the suppression of the M-current.

The understanding of the precise mechanism of M-current regulation by neurotransmitters had also been elusive for over three decades[6]. Previously, PIP_2 depletion had been considered the principal mechanism in M-current suppression since rapid depletion and recovery of PIP_2 correlate with M-current amplitudes[7–10]. My work reported in Chapter Two contributed to elucidating how other second messenger signaling events are integrated during muscarinic-mediated suppression of the M-current. The data suggest that the signaling pathway of M-channel suppression occurs in three steps in a model outlined in Figure 5.2. First, PKC phosphorylation dissociates CaM from KCNQ2 subunit; second, CaM-deficient KCNQ2 is less able to associate with PIP_2; and third, the impaired ability to interact with PIP_2 leads to the collapse of the channel pore[11]. PKC activation had been quickly identified as a candidate mediator in Gq-protein coupled receptor-mediated M-current suppression pathway[12]. However, its contribution was not widely accepted, as some phorbol esters did not suppress the current[13–15].

Additionally, staurosporine, a pharmacological PKC inhibitor, did not interfere with muscarinic suppression of the M-current[16,17]. Identification of the key PKC phosphorylation residue on KCNQ2 subunit, S541 (rat), and its physiological role in the suppression of the M-channel clarified the role of PKC (Figure 2.8). These findings also tie in with previous reports that anchoring of PKC by AKAP79/150 modifies the susceptibility of PKC to pharmacological agents including staurosporine[18,19]. Furthermore, we were able to clarify the role of CaM in muscarinic receptor-mediated M-current suppression by immunoprecipitation and FRET analyses, which revealed that CaM dissociation from KCNQ2 subunit is associated with the suppression of the M-current (Figures 2.6 & 2.7). Our mutant studies not reported here offered strong correlations between KCNQ2–CaM binding and PIP_2-related events, which suggests that they are closely related. Thus, we think that CaM dissociation triggers a reduction in PIP_2 affinity, which, together with concomitant depletion of PIP_2, leads to the suppression of the M-current upon muscarinic stimulation. Together, these findings contributed to the elucidation of the cascade of signaling events, which laid ground for a new view on muscarinic-mediated regulation of the M-current. The conclusions of this work emphasize the significance of signaling complexes as a point of convergence of overlapping modulatory signaling pathways. In a broader context, we provide evidence that seemingly redundant actions of PKC, CaM and PIP_2 act synergistically to create a fail-safe mechanism for the M-current regulation.

Characterization of novel mouse line, KCNQ2(S559A)

Based on the findings mentioned above, we generated a novel knock-in mouse model, KCNQ2(S559A), described in Chapter Three. These mice appeared to have normal baseline characteristics as compared to wild-type, namely normal rate of growth, brain morphology as well as a normal phenotype on basic behavioral tasks. Electrophysiological characterization of

neurons from KCNQ2(S559A) mice showed that their basic properties such as input resistance, cell capacitance as well as standing current amplitudes were comparable to those of wild-type. However, hippocampal, cortical, and SCG neurons from KCNQ2(S559A) mice showed attenuated suppression in response to muscarinic agonist, oxo-M. We tested four different doses of oxo-M, ranging from 0.3 μM to 10 μM and observed an approximately 10-fold decrease in oxo-M sensitivity in mutant neurons compared to wild-type. However, to conduct a more thorough and complete characterization of KCNQ2(S559A) resistance to muscarinic stimulation, it will be beneficial to perform a full dose response on neurons from wild-type and KCNQ2(S559A) mice. Additionally, since we believe that KCNQ2(S559A) mutation attenuates neurotransmitter-induced M-current suppression *in vivo*, electrophysiological studies using agonists that act on various Gq-protein coupled receptors will need to be carried out in the future to prove this hypothesis.

Role of M-current suppression in learning and memory

Although KCNQ2(S559A) mice showed a normal phenotype on the battery of basic behavioral tests, they exhibit some phenotypic differences as compared to their wild-type littermates. One of such differences, a deficit in long-term recognition memory, is covered in Chapter Four. KCNQ2(S559A) mice showed an impairment that was specific to consolidation of recognition memories that require cortical function, particularly that of perirhinal cortex[20–22]. On the other hand, the mutation did not have an apparent effect on hippocampus-dependent memories. The observed impairment correlated with lower neuronal activation in PRH of KCNQ2(S559A) brains, as measured by immunohistochemistry for c-fos. These findings suggest a very specific role for M-current suppression in memory processing. However, from our study we cannot positively conclude whether consolidation of recognition memory requires M-current

suppression in PRH or in the regions that send projections to PRH such as CA1 of the hippocampus or primary sensory areas. Thorough and extensive follow-up studies are desirable to identify precise molecular pathways and behavioral effects of M-current regulation in cognitive function. Since the observed memory deficit requires cortical function, it would be sensible to perform a detailed characterization of cortical layers in the KCNQ2(S559A) brain by using both electrophysiology and immunohistochemistry. Patients suffering from Alzheimer's disease exhibit characteristic neurofibrillary tangles in PRH very early in disease progression[23] as well as significant thinning of perirhinal and entorhinal cortices[24]. If memory consolidation requires M-current suppression in cortical structures, it may explain why KCNQ inhibitor linopirdine did not prove efficacious in clinical trials.

Finally, although we saw a lower c-fos activation induced by NOR training in KCNQ2(S559A) PRH as compared to wild-type, it was significantly higher compared to that from home cage KCNQ2(S559A) mice. It is unclear why significant c-fos expression induced by NOR training was insufficient for recognition memory consolidation in KCNQ2(S559A) mice. We speculate that neuronal hyperexcitability induced by M-current suppression may activate activity-dependent transcription factors in PRH that are required for successful consolidation of recognition memory. Further studies including genomic profiling would be necessary to identify which genes may be up- or down-regulated in response to such hyperexcitability. Alternatively, neuronal hyperexcitability could induce structural changes of synapses that would not occur in the KCNQ2(S559A) mice.

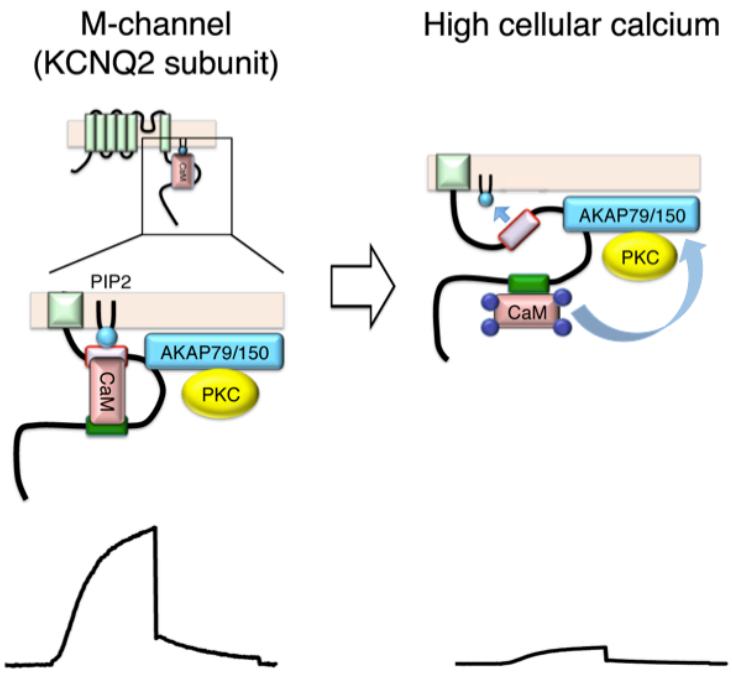

Figure 5.1. Schematic diagram of Ca^{2+}-induced KCNQ2 channel complex rearrangement.

Intracellular Ca^{2+} release triggers a conformational change of CaM, which leads to a change in configuration of the channel complex. This change reduces KCNQ2 affinity for PIP_2, which leads to current suppression. AKAP79/150 retains Ca^{2+}-bound CaM for rapid current recovery.

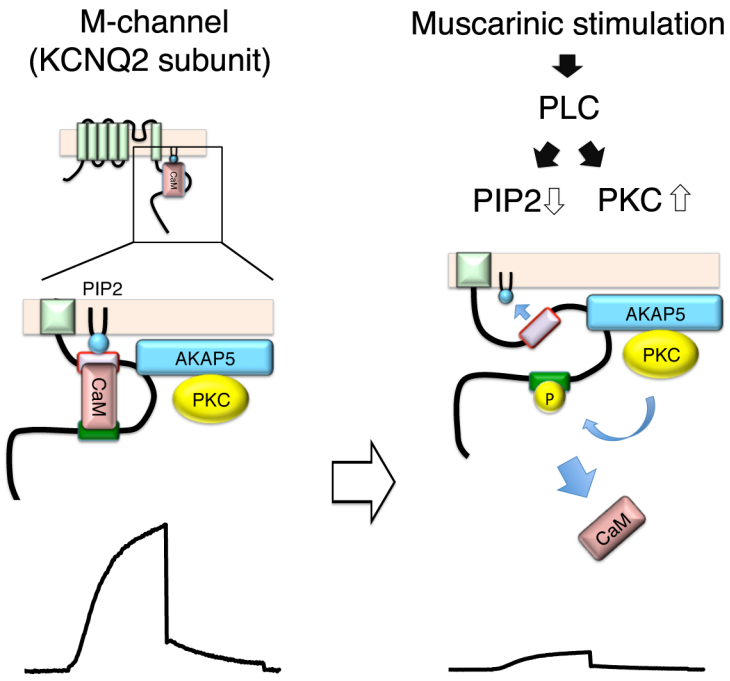

Figure 5.2. Schematic diagram of muscarinic receptor activation-induced KCNQ2 channel complex rearrangement.

Muscarinic receptor stimulation activated PKC, which phosphorylates KCNQ2 subunit. PKC phosphorylation dissociates CaM from KCNQ2, impairing the ability of KCNQ2 to associate with PIP_2. This leads to the collapse of the channel pore and, therefore, current suppression.

References

1. Kirkwood, A. & Lisman, J. E. Action potentials produce a long-term enhancement of M-current in frog sympathetic ganglion. *Brain Res.* **580,** 281–287 (1992).
2. Selyanko, A. A. & Brown, D. A. Intracellular calcium directly inhibits potassium M channels in excised membrane patches from rat sympathetic neurons. *Neuron* **16,** 151–162 (1996).
3. Gamper, N. & Shapiro, M. S. Calmodulin Mediates Ca2+-dependent Modulation of M-type K+ Channels. *J. Gen. Physiol.* **122,** 17–31 (2003).
4. Shahidullah, M., Santarelli, L. C., Wen, H. & Levitan, I. B. Expression of a calmodulin-binding KCNQ2 potassium channel fragment modulates neuronal M-current and membrane excitability. *Proc. Natl. Acad. Sci.* **102,** 16454–16459 (2005).
5. Bal, M., Zhang, J., Hernandez, C. C., Zaika, O. & Shapiro, M. S. Ca2+/calmodulin disrupts AKAP79/150 interactions with KCNQ (M-Type) K+ channels. *J. Neurosci.* **30,** 2311–2323
6. Brown, D. A. & Adams, P. R. Muscarinic suppression of a novel voltage-sensitive K+ current in a vertebrate neurone. *Nature* **283,** 673–676 (1980).
7. Suh, B. C. & Hille, B. Recovery from muscarinic modulation of M current channels requires phosphatidylinositol 4,5-bisphosphate synthesis. *Neuron* **35,** 507–520 (2002).
8. Delmas, P. & Brown, D. A. Pathways modulating neural KCNQ/M (Kv7) potassium channels. *Nat. Rev. Neurosci.* **6,** 850–862 (2005).
9. Winks, J. S., Hughes, S., Filippov, A. K., Tatulian, L., Abogadie, F. C., Brown, D. A. & Marsh, S. J. Relationship between membrane phosphatidylinositol-4,5-bisphosphate and

receptor-mediated inhibition of native neuronal M channels. *J. Neurosci.* **25,** 3400–3413 (2005).

10. Suh, B.-C., Inoue, T., Meyer, T. & Hille, B. Rapid chemically induced changes of PtdIns(4,5)P2 gate KCNQ ion channels. *Science* **314,** 1454–1457 (2006).
11. Hansen, S. B., Tao, X. & MacKinnon, R. Structural basis of PIP2 activation of the classical inward rectifier K+ channel Kir2.2. *Nature* **477,** 495–498 (2011).
12. Higashida, H. & Brown, D. A. Two polyphosphatidylinositide metabolites control two K+ currents in a neuronal cell. *Nature* **323,** 333–335 (1986).
13. Dutar, P. & Nicoll, R. A. Classification of muscarinic responses in hippocampus in terms of receptor subtypes and second-messenger systems: electrophysiological studies in vitro. *J. Neurosci.* **8,** 4214–4224 (1988).
14. Marrion, N. V. Control of M-current. *Annu. Rev. Physiol.* **59,** 483–504 (1997).
15. Suh, B. C. & Hille, B. Does diacylglycerol regulate KCNQ channels? *Pflugers Arch. Eur. J. Physiol.* **453,** 293–301 (2006).
16. Bosma, M. M. & Hille, B. Protein kinase C is not necessary for peptide-induced suppression of M current or for desensitization of the peptide receptors. *Proc. Natl. Acad. Sci.* **86,** 2943–2947 (1989).
17. Shapiro, M. S., Roche, J. P., Kaftan, E. J., Cruzblanca, H., Mackie, K. & Hille, B. Reconstitution of muscarinic modulation of the KCNQ2/KCNQ3 K(+) channels that underlie the neuronal M current. *J. Neurosci.* **20,** 1710–1721 (2000).
18. Hoshi, N., Langeberg, L. K., Gould, C. M., Newton, A. C. & Scott, J. D. Interaction with AKAP79 modifies the cellular pharmacology of PKC. *Mol. Cell* **37,** 541–550 (2010).

19. Smith, I. M. & Hoshi, N. ATP competitive protein kinase C inhibitors demonstrate distinct state-dependent inhibition. *PLoS One* **6,** (2011).

20. Brown, M. W. & Aggleton, J. P. Recognition memory: what are the roles of the perirhinal cortex and hippocampus? *Nat. Rev. Neurosci.* **2,** 51–61 (2001).

21. Suzuki, W. A. Untangling memory from perception in the medial temporal lobe. *Trends. Cogn. Sci.* **14,** 195–200 (2010).

22. Feinberg, L. M., Allen, T. A., Ly, D. & Fortin, N. J. Recognition memory for social and non-social odors: differential effects of neurotoxic lesions to the hippocampus and perirhinal cortex. *Neurobiol. Learn. Mem.* **97,** 7–16 (2012).

23. Augustinack, J. C., Huber, K. E., Stevens, A. A., Roy, M., Frosch, M. P., van der Kouwe, A. J. W., Wald, L. L., Van Leemput, K., McKee, A. C. & Fischl, B. Predicting the location of human perirhinal cortex, Brodmann's area 35, from MRI. *Neuroimage* **64,** 32–42 (2013).

24. Juottonen, K., Laakso, M. P., Insausti, R., Lehtovirta, M., Pitkänen, a., Partanen, K. & Soininen, H. Volumes of the entorhinal and perirhinal cortices in Alzheimer's disease. *Neurobiol. Aging* **19,** 15–22 (1998).